Molecular Assemblies as Drug Carriers for Topical Applications(Dissertation_全文)

AUTHOR(S):

Kawakami, Kohsaku

Molecular Assemblies as Drug Carriers for Topical Applications

Kohsaku Kawakami

2000

Contents

Preface

Amphiphiles, which consist of hydrophilic and hydrophobic groups, form various types of aggregates in both polar and apolar media.[1] The formation of such aggregates is mainly controlled by physical forces such as hydrophobic, electrostatic, and van der Waals interactions. Some of them are spontaneously formed, while others can be prepared under external mechanical forces. The former aggregates are in the equilibrium state, and their structures are controlled by physical interactions. However, the latter aggregates are not in the equilibrium state, which means that their structures can be controlled by the preparation methods. Examples of the equilibrium and non-equilibrium structures consisting of amphiphiles are illustrated in Figure 1 and 2, respectively.

The types of the aggregates in the equilibrium state formed by particular amphiphiles strongly depend on their molecular shape and concentration. Upon increasing the amphiphile concentration, there is generally change in the phase structures in the order of micelle, hexagonal, and lamellar as shown in Figure 1. The reversed structures for each phase can also be observed in the apolar media except for the lamellar phase.

Figure 2 shows the most representative non-equilibrium aggregates in the pharmaceutical studies. Oil-in-water emulsions, which are frequently called as "emulsions" simply, are oil droplets coated by surfactant shells. Although it is also possible to prepare emulsions without surfactants, their physical stability is usually not high enough due to the high interfacial energy, which enhances their coalescence. Therefore, it is difficult to utilize them as drug carriers. The preparation of the reversed type emulsions, water-in-oil emulsions, is also possible. However, they are not often utilized, because formulations are usually administered into water-rich atmospheres, in which water-in-oil emulsions cannot mix well with the surrounding aqueous phase or are destroyed easily by excess water. Emulsions are regarded as promising drug carriers for hydrophobic drugs, because they can be solubilized at

high concentration into the oil core.[2] It is also reported that the solubilized drugs in emulsions behave differently from free drugs after administration.[3-5] For example, the entrapped drugs in the emulsion core remain longer in the circulation than free drugs after the injection. The tissue distribution of drugs is also different, because that of the entrapped drugs depends on the fate of the emulsion droplets. Therefore, emulsions are regarded as convenient drug carriers for the controlled release or the targeting of drugs.

Liposomes,[6] which can be defined as vesicles composed of lipids, have been the most attractive drug carriers[7-14] because of their easily controllable properties,[15-18] low toxicity, and ability of incorporating various kinds of drugs. Figure 3 shows how drugs can be loaded into liposomes and how liposomes can be functionized. As can be seen, liposomes can serve as carriers for both hydrophilic and hydrophobic drugs. Surface modification is usually done to enhance their physical stability, to avoid the serum protein binding on surfaces which leads to their rapid clearance from the circulation,[8] and to deliver liposomes to the desired site. Liposomes, like emulsions, can also alter the fate of drugs in vivo. The administration route studied most has been the injection, while other routes such as the transdermal,[19-21] oral,[22-24] and ocular[25-27] routes have also been tried actively. Although the usage of liposomes as drug carriers has a long history of more than 20 years, new ideas continue to be put forth, such as applications for photodynamic therapy,[28,29] vaccination,[14,30] and gene transfer.[14,31-33]

However, some problems stand in the way of the development of liposomal products.[34-37] For example, the characteristics of liposomes prepared on a laboratory scale cannot always be reproduced in large-scale production. Such a problem arises because liposomes are not in the equilibrium state. Therefore, usage of the equilibrium structure, such as microemulsions[38] including cubic phase,[39-43] as drug carriers has been increasing. Although micelles are the most widely-known type of aggregate in the equilibrium state, they are hardly utilized as drug carriers due to the low solubilization capacity of drugs. To overcome this problem, apolar solvents are

introduced into the hydrophobic core of micelles. These "swollen micelles" are called as oil-in-water microemulsions. The inverted structure is also known as water-in-oil microemulsions. These aggregates have a very similar morphology to the emulsions introduced above. However, they can exist as equilibrium structures due to the extremely low interfacial energy.

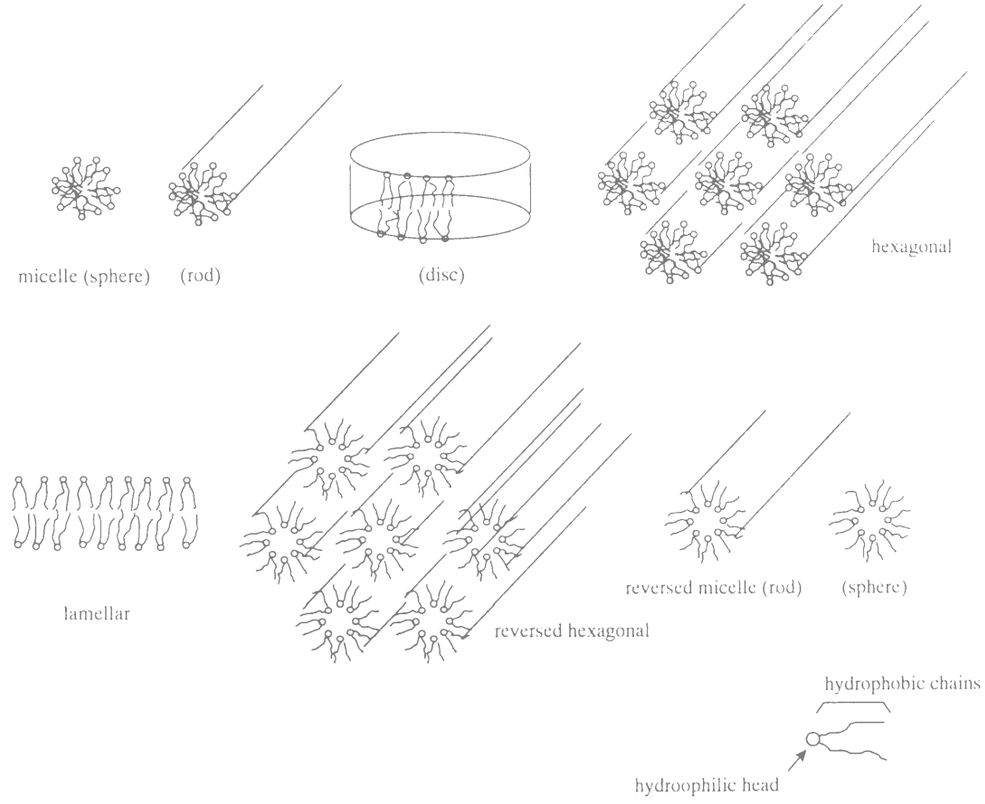

Figure 1. Representative equilibrium structures formed by amphiphiles.

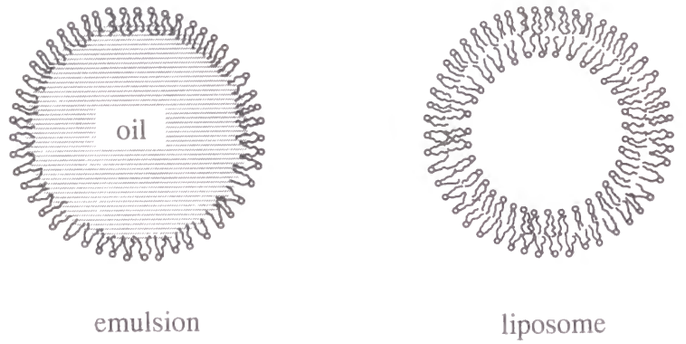

Figure 2. Representative non-equilibrium structures formed by amphiphiles.

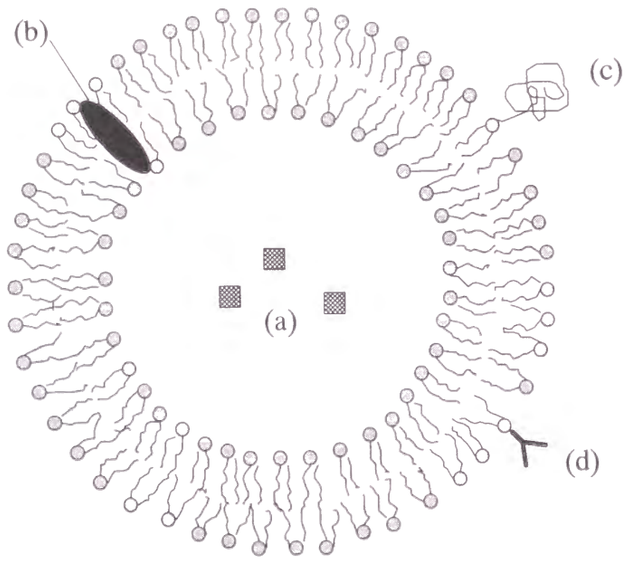

Figure 3. A liposome particle as a drug carrier. (a) Hydrophilic drugs are incorporated into the aqueous core. (b) Hydrophobic drugs are loaded into the lipid membrane. (c) Poly(ethylene glycol)-attached lipids are frequently used to stabilize liposome particles. The PEG-decorated liposome is usually called as a "stealth liposome." (d) Immobilized antibodies can act as a sensor for site-specific targeting of drug-loaded liposomes.

Microemulsions can be defined as thermodynamically stable isotropic solutions composed of at least oil, water, and surfactants. Because they are surrounded by liquid surfactant membranes, they may act as a "soft" drug reservoirs whose formation and deformation are easily controlled by external factors such as temperature and ion strength. In other words, the uptake of drugs into microemulsion droplets and their release can proceed promptly. However, it means that the solubilization of drugs into microemulsion droplets should be investigated in detail, because the characteristics and even the existence of the droplets can be affected significantly by the guest drugs.

In this thesis, two representative types of aggregates mentioned above, liposomes as representative of a non-equilibrium structure and microemulsions as that of equilibrium structure, are discussed from the standpoint of their use as drug carriers for topical applications.[18-20,24-26,44,45] Drugs are usually solubilized or dispersed into homogeneous matrices such as hydrogels or waxes for the transdermal drug delivery. However, when active agents are loaded onto the molecular assemblies as shown in Figure 4, they can remain longer on the skin or mucosa due to the great compatibility between the aggregates and the skin. The enhanced solubility of drugs into the formulation is another advantage of using molecular assemblies as carriers. In addition, the enhanced penetration rate of drugs into skin is also examined in some cases.

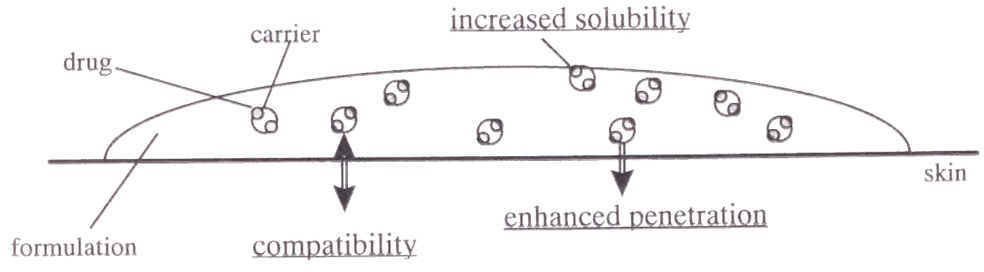

Figure 4. Schematic representation of the carrier-containing formulation for the transdermal drug delivery.

When molecular assemblies are contained as drug carriers in the formulations, their designs are very complicated. This thesis focuses on how to design and characterize such carrier-containing formulations. Chapters 1 through 3 examine liposomes and Chapter 4 discusses the use of water-in-oil microemulsions from the viewpoint of utilizing them as drug carriers for the transdermal drug delivery.

The formulation for the transdermal drug delivery has some distinctive features. The first is the relatively large amount of drug usually needed in the formulation because of the high barrier efficiency of the skin. Another reason for this is that a large part of the formulation may be removed before the drug can penetrate into the skin. Such large amounts are needed even when molecular assemblies are used as drug carriers. However, it is frequently difficult to disperse drugs efficiently on the carriers while maintaining the morphology of the aggregates. This problem will be considered in Chapters 1 and 2, which discuss a new method for investigating the compositional homogeneity of liposomal membranes and the mechanism of destroying the liposomal structure with an excess amount of oil-soluble drugs. Another feature to keep in mind in the design of topical formulations is that they should have a high viscosity to prevent their being washed away easily. This can be prevented by adding a hydrophilic polymers. What needs to be considered here is the fact that hydrophilic polymers are often used without considering their effect on the molecular assemblies, although they may affect their structure and dispersity. The effect of adding hydrophilic polymers on liposome dispersions will be discussed in Chapter 3. Chapters 1 and 2 also present new various methodologies for studying liposomes. These methods are applicable for fundamental studies on liposomes as well as for the study of topical formulations.

In the case of equilibrium structures such as microemulsions employed as drug carriers, the drug incorporation process into the carriers must be studied in detail. This is because it may alter the morphology or even the existence of microemulsion droplets as mentioned earlier. This issue will be treated in Chapter 4. These discussions are offered with the hope that they can lead to important information for designing new topical formulations containing molecular assemblies as drug carriers.

References

(1) Israelachvili, J. N. "Intermolecular and Surface Forces, 2nd ed." Academic Press, London, **1991**.

(2) Müller, R. H., Benita, S., Böhm, B. H. L. "Emulsions and Nanosuspensions for the Formulation of Poorly Soluble Drugs." Medpharm Scientific Publ., Stuttgart, **1998**.

(3) Mizushima, Y., Yanagawa, A., Hoshi, K. *J. Pharm. Pharmacol.* **1983**, *35*, 666.

(4) Lin, S. Y., Wu, W. H., Lui, W. Y. *Pharmazie* **1992**, *47*, 439.

(5) Takino, T., Konishi, K., Takakura, Y., Hashida, M. *Biol. Pharm. Bull.* **1994**, *17*, 121.

(6) Bangham, A. D.; Horn, R. W. *J. Mol. Biol.* **1964**, *8*, 660.

(7) Knight, C. G. "Liposomes; From Physical Structure to Therapeutic Applications." Elsevier, Amsterdam, **1981**.

(8) Senior, J. H. *Crit. Rev. Ther. Drug Carrier Syst.* **1987**, *3*, 123.

(9) Lasic, D. D. "Liposomes; From Physics to Applications." Elsevier, Amsterdam, **1993**.

(10) Gregoriadis, G. "Liposome Technology." CRC, Boca Raton, FL, **1993**.

(11) Lasic, D. D.; Papahadjopoulos, D. *Science* **1995**, *267*, 1275.

(12) Sharma, A.; Sharma, U. S. *Int. J. Pharm.* **1997**, *154*, 123.

(13) Gulati, M.; Grover, M.; Singh, S.; Singh, M.; *Int. J. Pharm.* **1998**, *165*, 129.

(14) Lasic, D. D. *Trends Biotechnol.* **1998**, *16*, 307.

(15) Oku, N.; Namba, Y. *Crit. Rev. Ther. Drug Carrier Syst.* **1994**, *11*, 231.

(16) Jones, M. N. *Adv. Colloid Interface Sci.* **1995**, *54*, 93.

(17) Ceh, B.; Winterhalter, M.; Frederik, P. M.; Vallner, J. J.; Lasic, D. D. *Adv. Drug. Delivery Rev.* **1997**, *24*, 165.

(18) Woodle, M. C. *Adv. Drug Delivery Rev.* **1998**, *32*, 139.

(19) Mezei, M.; Gulasekharam, V. *Life Sci.* **1980**, *26*, 1473.

(20) Gabrijelcic, V.; Šentjurc, M. *Int. J. Pharm.* **1995**, *118*, 207.

(21) Kim, M. K.; Chung, S. J.; Lee, M. H.; Cho, A. R.; Shim, C. K. *J. Control. Release* **1997**, *46*, 243.

(22) Patel, H. M.; Ryman, B. E.; *FEBS Lett.* **1976**, *62*, 60.

(23) Hemker, H. C.; Muller, A. D.; Hermens, W. Th.; Zwaal, R. F. A. *Lancet* **1980**, *1*, 70.

(24) Nishida, Y.; Kamatani, N.; Miyamoto, T. *J. Pharm. Pharmacol.* **1984**, *36*, 354.

(25) Schaeffer, H. E.; Krohn, D. L. *Invest. Ophthalmol. Vis. Sci.* **1982**, *21*, 220.

(26) Davies, N. M.; Farr, S. J.; Hadgraft, J.; Kellaway, I. W. *Pharm. Res.* **1992**, *9*, 1137.

(27) Mezei, M.; Meisner, M. "Liposomes and Nanoparticles as Ocular Drug Delivery Systems. Biopharmaceutics of Ocular Drug Delivery." CRC Press, Boca Raton, FL, **1993**.

(28) Ricchelli, F.; Nikolov, P.; Gobbo, S.; Jori, G.; Moreno, G.; Salet, C. *Biochim. Biophys. Acta* **1994**, *1196*, 165.

(29) Isele, U.; Schieweck, K.; Kessler, R.; van Hoogevest, P.; Capraro, H. G. *J. Pharm. Sci.* **1995**, *84*, 166.

(30) Donnelly, J. J.; Ulmer, J. B.; Shiver, J. W.; Liu, M. A. *Annu. Rev. Immunology* **1997**, *15*, 617.

(31) Lappalainen, K.; Urtti, A.; Soderling, E.; Jaaskelainen, I.; Syrjanen, K.; Syrjanen, S. *Biochim. Biophys. Acta* **1994**, *1196*, 201.

(32) Lee, R. J.; Huang, L. *Crit. Rev. Ther. Drug Carrier Syst.* **1997**, *14*, 173.

(33) Chonn, A.; Cullis, P. R. *Adv. Drug Delivery Rev.* **1998**, *30*, 73.

(34) Ausborn, M.; Nuhn, P.; Schreier, H. *Eur. J. Pharm. Biopharm.* **1992**, *38*, 133.

(35) Isele, U.; van Hoogevest, P.; Hilfiker, R.; Capraro, H. G.; Schieweck, K.; Leuenberger, H. *J. Pharm. Sci.* **1994**, *83*, 1608.

(36) Lawrence, M. J. *Eur. J. Drug Metab. Pharmacokinet.* **1994**, *3*, 257.

(37) Hirota, S. *Int. J. Pharm.* **1998**, *162*, 185.

(38) Hoar, T. P.; Schulman, J. H. *Nature*, **1943**, *152*, 102.

(39) Lindblom, G.; Rilfors, L. *Biochim. Biophys. Acta* **1989**, *988*, 221.

(40) Engström, S. *Lipid Tech.* **1990**, *2*, 42.

(41) Alexandridis, P.; Olsson, U.; Lindman, B. *Langmuir* **1996**, *12*, 1419.

(42) Chang, C. M.; Bodmeier, R. *J. Control. Release* **1997**, *46*, 215.

(43) Koynova, R.; Tenchov, B.; Rapp, G. *Biochim. Biophys. Acta* **1997**, *1326*, 167.

(44) Osborne, D. W., Ward, A. J. I., O'neill, K. J. *J. Pharm. Pharmacol.* **1991**, *43*, 451.

(45) Bolzinger, M. A., Thevenin, M. A., Carduner, C., Poelman, M. C. *Int. J. Pharm.* **1998**, *176*, 39.

Chapter 1

Capillary Electrophoresis for Analysis of Liposome Dispersions

1-1. Mobility of Liposomes Evaluated by Capillary Electrophoresis

Introduction

Capillary electrophoresis (CE)[1] is a newly developed method which enables separation of small solutes by their size and amount of charge. CE has some advantages, compared with the conventional liquid chromatography technique. For example, CE separation can be completed on the faster time scale, require only a small amount of injection volume, and can be performed under aqueous conditions in most cases.

Recently, various applications of CE have been developed. As for large molecules and particles, such as hydrophilic polymers[2] and polystyrene nanoparticles,[3] they are separated successfully by CE. However, as for the liposomes,[4,5] their behavior in capillary columns is not well understood, even though the CE application to liposomes are also under development. In this section, we discuss the behavior of liposomes in the CE analysis as the preparation of Chapters 1-2 and 1-3.

Principle of CE analysis

CE enables the separation of small solutes by their size and amount of charge as mentioned in Introduction. The experimental setup and the principle of the separation are illustrated in Figure 1-1. Each end of a capillary column is immersed in a running buffer vial. The buffer vial into which the sample-injection end of the column is inserted is maintained at positive high voltage, and the vial at the other side is held at ground. The sample injection is done by replacing the buffer vial with a sample vial and applying pressure to the sample vial to force a small aliquot of sample into the capillary. After the injection, the sample vial is returned to its original place and replaced with the buffer vial and the separation is started. The electrophoretic

mobility of solutes, μ, is given by

$$\mu = \frac{v}{E} = \frac{q}{6\pi\eta r} \qquad (1\text{-}1)$$

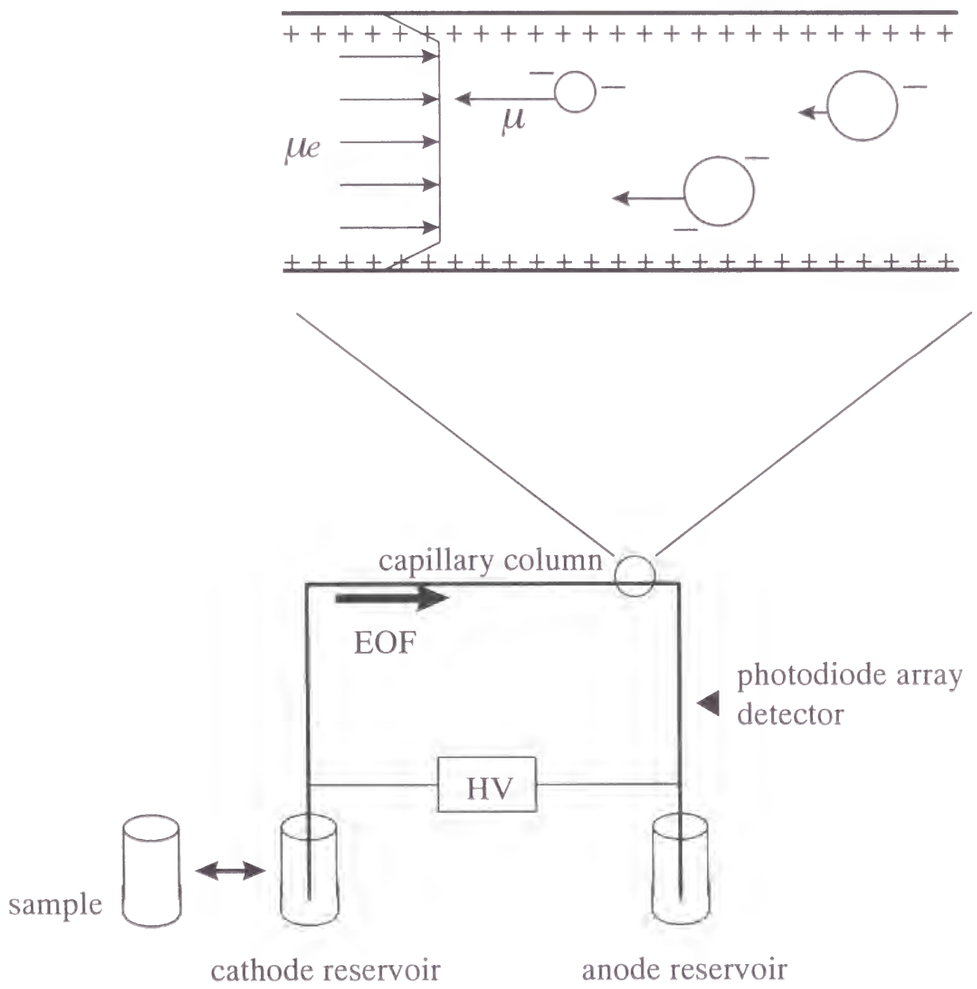

Figure 1-1. Diagram of CE setup.

where v, E, q, η, and r are the velocity of solutes, electric field, charge of solutes, viscosity of the continuum phase, and radius of solutes, respectively. For large particles like liposomes, electrophoretic retardation and relaxation effect must be taken into account. In this case, equation (1) is replaced with[6]

$$\mu = \frac{v}{E} = f(\kappa a)\frac{2\varepsilon_r \varepsilon_o \zeta}{3\eta} \qquad (1\text{-}2)$$

where κ, a, $f(\kappa a)$, ε_r, ε_o, and ζ are the Debye-Hückel parameter, radius of particles, Henry's coefficient, relative permittivity of continuum phase, permittivity of vacuum, and the ζ-potential, respectively. From this equation, we can speculate that the mobility increases with the charge when the radius is fixed, and also, with the radius when the amount of charge is fixed because the Henry's coefficient is an increasing function from 1 to 1.5 with κa. The apparent mobility μ_a is the sum of the real mobility, μ, and the mobility of the electroosmotic flow (EOF), μ_e, i.e.,

$$\mu_a = \mu + \mu_e . \qquad (1\text{-}3)$$

The migration time, t_m, is expressed as

$$t_m = \frac{L}{\mu_a E} \qquad (1\text{-}4)$$

where L is the effective length of the capillary. However, it should be noted that the following assumptions must be made to apply this theory to liposomes. (1) Each particle is supposed to behave as a rigid sphere. (2) The particle-particle interaction and the particle-wall interaction are ignored. (3) Electroosmotic flow is the plug flow Recently, some attempts to use this technique were made to characterize liposomal dispersions, with successful application to the size distribution[4] and quantification of

phospholipids.[5]

Experimental Section

Materials. Dipalmitoylphosphatidylcholine (DPPC) and distearoyl-phosphatidylglycerol (DSPG) were purchased from Nippon Fine Chemicals. All chemicals were at least of reagent grade and used as supplied.

Preparation of Liposome. Liposome dispersions were prepared by freeze-dry method as shown in Figure 1-2. First, weighed lipid powder was dissolved in tert-butyl alcohol at 65°C, which is above the phase transition temperature of phospholipids. The alcohol solution was freeze-dried, and the powder obtained was dispersed in a 10 mM phosphate buffer of pH 8.0, also at 65°C. The size of the liposomal particles was controlled with a high pressure emulsifier, Extruder™ (Lipex Biomembranes) with polycarbonate membranes. Size distributions were determined by the laser light scattering method (Coulter N4 plus).

Capillary Electorphresis. The CE analysis was performed by Hewlett Packard 3D CE system, using a fused silica capillary column (50 μm id × 56 cm). The running buffer was the same as the solution buffer. Before each run, 20 minutes flushing with buffer at 60°C, 2 minutes with methanol at 35°C, and 2 minutes with 0.1 M NaOH at 35°C are performed. These steps were conducted to prevent the clogging in the column, although it did not often occur. The injection was done from cathode side by pressuring the dispersion up to 50 mbar for 10 seconds unless otherwise mentioned, followed by injection of the buffer for 100 seconds at the same pressure. The voltage and temperature were set to be 30 kV and 25°C, unless otherwise mentioned. The voltage, current, and temperature were monitored during the measurement to confirm that they all remained to be constant.

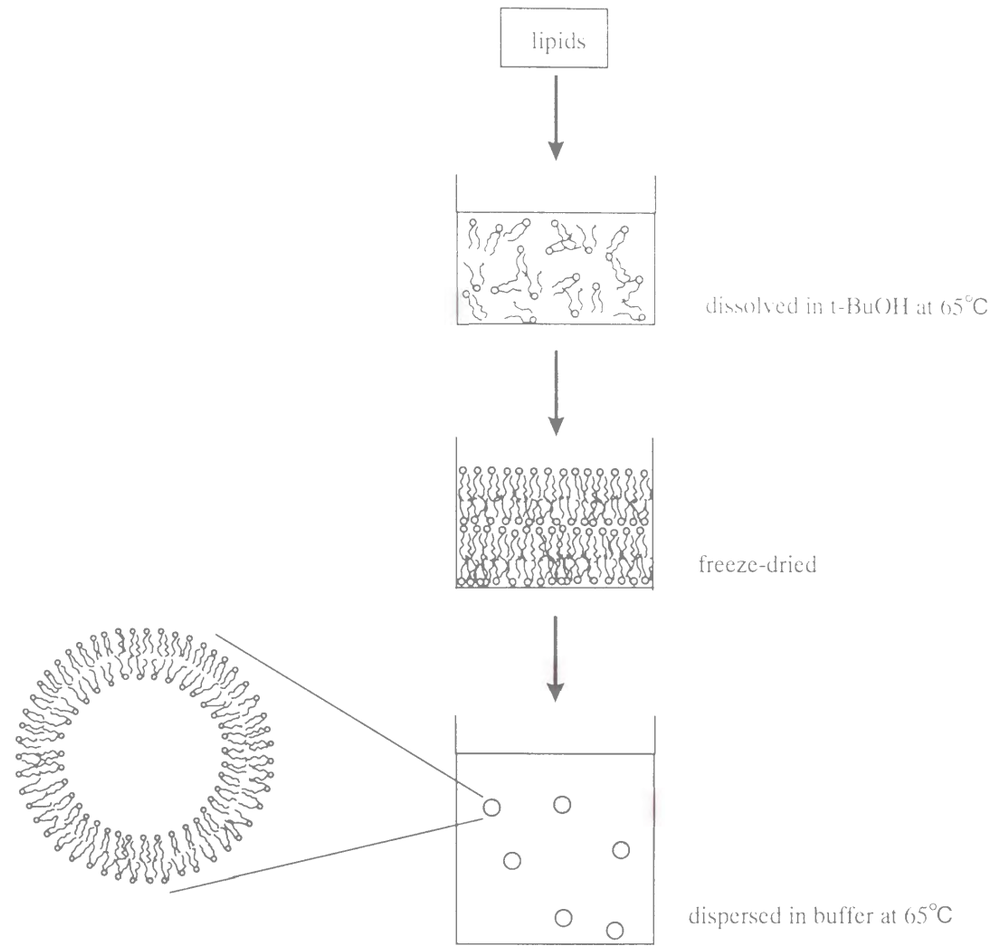

Figure 1-2. Schematic presentation of the preparation process of liposome.

Results and discussion

Dependence of Migration Time on Charge of Liposomes. Theoretically, the migration time of particles will be shorter as the amount of negative charge decreases. The change of the migration time with the ratio of dosed negatively charged phospholipids is shown in Figure 1-3. Liposomes are composed of DPPC and DSPG with various ratios. For both injection volume, the charge trend agrees with the prediction made from Equation 1-4, except that there was the dependence on the injection volume. The effect of the injection volume will be discussed later.

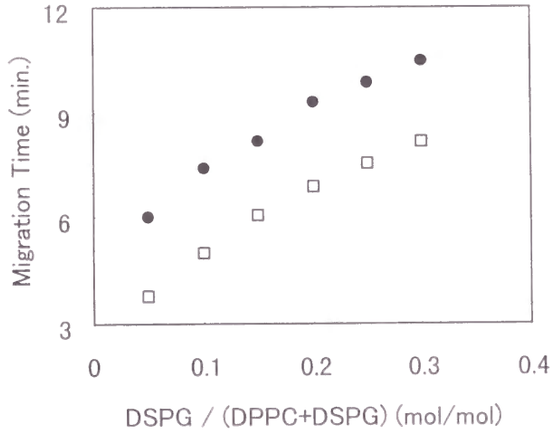

Figure 1-3. Dependence of migration time on charge of liposomes. Injection time (proportional to injection volume) was 10 sec. (□) and 30 sec. (●), respectively.

Dependence of Migration Time on Size of Liposomes. The migration time of the negatively charged particles will become shorter as the size decreases. In Figure 1-4, the change of the migration time with the size is shown when the size and the injection volume are altered. Liposomes are composed of DPPC/DSPG = 10/1 (molar ratio). The size distributions were determined by the light scattering method to be nearly monodisperse for all dispersions. For both injection volume, the effect of size seems to agree with the features predicted by Equation 1-4, except that there was a dependence on the injection volume. The reason for the dependence on the injection volumes is thought to be as follows. First, the plug flow must be disrupted when liposomal particles occupy a large proportion of the cross-sectional area in the capillary. If this is the case, the migration time should become longer than that of the expected value from Equation 1-4 as the diameter increases. Hence the electrophoretic mobility of liposomal particles can be expressed as

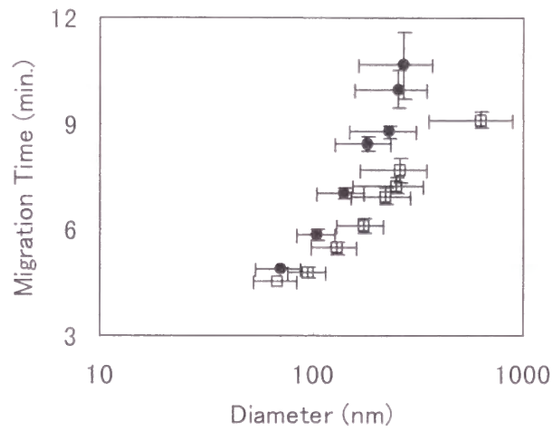

Figure 1-4. Dependence of migration time on size of liposomes. Injection time (proportional to injection volumes) was 10 sec. (□) and 30 sec. (●), respectively. Error bars represent the standard deviations.

$$\mu = \frac{L}{E}\left(\frac{1}{t_m} - \frac{1}{t_0}\right) \qquad (1\text{-}5)$$

where t_0 is the migration time of neutral particles, which could be determined by extrapolating the data of Figure 1-3 to DSPG/(DPPC + DSPG)=0. The evaluation of μ from Equation 1-5 indicates that the ratio between the maximum and minimum values of μ for the maximum size difference is 2.1. However, this value is much greater than the maximum ratio, 1.5, which is predicted using Equation 1-2 for much wider size difference. Therefore, we conclude that the increase of the migration time with the diameter cannot be explained only by Equation 1-2. When either the diameter of liposomal particles or the injection volume increased, we observed the broadening of the peak widths. Therefore it is very likely that the disrupt of the plug flow occurs. In addition, it is also possible to think that the softness of the lipid membranes affect the migration time, i.e., larger particles deform more easily and such deformation may prevent liposomal particles from moving with the electroosmotic flow. Anyway, it was confirmed that the migration time of liposomal particles was controlled by the diameter.

Application to the Analysis of Size Distributions. From the results mentioned above, we can expect that the size distribution of liposomes may be analyzed by the CE measurement, if the charged components are homogeneously distributed. In Figure 1-5, we present the electropherograms of liposomes of 100 nm and 200 nm in diameter, and that of their equimolar mixture. As can be seen, the electropherogram of the mixture is approximately given by the summation of those of the monodisperse samples, suggesting that the CE analysis can be a powerful tool for investigating the size distribution of liposomes as implied by Roberts et al.[4] The most common technique for measuring the size distribution of colloidal particles has been the light scattering method. However, the interpretation of the obtained data sometimes fails when the distribution is bimodal. On the other hand, since the CE analysis is based on a very simple principle, it offers a great possibility of being a very powerful tool for

measuring the size distribution of particles. Actually, the bimodal sample in Figure 1-5 was analyzed to be monodisperse by the light scattering method. The upper limit of liposome size which can be detected by this technique was ca. 1 μm, because larger liposomes than this size gave too broad peaks to be investigated. This may be due to the disruption of the plug flow as mentioned earlier.

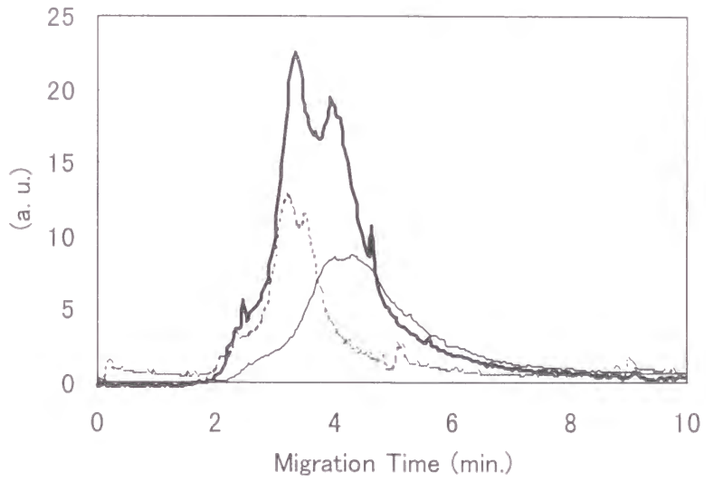

Figure 1-5. Electropherograms of liposomes (DPPC/DSPG = 10/1) of 100 nm (---), 200 nm (—) in diameter, and the mixture of these liposomes of equal volume (—). Temperature was 50 ℃.

Summary

The behavior of liposomes in the CE analysis was investigated and proved to agree roughly with the prediction from the theory for small solutes, although the disruption of the plug flow or deformation of liposomes seemed to occur. As one of the applications, the possibility for determining the size distribution are presented. These results demonstrate that the CE will be a hopeful tool to investigate various characteristics of liposomes as shown in Chapters 1-2 and 1-3.

1-2. Compositional Homogeneity of Liposomal Membranes

Introduction

In pharmaceutical fields, liposomes have been regarded as hopeful drug carriers[7,8] for more than 30 years. However, despite much effort, there are only a few liposomal products on the market. One of the major reasons is the difficulty in scaling-up of the production process. Therefore it can be said that methods for preparing liposomal formulations are still under development from an industrial point of view. Because the preparation methods affect the characteristics of liposome structures significantly, the products must be characterized to evaluate new[9] or up-scaled[10] preparation process. Most methods for characterizing various aspects of products have already been established. However, that for observing compositional homogeneity requires further development.

The most popular method for determining compositional homogeneity is differential scanning calorimetry.[11] However, there are limitations to the application mainly due to the small transition enthalpy of lipids in the membranes. In other words, there are so many requirements to detect the transition peak clearly. For example, the higher the curvature of the membrane is, the more difficult it is to detect the transition peaks of constituent lipids. The same problem arises when cholesterol, a well-known membrane stabilizer, is added. An alternative method is free-zone electrophoresis, which was introduced to investigate the charge density.[12,13] However this technique entails a long procedure and can be used only when the homogeneity of charged components is examined. Fluorescent probes can also be applied to evaluate several kinds of homogeneity.[14] However, it is suspected that probes themselves are distributed homogeneously in some cases. In addition, even though the distribution of probes is homogeneous, this method cannot be adopted for quality control. It is because there are few cases in which guest molecules in the products can be treated as fluorescent probes.

In this section, we report the application of CE to the detection of compositional

homogeneity of liposomal membranes, which remains a problem in this field. The concept of this study is as follows. In the case of charged guest molecules distributed on monodispersed liposomal membranes, the zeta potential of each particle is the only factor which controls the migration time in the analysis as shown by Equations 1-2 through 1-4. Therefore, all the particles would be detected as a single peak if the guest molecules are homogeneously dispersed on the membranes, i.e., the amount of charge per particle is the same. However, several distinguishable peaks will be observed if they are dispersed heterogeneously. Even if the guest molecules are non-charged but have UV or visible light absorption, the signal ratio obtained at two different wavelengths would enables us to investigate the homogeneity. When they are dispersed homogeneously, the signal ratio obtained at two different wavelengths, one of which should be chosen to be that at which maximal absorption of guest molecules occurs, will show a constant value. However, this would not be the case for the heterogeneous distribution.

Experimental Section

Materials. α-tocopheryl acetate (Toc) was supplied from Shionogi & Co. Dimyristoylphosphatidylcholine (DMPC) and dipalmitoyl-phosphatidylglycerol (DPPG) were purchased from Nippon Fine Chemicals. Other lipids were the same as stated in the previous section. All chemicals were at least of reagent grade and used as supplied.

Preparation of Liposome. Two types of liposomal dispersions, which were expected to be homogeneous and heterogeneous ones, were prepared by two different methods. For the homogeneous one, weighed lipid powder with or without Toc was dissolved in tert-butyl alcohol at 65°C. The alcohol solution was freeze-dried, and the powder obtained was dispersed in 10 mM phosphate buffer at pH 8.0, also at the same temperature. The size of the liposomal particles was controlled with Extruder™

(Lipex Biomembranes) using polycarbonate membranes, except that small liposomes of 20 nm in diameter were produced using Nanomizer™ (Sayama Trading). Heterogeneous one were prepared by dispersing all components in buffer solution with heating, followed by the same process of sizing treatment. The size distribution was determined by dynamic light scattering method (Coulter N4 plus).

Capillary Electrophoresis. The CE analysis of the liposomes was performed as described in the previous section.

Results and Discussion

Dispersity of Charged Components. When charged components are loaded as the guest molecules on liposomal membranes, we should be able to detect the homogeneity of the membrane from the shape of peaks as mentioned above. Figure 1-6 presents electropherograms for the samples with the same composition but prepared by different methods. The signals were detected at 220 nm. These dispersions were composed of DMPC/DPPG=16/3 in molar ratio, and the diameter was controlled to be 20 nm because smaller liposomes showed sharper peaks. As expected, the freeze-dried sample showed a single peak, while the directly-dispersed sample had several broad peaks. Since the diameter of both samples was confirmed to be monodisperse, this difference must be due to the difference of the compositional homogeneity, i.e., the difference of the charge density of individual particles.

As another interpretation of the peak-splitting , the fusion of liposome particles can also be assumed. It is well-known that the compositional heterogeneity of lipid membranes often leads to the fusion of liposomes. Therefore, it may be another reason for the peak-splitting, although it also reflects the heterogeneity of the membranes.

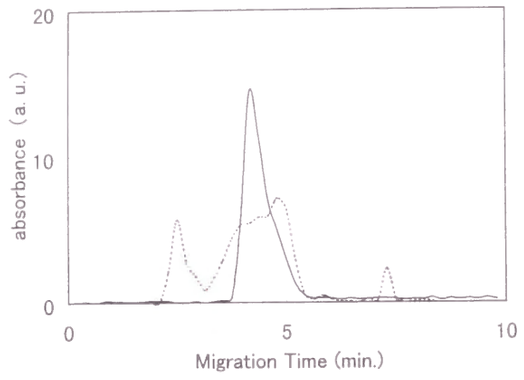

Figure 1-6. Comparison of electropherograms for two preparation methods; freeze-dry method (——) and directly-disperse method (-----). Particle diameter was adjusted to be 20 nm. DMPC/DPPG=16/3 in molar ratio.

Dispersity of Noncharged Components. As a next step, Toc, which is known as a highly oil-soluble drug, was loaded as a noncharged guest molecule on DMPC/DPPG membranes. It was confirmed that almost all the Toc added was incorporated in the lipid membranes and only a trace amount was found in the aqueous phase. To avoid the charge heterogeneity, DMPC and DPPG were freeze-dried in advance even for the directly-dispersed sample. The wavelengths selected were 220 nm and 285 nm at which the maximal absorption of Toc was attained. The diameter of particles was adjusted to be 200 nm because broader peaks make the analysis easier. Figure 1-7 shows the signal ratio at two wavelengths for the composition of DMPC/DPPG/Toc = 16/3/1 in molar ratio but prepared by different methods. Apparently, the directly-dispersed sample gave a more disordered signal-ratio than the freeze-dried one. Quantitative analysis of the degree of the disorder was also successful. First, we calculated the averaged signal ratio, R_{ave}, by

$$R_{ave} = \frac{\int A(t)R(t)dt}{\int A(t)dt} \qquad (1\text{-}6)$$

where A(t) is the signal at 220 nm and R(t) the signal ratio (A_{220}/A_{285}), respectively. Integration was done within the range where the value of A(t) was greater than 5% of the peak value. The variance of R(t), S^2, which can be regarded as the degree of disorder, was calculated by

$$S^2 = \frac{\int A(t)(R_{ave} - R(t))^2 dt}{\int A(t)dt}. \qquad (1\text{-}7)$$

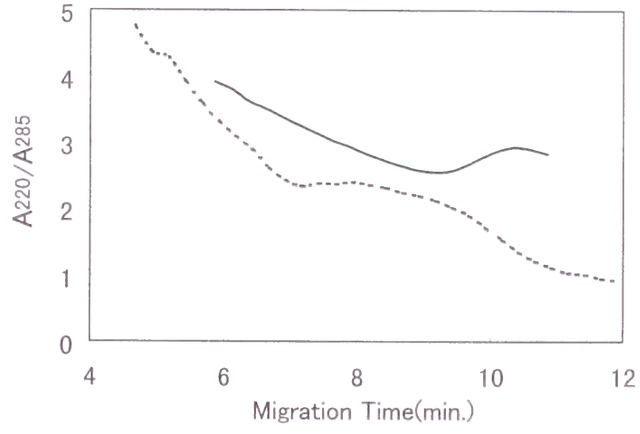

Figure 1-7. Comparison of the signal ratio at 220 nm and 285 nm (shown as A_{220}/A_{285}) between two preparation methods. Line types are same as Figure 1-6. The particle diameter was adjusted to be 200 nm. DMPC/DPPG/Toc=16/3/1 in molar ratio.

S^2 was calculated to be 0.082 for the freeze-dried sample and 0.32 for the directly-dispersed sample. This value was reproducible for the freeze-dried samples although the shape of the signal ratio was not always the same. Generally, S^2 for freeze-dried samples is smaller than 0.1. When Toc was not loaded, the values were smaller than 0.05. However, directly-dispersed samples gave larger values than 0.3. Therefore, we concluded that this analysis can also be used for detecting the homogeneity of the noncharged components. Some extent of the disorder observed for the freeze-dried sample may be attributed to a certain degree of heterogeneity, and this was reproducible also for liposomes prepared by the most conventional lipid-film method. It may be partially due to the fact that all lipids were in the gel state.

Summary

We present a new application of CE as a tool for the detection of compositional homogeneity of liposomal membranes. The homogeneity of the charged components is evaluated from the peak splitting and that of the noncharged components from the signal ratio at two wavelengths for monodispersed samples. This technique offers a powerful means for quality control of liposomal products.

1-3. Rigidity of Liposomal Membranes

Introduction

This section discusses the investigation of the rigidity of liposomal membranes as another application. Although the membrane rigidity of liquid films for microemulsions has been evaluated by means of the measurements of interface tension[15-17] and light scattering,[15-20] no experimental observation has been done for lipid bilayers. We found that the CE has a possibility to be a powerful tool for evaluating the membrane rigidity of various liquid membranes.

The principle of CE separation described in Section 1-1 is based on a theory in which a balance between the electrostatic force F_e and the friction force F_f is assumed. However, by taking into account the bending energy of lipid membranes, we can obtain the following equation:

$$F_e(\xi) = F_f(a,\xi) + \Delta F_f(\alpha,K), \qquad (1\text{-}8)$$

where α and K represent the shape of liposomes and the bending constant,[21-23] respectively. ΔF_f is expected to be negative because deformable particle can reduce the friction force. Therefore, the "soft" liposomes would give large μ values, which lead to delayed detection, i.e., a long migration time.

As described later in the text, when the bilayers were softened by incorporating cholesterol or short chain lipids, the migration time was delayed. In the experiment to observe the dependence on temperature, the relation of the viscosity versus the migration time showed a discontinuous point near the phase transition temperature, which could be elucidated in terms of the change of the membrane rigidity due to the gel/liquid crystal transition. These observations support the assumption described above.

Experimental Section

Materials. Didecanoylphosphatidylcholine ($DC_{10}PC$) was obtained from Nippon Fine Chemicals. Cholesterol was purchased from Nacalai Tesque. Other lipids were the same as stated in the previous section. Polystyrene standard particles was supplied from Dow Chemicals. All chemicals were at least of reagent grade and used as supplied.

Preparation of Liposome. Liposomal dispersions were prepared by the freeze-dry method described in the previous section. The size of the liposomal particles was controlled to be 100 nm with Extruder™ (Lipex Biomembranes) using polycarbonate membranes.

Capillary Electrophoresis. The CE analysis was performed as described in the previous sections.

Results and Discussion

Dependence of Migration Time on Membrane Composition. Table 1-1 shows the migration time of various liposomes. As can be seen, the addition of cholesterol to DPPC/DSPG liposomes made the migration time longer in gel state and shorter in liquid crystal state. This result can be well elucidated by supposing that the detection of "soft" liposomes is delayed due to the shape-change as mentioned earlier. Addition of the short chain lipids ($DC_{10}PC$), which is also known to soften the membrane,[23,24] made the migration time longer in both physical states. This was also observed when the chain length of all the constituent lipids was shortened.

Table 1-1. Migration time of various liposomes (min.)

Composition (molar ratio)	t_m (25℃)	t_m (50℃)	Diameter (nm)
DPPC/DSPG = 10/1	5.09 ± 0.13	3.00 ± 0.11	112.2 ± 1.7
DPPC/DSPG/Cholesterol = 8/1/2	6.35 ± 0.10	2.77 ± 0.07	116.8 ± 2.0
DPPC/DSPG/$DC_{10}PC$ = 10/1/0.5	6.75 ± 0.08	3.25 ± 0.03	118.3 ± 1.3
DMPC/DPPG = 10/1	5.92 ± 0.14	3.11 ± 0.03	112.7 ± 1.3

All experiments were repeated three times and results are shown as averaged values ± standard deviations. Diameter of liposomes were analyzed by dynamic light scattering method (Coulter N4 plus).

Here it should be noted about the change of the charge density by the alteration of constituent lipids, since it also has a possibility to affect the migration time. When cholesterol is incorporated in lipid membranes, it is well known that the membranes become condensed,[25] that is, the occupied area per lipid molecule becomes small. The incorporation of 25 mol% of cholesterol to DPPC membrane yields a bilayer that is 1.15 times thicker in liquid crystal state. If we assume that the total volume of membranes is constant,[23] the charge density also becomes 1.15 times higher. However, according to our previous results shown in Chapter 1-2, this difference of the charge density leads to only a minor effect on the migration time. This is also the case for the difference between DPPC and DMPC membranes,[26,27] since the difference in the charge density can be estimated as 1.10 times in gel state and 1.01 times in liquid crystal state. Thus, the change of the migration time shown in Table 1-1 can be elucidated in terms of the change of the membrane rigidity.

Phase Transition Behavior of Lipid Bilayer. By changing the temperature of the capillary column, we can also alter the membrane rigidity. Unless the membrane rigidity is a factor influencing electrophoretic mobility, the migration time should be proportional to the medium viscosity according to Equations 1-2 through 1-4. The change in the size of liposomes with temperature is not significant.[26,27] Figure 1-8

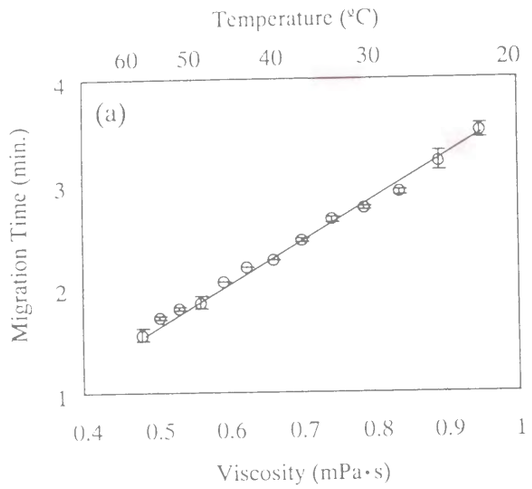

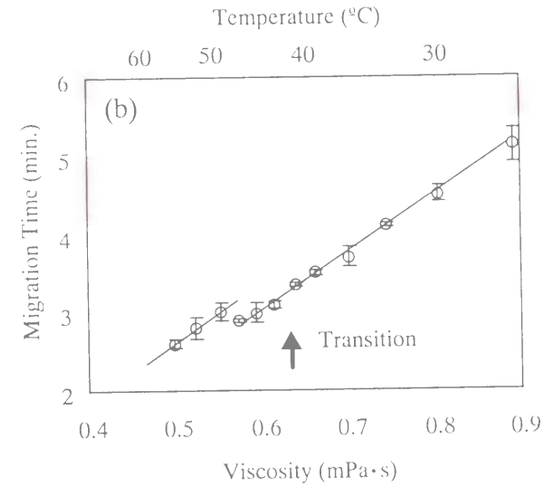

Figure 1-8. Dependence of the migration time of (a) 100 nm polystyrene standard particles and (b) DPPC/DSPG liposome (10/1 in molar ratio) on medium viscosity. The medium viscosity was varied by changing the temperature of the capillary column. All experiments were repeated three times, and averaged values are shown here. Error bars represent standard deviations.

shows the dependence of the migration time of the polystyrene standard particles and the DPPC/DSPG liposome on the medium viscosity, which was varied by changing the temperature. The main transition point obtained from DSC measurement is also indicated. As can be seen, a proportional relationship was observed for polystyrene particles, suggesting that rigid spheres behaved ideally. However, when liposomes were used, a discontinuous point was observed at temperature slightly above the transition point. Taking into account the earlier conclusion derived from Table 1-1, this discontinuity point seems to be where all the constituent lipids alter their physical state into liquid crystal with subsequent softening of the membrane. To check this hypothesis, 20 mol% of DPPC was replaced with cholesterol, whose addition is known to reduce the transition temperature, and the obtained result is shown in Figure 1-9. The discontinuity point shifted in the direction of higher viscosity, that is, lower temperature, as expected. In addition, it also appeared at the temperature slightly above the transition point. As shown in the same figure, this was also the case for the DMPC/DPPG liposomes, which has a much lower transition temperature, although the clarity of the discontinuity was reduced.

As introduced above, the membrane rigidity was found to be one of the important factors controlling the migration time of liposomes. Futher progress in this work may enable us to estimate the bending constants of various liquid membranes.

Summary

Capillary electrophoresis was demonstrated as a new powerful tool for observing the membrane rigidity of lipid bilayers. When the bilayers were softened by incorporating cholesterol or short chain lipids, the migration time was delayed. In the experiment of the temperature dependence, the relation of viscosity versus migration time showed a discontinuous point near the phase transition temperature, which could be elucidated in terms of the change in the membrane rigidity due to the gel/liquid crystal transition. It is likely that the membrane rigidity significantly affects the electrophoretic mobility of liposome particles.

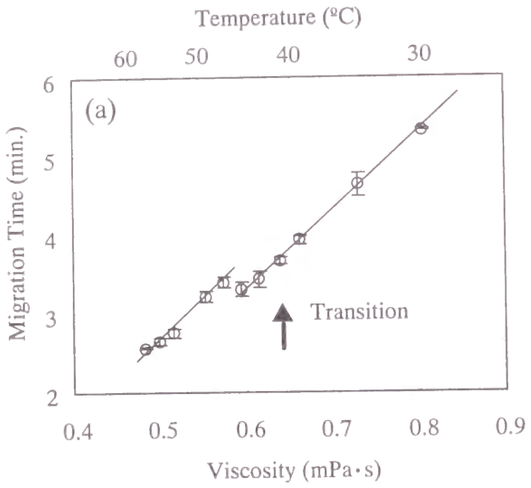

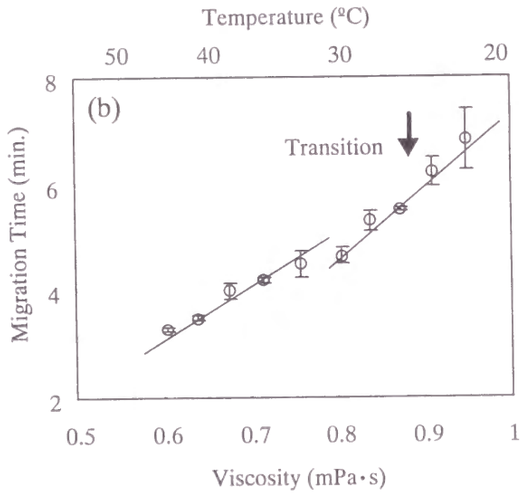

Figure 1-9. Dependence of the migration time of (a) DPPC/Cholesterol/DSPG liposome (8/2/1 in molar ratio) and (b) DMPC/DPPG liposome (10/1 in molar ratio) on medium viscosity.

References

(1) Holland, L. A., Chetwyn, N. P., Perkins, M. D., and Lunte, S. M., *Pharm.Res.* **1997**, *14*, 372.

(2) Amankwa, L. N.; Scholl, J.; Kuhr, W. G. *Anal. Chem.* **1990**, *62*, 2189.

(3) VanOrman, B. B.; McIntire, G. L. *J. Microcolumn Separations* **1989**, *1*, 289.

(4) Roberts, M. A., Locascio-Brown, L., MacCrehan, W. A., and Durst, R. A., *Anal. Chem*. **1996**, *68*, 3434.

(5) Tsukagoshi, K., Okumura, Y., Akasaka, H., Nakajima, R., and Hara, T., *Anal. Sci*. **1996**, ***12***, 869.

(6) Wiersema, P. H., Loeb, A. L., and Overbeek, J. Th. G., *J. Colloid Interface Sci.* **1966**, *22*, 78.

(7) Lasic, D. D.; Papahadjopoulos, D. *Science* **1995**, *267*, 1275.

(8) Sharma, A.; Sharma, U. S. *Int. J. Pharm.* **1997**, *154*, 123.

(9) Frederiksen, L.; Anton, K.; van Hoogevest, P.; Keller, H. R.; Leuenberger, H. *J. Pharm. Sci.* **1997**, *86*, 921.

(10) Isele, U.; van Hoogevest, P.; Hilfiker, R.; Capraro, H. G.; Schieweck, K.; Leuenberger, H. *J. Pharm. Sci.* **1994**, *83*, 1608.

(11) Mabrey-Gaud, S. "Liposomes: From Physical Structure to Therapeutic Applications" (Knight,C.G., ed.), Elsevier, Amsterdam, **1981**.

(12) De Cuyper, M.; Joniau, M.; Dangreau, H. *Biochemistry* **1983**, *22*, 415.

(13) Kessler, R.; Manz, H. -J. *Electrophoresis* **1990**, *11*, 979.

(14) Davenport, L. *Methods.Enzymol*. **1997**, *278*, 487.

(15) Binks, B. P.; Meunier, J.; Abillon, O.; Langevin, D. *Langmuir* **1989**, *5*, 415.

(16) Sicoli, F.; Langevin, D. *J. Phys. Chem.* **1995**, *99*, 14819.

(17) Gradzielski, M.; Langevin, D.; Sottmann, T.; Strey, R. *J. Chem. Phys.* **1997**, *106*, 8232.

(18) Nallet, F.; Roux, D.; Prost, J. *Phys. Rev. Lett.* **1989**, *62*, 276.

(19) Roux, D.; Nallet, F.; Freyssingeas, E.; Porte, G.; Bassereau, P.; Skouri, M.; Marignan, J. *Europhys. Lett.* **1992**, *17*, 575.

(20) Ponsinet, V.; Fabre, P. *J. Phys. Chem.* **1996**, *100*, 5035.

(21) Helfrich, W. *Z. Naturforsch.* **1973**, *28c*, 693.

(22) Winterhalter, M.; Helfrich, W. *J. Phys. Chem.* **1988**, *92*, 6865.

(23) Szleifer, I.; Kramer, D.; Ben-Shaul, A.; Gelbart, W. M.; Safran, S. A. *J. Chem. Phys.* **1990**, *92*, 6800.

(24) Lemmich, J.; Mortensen, K.; Ipsen, J. H.; Hønger, T.; Bauer, R.; Mouritsen, O. G. *Eur. Biophys. J.* **1997**, *25*, 293.

(25) Sankaram, M. B.; Thompson, T. E. *Biochemistry* **1990**, *29*, 10676.

(26) Janiak, M. J.; Small, D. M.; Shipley, G. G. *Biochemistry* **1976**, *15*, 4575.

(27) Janiak, M. J.; Small, D. M.; Shipley, G. G. *J. Biol. Chem.* **1979**, *254*, 6068.

Chapter 2

Characterization of Liposome Dispersions for Topical Applications

2-1. A New Method for Determining the Entrapped Volume

Introduction

The entrapped volume, which depends on their size, composition and lamellarity, is one of the most significant properties in studies of liposomes.[1] Although various methods for evaluating the entrapped volume have been developed,[1-9] simpler ones are still required. Most of the methods utilize the fluorescent probe such as calcein or carboxyfluorescein. The popular method has been the method in which liposomes are separated from the free fluorescent probes by gel permeation chromatography. However, it apparently requires a very complicated procedure. An alternative method is to utilize the quenching phenomena caused at high probe concentration or the addition of cations such as cobalt or copper. However, we are not certain that the probe-containing liposomes are really the same as those free from probes when the probe concentration is very high, and the amount of cations to add and the conditions for solubilizing liposomes are also sometimes difficult to be decided. One possible solution is the use of ESR,[3] but the instrument is not popularly used . As one solution, we developed a very simple method to use fluorescent probes at very low concentration.

Principle

Although our method also requires fluorescent probes, their concentration is much lower than that of the traditional methods. The principle of our method is illustrated in Figure 2-1. First, liposome dispersions are prepared using an aqueous solution of a fluorescent probe. We define the total volume of the dispersion, the total entrapped volume of liposomes, and the concentration of the fluorescent probes as V, v, and C_{in}, respectively. When the dispersion is diluted d times by the probe-free buffer solution,

the continuum phase is diluted more than d times because the entrapped phase is not diluted at all. The leakage of probes from the entrapped phase was confirmed to be negligible above the phase transition temperature of constituent lipids. The probe concentration in the continuum phase after this dilution process is defined as C_{out}, and the probe concentration when we suppose that there are no liposomes as C_{total} (= C_{in} / d). In other words, C_{total} is the concentration when the liposome-free probe solution is diluted d times. Thus, we can write as

$$C_{total}V = C_{in}v + C_{out}(V - v). \qquad (2\text{-}1)$$

This equation is rewritten as

$$\frac{v}{V} = \frac{C_{total} - C_{out}}{C_{in} - C_{out}}. \qquad (2\text{-}2)$$

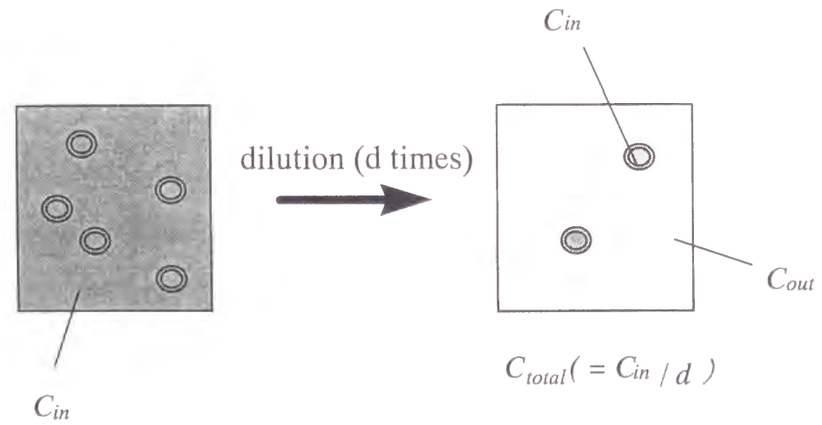

Figure 2-1. The dilution process of liposome dispersion.

Therefore, the entrapped volume Ev (= dv / V) can be calculated from

$$Ev = \frac{d(C_{total} - C_{out})}{C_{in} - C_{out}}. \qquad (2\text{-}3)$$

This equation shows that the measurement of C_{in} and C_{out} gives the entrapped volume. C_{in} is equal to the concentration of the probe solution, which was used to prepare the liposome dispersions. C_{out} was measured after filtering the liposome dispersions with syringe filters as described in the experimental section.

Experimental Section

Materials. Hydrogenated soybean lecithin (HSL) and dipalmitoylphosphatidyl-choline (DPPC) were obtained from Nippon Oil & Fats. HSL consisted of ca. 87% of distearoylphosphatidylcholine (DSPC) and ca. 13% of DPPC. Distearoyl-phosphatidylglycerol (DSPG), dioctadecyldimethylammoniumchrolide (DODAC), and cholesterol were supplied from Nippon Fine Chemicals, Tokyo Kasei, and Nacalai Tesque, respectively. Polyoxyethylene(10) Octylphenyl Ether (Triton X-100) was purchased from Wako Pure Chemicals. 5-(and-6)-carboxyfluorescein (CF) was obtained from Molecular Probes. All the reagents were of the highest purity available and used as supplied.

Preparation of Liposomes. Liposomes were prepared by the freeze-dry method. First, all lipids were dissolved in *tert*-butyl alcohol above their phase transition temperature. The alcohol solution was freeze-dried, and the obtained powder was dispersed by vigorous vortexing in CF-containing 10 mM phosphate buffer of pH 6.5, also above the temperature. The final concentration of total lipids was kept to be 50 mg/ml.

Dynamic Light Scattering. The diameter of liposomes was measured by He-Ne

laser light scattering (Coulter N4 plus). The scattering angle was 90 ° and the data was analyzed by the cumulant method to yield the mean intensity-weighted diameter. Measurements were performed in the presence of fluorescent probes and repeated 3 times.

Quenching Method. As the widely accepted method to quantify the entrapped volume of liposomes, we employed the quenching method. The liposome dispersions were prepared using the phosphate buffer containing ca. 50 mM CF, of which the pH was pre-adjusted to be 7.0 using sodium hydroxide. pK_a value of CF is ca. 6.4. At this concentration, the fluorescence from CF was confirmed to be quenched completely. The dispersions were diluted 50000 times and subjected to fluorescent measurements. The excitation and the emission wavelength were 494 nm and 517 nm, respectively. The intensity, denoted as I_0, was attributed to that from the CF molecules in the continuum phase. As a next step, 10 wt % Triton X-100 aqueous solution of the one tenth volume was added to the dispersions, and the mixtures were incubated at 65°C for 30 minutes. After this heat treatment, the mixtures were cooled to the room temperature and the fluorescent measurements were carried out. The obtained intensity, denoted as I_t, was interpreted as that from the CF molecules both in the continuum phase and the entrapped phase. The entrapped volumes to liposomes could be calculated from the following equation:

$$Ev = \frac{1.1I_t - I_0}{I_0} \qquad (2\text{-}4)$$

The measurements for the same dispersion were repeated 3 times and the mean values and standard deviations were calculated.

Dilution Method. At first, the liposome dispersions were prepared using the phosphate buffer containing the CF of an arbitrary concentration. The obtained dispersion was diluted with the phosphate buffer d times, which was checked by weight carefully. When the concentration of the membrane-constituent components is

high, d should be corrected by subtracting the weight of the components. In our experiment, we carried out this correction for all measurements. Ev was calculated by the equation,

$$Ev = -\frac{d\left(F_{total} - F_{out}\right)}{\left(F_{in} - F_{out}\right)} \qquad (2\text{-}5)$$

where F_{in}, F_{out}, and F_{total} are the fluorescent intensity from the entrapped phase, the continuum phase, and the whole solution when we suppose there are no entrapped volumes, respectively. F_{in} could be measured by diluting the CF phosphate buffer solution. F_{total} could be calculated from F_{in} and d. F_{out} was measured by filtering the dispersions using syringe filters composed of the polyvinylidene fluoride membranes and the glass microfiber prefilters to eliminate the large components - namely, liposome particles (Whatman GD/X, pore size 0.45 μm). Prefilters are essential for this analysis to reduce the back pressure, which may cause the deformation of liposomes or leakage of CF from the entrapped phase, during the filtering process.

Quantification of HSL. Quantification of HSL was performed by HPLC, which was a slight modification of the method of Hurst et al.[7] The column used was a μ-Bondasphere 5C18-100Å 150 × 3.9 mm I.D. (Waters) and the detection was at 210 nm. Acetonitrile/methanol/water = 65/21/14 (v/v) was used as the mobile phase with the flow rate at 0.8 ml/min. The injection volume was 30 μl. Each sample was dissolved and diluted in isopropyl alcohol of HPLC grade to yield an adequate final concentration before the analysis.

Results and Discussion

Optimization of Dilution Rate. First, we tried to optimize the *d* value. Figure 2-2 shows the calculated entrapped volume when 100 or 200 μM CF solution was employed to prepare liposome dispersions. The liposome consisted of HSL, and the results were expressed as a function of the final CF concentration, C_{total}. As can be seen, the dilution rate had no significance when CF concentration was higher than 0.5 μM regardless of the initial CF concentration. We selected 1 μM as the final CF concentration for the following experiments.

Figure 2-3 shows the dependence on the initial CF concentration for HSL liposome. In this figure, some deviation should be allowed for, because the dispersions were not the same. It shows that the initial concentration also had a minor influence on the calculated entrapped volumes. To minimize the effect of the fluorescent probes on the property of liposomes, it seems favorable to select an initial CF concentration of ca. 50 - 100 μM.

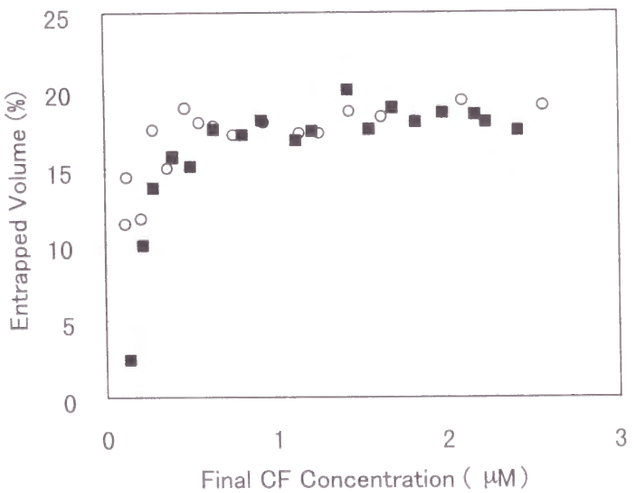

Figure 2-2 . Calculated entrapped volumes as a function of the final CF concentration. The initial CF concentration was 200 μM (■) and 100 μM (○).

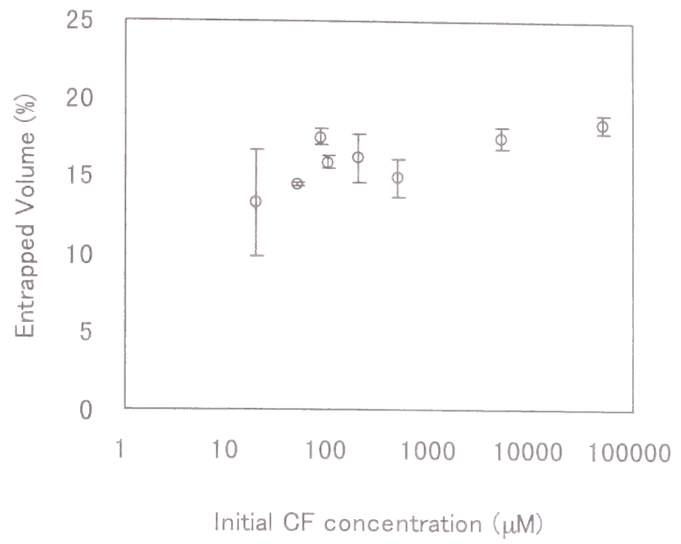

Figure 2-3. Calculated entrapped volumes as a function of the initial CF concentration.

The "dilution method" was validated by comparing it with the conventional "quenching method." To make it possible to use the same dispersions for different determination methods, we employed the "quenching method" as the conventional one. Therefore, the liposome dispersions were prepared using 50 mM CF solution. Table 2-1 shows the entrapped volume of various liposomes obtained by the two different methods. Each measurement was done three times, and the mean values and standard deviations are presented in the table. As can be seen, all values determined by our "dilution method" agreed approximately with those obtained by the "quenching method," although our method yielded slightly lower values. It seems that this difference arose from the shielding of light in fluorescent measurements by coexisting liposome particles in the quenching method, which would lead to underestimation of I_0 in Equation 2-4. Another possibility is overestimation in the correction of *d* due to the high lipid concentration in the dilution method. On the

other hand, the values from HSL/cholesterol liposome showed the reverse tendency. This must be due to the incomplete solubilization of liposomes by Triton X-100[8] in the quenching method. Therefore, we concluded that our method has adequate or superior ability to replace the traditional methods. However, we must keep in mind that the experiment must be performed below the transition temperature of constituent lipids to prevent liposome particles from passing through the syringe filter. When liposomes are composed of saturated lipids, our method can be very useful and convenient due to its very simple procedure and high reproducibility.

Table 2-1. Comparison of the calculated entrapped volume by two different methods

Liposomes	Entrapped volumes (%)[a]		Diameter (μm)[a]
	Dilution method	Quenching method	
HSL	18.4 ± 0.57	21.4 ± 1.74	2.20 ± 0.15
HSL/DPPG=10/1[b]	22.9 ± 1.11	27.0 ± 3.48	1.05 ± 0.04
HSL/DODAC=10/1[b]	6.6 ± 0.56	7.3 ± 0.83	3.91 ± 0.50
DPPC/DSPG=10/1[b]	17.0 ± 0.48	18.2 ± 1.79	1.25 ± 0.06
HSL/cholesterol=10/1[b]	5.0 ± 1.12	2.6 ± 1.62	6.24 ± 0.85

[a]mean ± standard deviations; [b]molar ratio

Summary

We have established a novel method for evaluating the entrapped volume of liposomes. The entrapped volume obtained by our method agreed very well with the result of the conventional method. In addition, our method offers the great advantages in the procedure and reproducibility.

2-2. Liposome/Emulsion Transition Induced by α-Tocopheryl Acetate

Introduction

α-Tocopherol, which is a highly hydrophobic molecule, can be found in various tissues and lipid membranes at the proportion of ca. 0.1 to 1 mol %.[9] Its major role in membranes has been regarded as that of an antioxidant agent.[10,11] In addition to this chemical effect, the membrane-stabilizing effect has also been under extensive study by many groups. This physical effect has recently been revealed to be another source of its antioxidant effect by Stillwell et al.[12] Their findings suggested that α-tocopherol is effective for the composition of a greater variety of membranes than cholesterol, because its chromanol ring fits well with various lipids due to its smaller size than the sterol ring. It can also exert the structuring effect at a much smaller amount than cholesterol. However, although the incorporation of α-tocopherol into lipid membranes has been investigated by a number of techniques, such as differential scanning calorimetry,[9,12-15] nuclear magnetic resonance,[12-14,16] electron spin resonance,[17,18] fluorescence,[12,19,20] and capillary electrophoresis,[21] the detailed mechanism and the distribution state of α-tocopherol in membranes needs further discussion.

In pharmaceutical and cosmetic fields, derivatives of α-tocopherol have been used as hydrophobic antioxidant agents in various products including liposomal formulations.[22-24] The reason for using derivatives is due to their higher chemical stability than α-tocopherol. They also have the ability to act as antioxidant agents for phospholipids and as physical membrane stabilizers in lipid membranes, although their physical characteristics such as hydrophobicity are modified by alteration of their chemical structure. In pharmaceutical and cosmetic products, the proportion of tocopherols in lipid membranes should be much higher than in naturally occurring membranes. It is not rare that it exceeds 1%. Even from this standpoint, the physical and chemical effects of adding tocopherols to lipid membranes should be understood better.

In this section, we focus on the physical effect of adding α-tocopheryl acetate (Toc) to liposomes made of hydrogenated soybean lecithin (HSL), from the viewpoint of practical importance in the pharmaceutical field. The addition of guest compounds to liposome dispersions has been known to result in various morphologies. The effect of the addition of surface-active components usually leads to the formation of mixed micelles,[25,26] whereas the addition of oils usually yields emulsions.[27-30] This was also the case with our system, although addition of a small amount of Toc leads to membrane stabilization. The resulting emulsion was a multiple type. We discuss the transition mechanism below, and also propose a thermodynamic model, which enables us to predict quantitatively the proportion of liposomes and emulsions.

Experimental Section

Materials. HSL and Toc were obtained from Nippon Oil & Fats (Tokyo, Japan) and Shionogi & Co. (Osaka, Japan), respectively. HSL consisted of ca. 87% of distearoylphosphatidylcholine and ca. 13% of dipalmitoylphosphatidylcholine. Pyrene and Polyoxyethylene(10) Octylphenyl Ether (Triton X-100) were purchased from Wako Pure Chemicals (Osaka, Japan). 5-(and-6)-carboxyfluorescein (CF) was supplied from Molecular Probes (OR, USA). All the reagents were of the highest purity available and used as supplied.

Preparation of Liposomes. Liposomes or liposome/emulsion mixtures were prepared by the freeze-dry method.[21,31] Briefly, all oil-soluble components were dissolved in tert-butyl alcohol at ca. 65°C, which is above the phase transition temperature of HSL. The alcohol solution was freeze-dried, and the obtained powder was dispersed by vigorous vortexing in 10 mM phosphate buffer of pH 6.5, also at the same temperature. The final concentration of total lipids was kept at 50 mg/ml.

Dynamic Light Scattering. The diameter of aggregates was measured by He-Ne

laser light scattering (Coulter N4 plus). The scattering angle was 90 ° and the obtained data was analyzed by the cumulant method. Each measurement was repeated 3 times and the obtained values of the mean diameter were averaged.

Separation of Liposomes. Liposome/emulsion mixtures were separated by ultra-centrifugation of 100,000g × 60 min. at 25°C. We carried out two-step centrifugation as depicted in Figure 2-4, because one-step centrifugation was not enough to purify each phase, as reported in early literature.[27] After the first centrifugation, the precipitates were separated from the other phases, that is, transparent middle phase and upper cream phase. The separated dispersions were re-dispersed by adding an adequate amount of buffer and vortexing, and subjected to the second centrifugation. The four resultant phases were named as shown in Figure 2-4. The purified "cream phase" was called phase 1 and the purified "precipitates" was called phase 4. Phase 2 was likely to include approximately the same type of molecular assemblies as phase 4, and phase 3 that of phase 1. The volume of phases 2 and 3 was much smaller than that of phases 1 and 4. We will mainly discuss phases 1 and 4 hereafter.

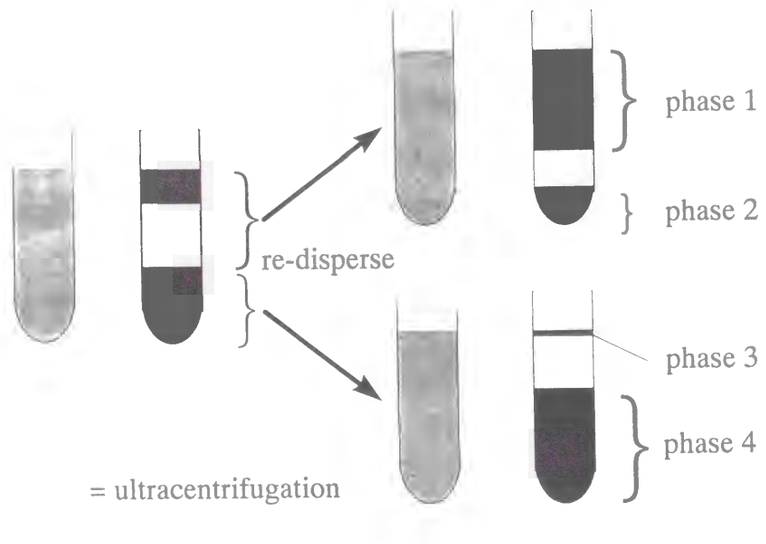

Figure 2-4. Ultracentrifugation procedure of liposome dispersions.

Measurement of Polarity in Lipid Membranes. The polarity of the hydrophobic region in the lipid membranes was investigated by incorporating pyrene as a fluorescent probe. Pyrene is known to be located in the middle of the acyl chain region[32] and its fluorescent spectrum greatly depends on the polarity of its surroundings.[28,33-35] Its spectrum splits into five sharp peaks and the most frequently used parameter is the peak ratio of the first peak and the third peak (I_1/I_3). The ratio increases with the increase of the polarity. Detailed experimental procedure is as follows. 200 ng of pyrene per 1 mg lipids was added before the freeze-dry step, and the liposomes were prepared as described. The obtained dispersions were diluted ca. 30000 times and subjected to fluorescent measurements. Phase 1 and phase 4 were also subjected to this measurement after adequate dilution. Excitation wavelength was set to 335 nm and the measurement of the spectrum from 350 nm to 500 nm followed. The first and the third peak were found at ca. 374 and 384 nm, respectively. The absence of dimer formation in all the measurements was confirmed by checking that there were no peaks around 450 nm. The ratio I_1/I_3 was calculated as the parameter to evaluate the polarity inside the lipid membranes.

Measurement of Entrapped Volume. The entrapped volume of liposomes was evaluated by the dilution method,[31] which can offer highly reproducible results as well as a simple experimental procedure as introduced in Chapter 2-1. The detailed principle and validity of this method are reported in the previous section.[31] First, the liposomal dispersions were prepared using phosphate buffer containing 100 μM CF. The obtained dispersion was diluted ca. 100 times with the phosphate buffer. This dilution rate, *d*, was checked by weight carefully. When the concentration of the membrane-constituent components is high, *d* should be corrected by subtracting the weight of the components. In our experiment, we carried out this correction for all the measurements. In this dilution process, the continuum phase was diluted more than *d* times since the entrapped phase was not diluted at all. This "excess dilution rate" provided the entrapped volume *Ev* by the equation,

$$Ev = \frac{d\left(F_{total} - F_{out}\right)}{\left(F_{in} - F_{out}\right)}, \qquad (2\text{-}6)$$

where F_{in}, F_{out}, and F_{total} are the fluorescent intensity from the entrapped phase, the continuum phase, and the whole dispersion when we suppose there are no entrapped volumes, respectively. F_{in} could be measured by diluting the CF phosphate buffer solution which was used to prepare liposome dispersions, since the probe concentration inside liposomes could be regarded as unchanged in the dilution process. F_{total} could be calculated from F_{in} and d. F_{out} was measured by filtering the dispersions using syringe filters composed of the polyvinylidene fluoride membranes and the glass microfiber prefilters to eliminate the large components (liposome particles) (Whatman GD/X, pore size 0.45 μm).

NMR Measurements. ^{31}P-NMR spectra were obtained on a Varian Unity Inova 500 spectrometer operating at 202.34 MHz. 300 μl of liposome (or emulsion) dispersion was introduced into a NMR tube manufactured by Shigemi (Tokyo, Japan), which could successively eliminate the effect of condensation of lipid aggregates at the top or bottom of the tube during measurements. The sample was allowed to equilibrate for 10 minutes at 60 °C, and subsequently, 512 free induction decays with a duration of 1 second were accumulated employing a 45° pulse with a recycle delay of 3 seconds. $MnCl_2$ was added to the dispersion to a final concentration of 20 mM, to eliminate signals originating from phosphate groups that are freely accessible by the paramagnetic Mn^{2+} ions. The difference in the peak area of the spectra recorded with and without Mn^{2+} was used to estimate the fraction of phospholipids at the surface of the liposomes.[30,36,37] The entrapped volume of liposomes was also roughly evaluated by comparing the peak area from phosphate ion with and without Mn^{2+}.

Freeze-Fracture Electron Microscopy. Freeze-fracture electron microscopy was performed by JEOL Hightech Co. (Tokyo, Japan). Platinum/carbon replicas of each sample were examined on a JEM-1010 transmission electron microscope.

Quantification of Toc and HSL. Quantification of Toc and HSL was performed

by HPLC. For Toc quantification, the column used was a Develosil ODS-5 150 × 4.6 mm I.D. (Nomura Chemicals, Aichi, Japan) and the detection was done by a UV detector at 285 nm. Methanol was used as the mobile phase with the flow rate at 1.5 ml/min. The injection volume was 50 μl. For HSL quantification, the method of Hurst et al.[7] was slightly modified. The column was a μ-Bondasphere 5C18-100Å 150 × 3.9 mm I.D. (Waters, MA, USA) and the absorbance was detected at 210 nm. Acetonitrile/methanol/water = 65:21:14 (v/v) was used as the mobile phase with the flow rate at 0.8 ml/min. The injection volume was 30 μl. Each sample was dissolved and diluted in isopropyl alcohol of HPLC grade to yield an adequate final concentration.

Results

Whole Entrapped Volume of Dispersion. The measurement of the entrapped volume is one of the most direct methods to prove the existence of liposomes. If the proportion of liposome decreases due to the destruction by Toc, it is natural to think that the entrapped volume becomes small. Figure 2-5 shows the calculated whole entrapped volume in the dispersion as a function of the Toc/HSL ratio. As can be seen, the decrease in the entrapped volume was observed as expected with the increase of Toc/HSL ratio.

NMR Measurements. The entrapped volume of liposomes is affected by the diameter, composition, and lamellarity of liposomes. Therefore, the lamellar number of liposomes should be evaluated to relate quantitatively the change in the entrapped volume to the destruction of liposomes. Figure 2-6 shows the ^{31}P-NMR spectra with or without the presence of paramagnetic Mn^{2+} ions, which cause the disappearance of signals originating from phosphate groups that are freely accessible. As can be seen, the signals of both phosphate ions (left) and phospholipids (right) diminished on the addition of Mn^{2+} to the HSL liposome dispersion. The change in the signal intensity

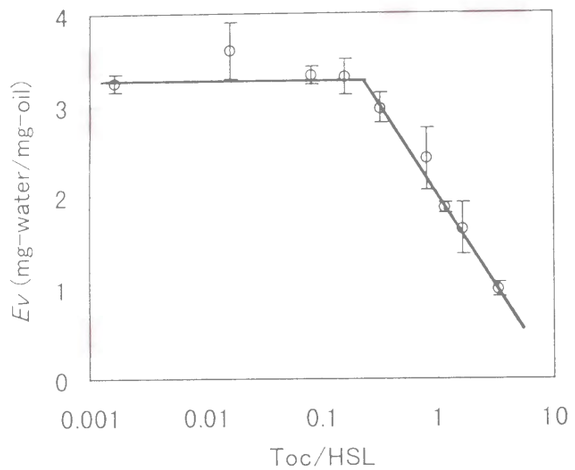

Figure 2-5. Entrapped volumes of HSL liposomes as a function of the total Toc/HSL ratio. Each measurement was repeated at least three times and the error bars show the standard deviation.

of phosphate ion enabled us to calculate approximately the entrapped volume of liposomes, and the obtained value agreed with that from the fluorescent measurement, although the sensitivity was not very high. On the other hand, the information on the lamellarity of the liposome could be obtained from the change in the signal intensity of phospholipid, because the proportion of the phospholipid belonging to the most outer layer could be converted to the lamellar number.[36,37] Figure 2-7 shows the model calculation for the proportion of phospholipids on the most outer layer. From our NMR measurements, we found that the proportion was estimated as ca. 30 % regardless of the Toc/HSL ratio below 0.6, suggesting that the lamellar number could be estimated to be ca. 2 on an average. Therefore, we concluded that the change in the entrapped volume was not affected by the change in the lamellarity, since the lamellar number did not depend on the Toc/HSL ratio and was itself very small.

(a)

(b)

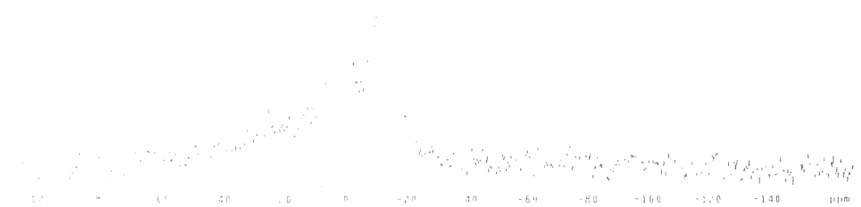

Figure 2-6. ^{31}P-NMR spectra of HSL liposome with (a) or without (b) the presence of 20 mM Mn^{2+} ions. The concentration of HSL was 50 mg/ml.

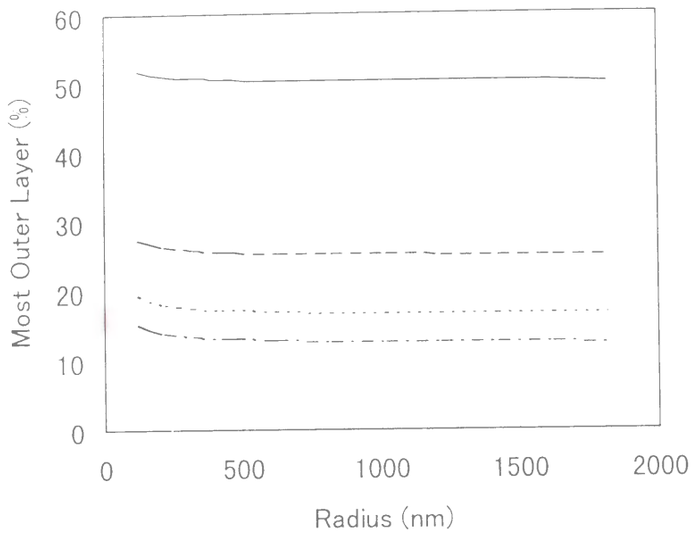

Figure 2-7. Calculated proportion of phospholipids belonging to the most outer layer of liposomes as a function of diameter and lamellar numbers. Layer numbers: 1 layer (unilamellar) (——), 2 layers (– – –), 3 layers (-------), and 4 layers (— - —). Membrane thickness and lamellar interval were assumed to be 4.2 nm and 2.7 nm, respectively.[38] The effect of Toc on the lamellar interval was neglected due to the low lamellar numbers.

We also measured the ^{31}P-NMR spectra of phase 1 and phase 4 with or without Mn^{2+} ions, and found that the spectra of both phases were very similar to that of HSL liposome. The proportion of phospholipids belonging to the most outer layer was evaluated as ca. 40-50 % for phase 1 and 30 % for phase 4, respectively. The reduction of the phosphate ion peak on addition of Mn^{2+} provided information on the existence of the entrapped volume, although the quantification did not seem to be possible. This observation revealed that phase 1, as well as phase 4, contains

significant amounts of entrapped volume, although it was much smaller (ca. 1/4) than that of phase 4.

Freeze-Fracture Electron Microscopy. To obtain direct information on the morphology of the molecular assemblies, transmission electron microscopy was performed. Figure 2-8 (a) and (b) shows the microstructure, which was found in the absence of Toc. As can be seen, there were two types of structure in the dispersion: (a) multilamellar structure and (b) unilamellar structure. The observed frequency was ca. 20 times higher for unilamellar structure, i.e., most aggregates were unilamellar liposomes, which seemed to be consistent with the result of NMR measurement. The structure found in phase 4 was similar to this.

On the other hand, a different type of structure was found in phase 1 as shown in Figure 2-8 (c). Small pools were enclosed in a large structure as pointed out by the arrows in the picture.

Polarity inside Lipid Membranes Evaluated using Whole Dispersion. As mentioned in the experimental section, the polarity inside the lipid membranes can be monitored by the hydrophobic fluorescent probe, pyrene. Table 2-2 shows the I_1/I_3 values of pyrene in various solvents as well as the literature data. It is clear that the increase in I_1/I_3 was observed with an increase of the polarity around the pyrene molecules. Figure 2-9 shows the dependence of I_1/I_3 on the Toc/HSL. With the increase of Toc/HSL, we observed a gradual decrease of I_1/I_3 for the whole dispersion with two breakpoints at Toc/HSL = 0.03 and 0.6. Hereafter, these characteristic molar ratios are called as R_1 and R_2, respectively. The reason we regarded 0.6 as a breakpoint will be discussed later. We can hypothesize two possible reasons for this decrease. First, it presents the "averaged" values of liposomes and emulsions, that is, the change in the proportion of liposomes and emulsions causes the change in the observed I_1/I_3. Second, the liposomal morphology is maintained but the property of the membranes is altered gradually. Of course, both may contribute to the decrease in I_1/I_3.

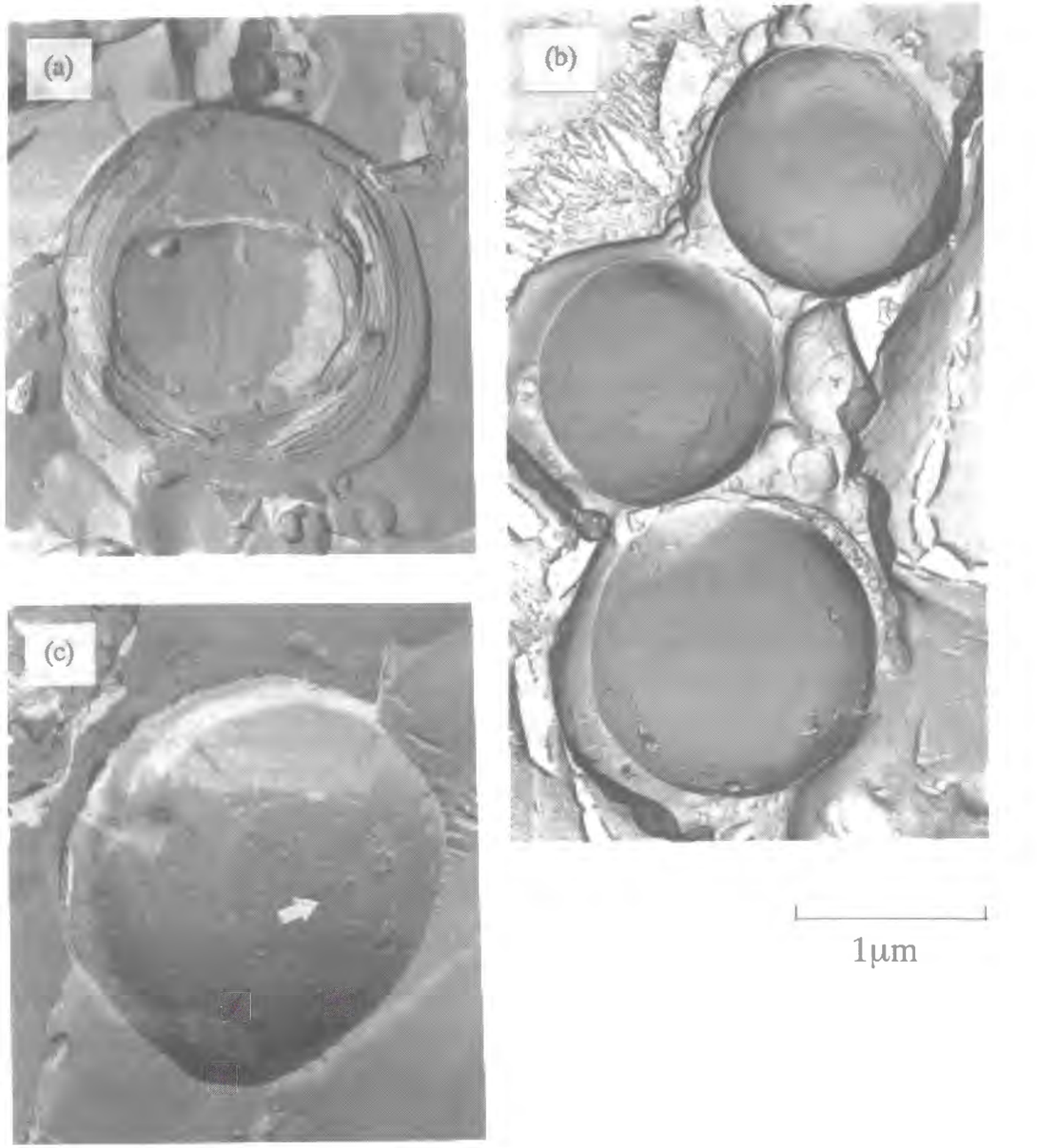

Figure 2-8. Freeze-fracture electron micrograph of particles found in different dispersions. (a) Multilamellar structure found in the absence of Toc, (b) unilamellar structure found in the absence of Toc (c) multiple structure found in phase 1.

Table 2-2. I_1/I_3 of pyrene in various solvents

Solvents	I_1/I_3
Water	1.49[d]
Acetonitrile	1.49
Methanol	1.19
Isopropyl alcohol	0.96
n-Hexane	0.56
Water	1.56[a], 1.49[b]
Soybean oil	0.70[b]
Pure hydrocarbon	0.61[a]
n-Decane	0.58[c]

[a]ref. 33; [b]ref 28; [c]ref 35; [d]0.5% of methanol is present.

Polarity inside Lipid Membranes Evaluated using Phase 1 and 4. To clarify the question mentioned above, we also measured the I_1/I_3 of phase 1 and 4, and the results are also shown in Figure 2-9. As can be seen, the values of phase 4 agreed completely with those of the whole dispersion at Toc/HSL < R_2, and became inconsistent at Toc/HSL > R_2. Therefore, we concluded that the gradual decrease of I_1/I_3 of the whole dispersions resulted from the gradual change in the membrane property below R_2, that is, the second hypothesis seemed reasonable in this range. Above R_2, I_1/I_3 for the whole dispersion is most likely to be controlled by the volume ratio of phase 1 and 4 since I_1/I_3 values of phase 1 and phase 4 are nearly constant,

that is, the first hypothesis seemed adequate in this range. The reason why I_1/I_3 for phase 1 became constant above R_2 was elucidated in terms of the formation of Toc core, and that for phase 4 was explained by the constant Toc/HSL ratio in phase 4, as it will be explained in Discussion.

Distribution of Toc and HSL. After the centrifugation process, the amount of Toc and HSL contained in each phase was measured. Figure 2-10 shows the distribution coefficient of component i, D_i, which is defined as

$$D_i = \frac{\sum_{j=1,3} A_i^j}{\sum_{j=2,4} A_i^j}, \qquad (i = Toc \text{ or } HSL) \qquad (2\text{-}7)$$

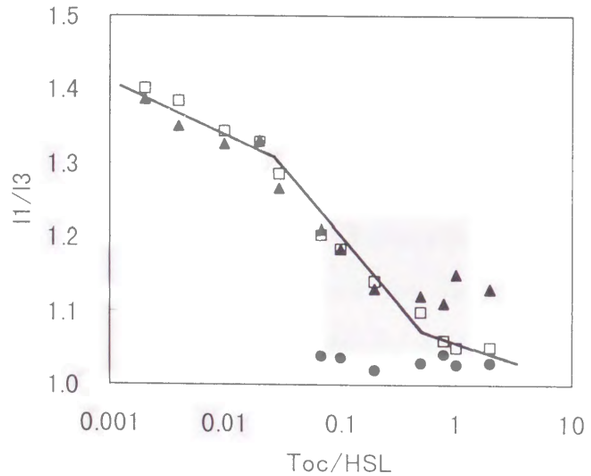

Figure 2-9. I_1/I_3 ratio of pyrene inside lipid membranes as a function of the total Toc/HSL ratio. Measurements were done for the whole dispersion (□), phase 1 (●), and phase 4 (▲).

where A_i^j is the amount of component i in phase j. This figure shows apparently that there is a breakpoint, at which both Toc and HSL in phase 1 (and 3) start to increase dramatically. The Toc/HSL ratio of the breakpoint was ca. 0.6.

Figure 2-11 shows the Toc/HSL ratio in phase 1 and phase 4 as a function of the total Toc/HSL ratio. This ratio in phase 1 increased significantly with an increase of the total Toc/HSL ratio, while that in phase 4 showed a gradual approach to 0.6. Therefore, we regarded 0.6 as the capacity of Toc in HSL membranes. These are why we employed 0.6 as a value of R_2 in Figure 2-9

Dynamic Light Scattering. Figure 2-12 presents the apparent diameter of the dispersed particles in phase 1 and phase 4 as a function of the total Toc HSL. This figure shows that the diameter of the particles in phase 4 was independent of Toc/HSL, while that in phase 1 increased with the increase of Toc/HSL. In the region of Toc/HSL > R_2, the particle size in both phases was nearly identical at ca. 2 μm.

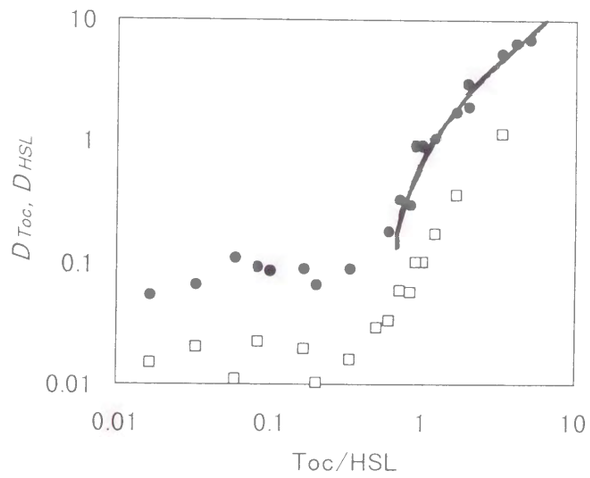

Figure 2-10. Distribution coefficient of Toc (●) and HSL (□), as a function of the total Toc/HSL ratio. The calculated line from Equation 2-10 is also shown.

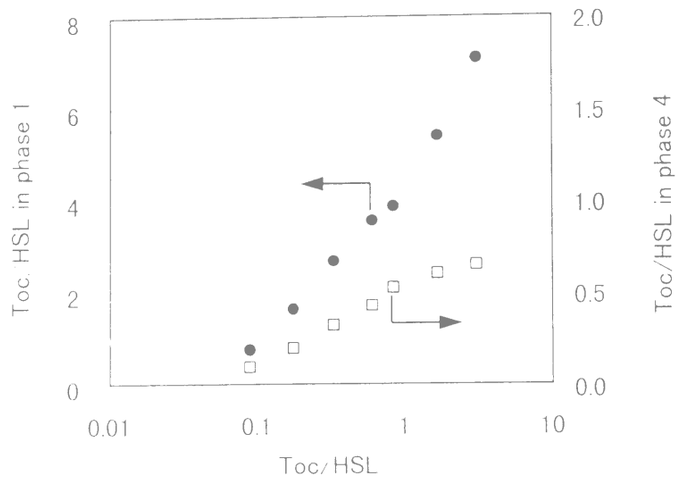

Figure 2-11. Toc/HSL ratio in each phase as a function of the total Toc/HSL ratio. Symbols represent phase 1 (●) and phase 4 (□).

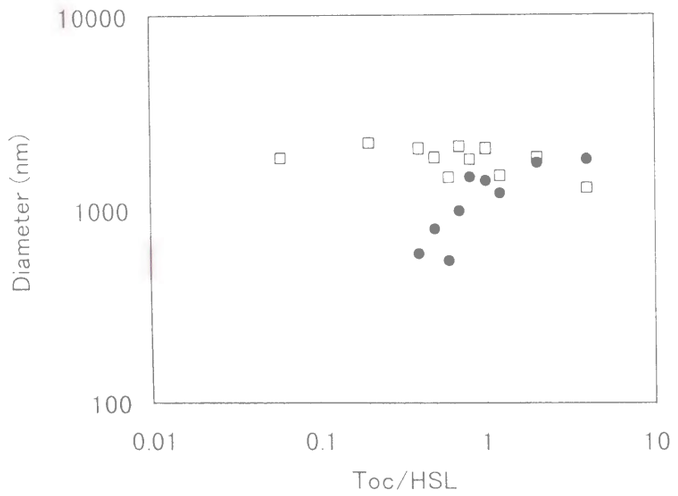

Figure 2-12. Apparent diameter of particles contained in phase 1(●) and phase 4 (□) as detected by laser light scattering method. Results are shown as a function of the total Toc/HSL ratio.

Discussion

Morphology of the Aggregations in Each Phase. The morphology of the aggregates in each phase can be estimated based on various investigations.

Phase 1 contains a very large amount of Toc compared to HSL, and the ratio depends strongly on the total Toc/HSL as shown in Figure 2-11. The polarity around pyrene molecules is much lower than that of liposomes and shows a constant value as can be seen in Figure 2-9. The constant values are likely to be evidence of the existence of Toc cores. In other words, pyrene molecules in phase 1 are preferably distributed in the Toc cores rather than in the membranes, since the I_1/I_3 values are not affected at all by the change in the Toc/HSL ratio in phase 1. These findings led us to the assumption that emulsions exist in phase 1. However, NMR measurements showed that there were entrapped water pools in phase 1 and half of the phospholipids were not in direct contact with the continuum phase. This was because the emulsions in phase 1 were of the multiple type as revealed by TEM observation.

Another TEM measurement revealed that phase 4 contains liposomes, although the picture was omitted to save space. The effect of the Toc on the morphology of liposomes was not observed. It is natural that the phase 4 contains only liposomes because large liposomes are known to precipitate by ultracentrifugation treatment. From measurements of the entrapped volume, distribution coefficients of Toc and HSL, and the I_1/I_3 ratio of pyrene, we found R_2 to be the ratio indicating where the morphology of liposomes begins to be altered. In other words, the capacity of Toc in the HSL bilayer membranes can be expressed by R_2. Therefore the Toc/HSL ratio in phase 4 should not exceed R_2 if this phase contains only liposomes, which was found to be the case as presented in Figure 2-11.

Model for Predicting the Distribution Coefficient of Toc Between Liposomes and Emulsions. The distribution of Toc between liposomes and emulsions could be easily predicted by the mean field approach described below. Although liposomes and emulsions are generally not in an actual equilibrium state, it is possible to

approximate our system by such a thermodynamic approach since no significant external force, such as high pressure or ultrasonic, was exerted on the dispersions during their preparation. Our liposomes were physically stable for at least 6 months at room temperature.

First we define the total number of each component as n, and the number of component i (Toc or HSL) in j phase (surface or core) as n_i^j, that is,

$$n = n_H + n_T = (n_H^S + n_H^C) + (n_T^S + n_T^C). \qquad (2\text{-}8)$$

Each component and phase are expressed only by the initial letter. Here, surface phase means the liposomal bilayer and emulsion monolayer. These two different membranes are approximated to be equivalent. Core phase means the Toc core of the emulsions. To simplify the calculation, we assume ${n^C}_H$ to be zero since the value is much smaller than ${n^C}_T$. Figure 2-13 shows the simplified picture of this model.

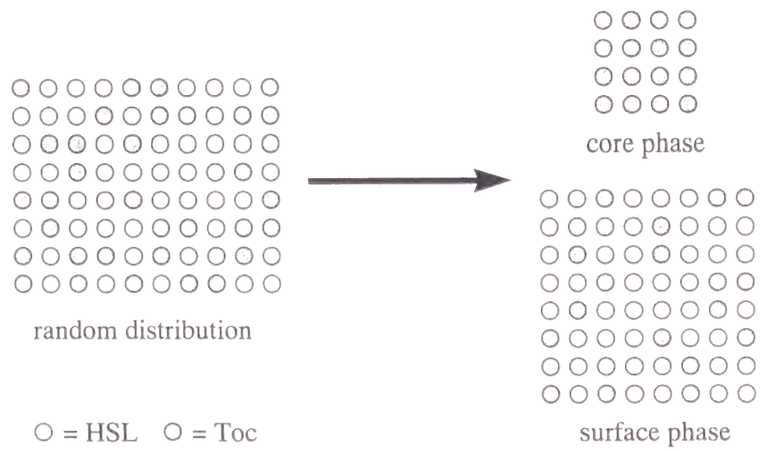

Figure 2-13. The simplified picture of the membranes and the core for the mean field calculation.

When Toc forms the core phases, the difference in free energy G compared to the random distributed state of all Toc molecules on HSL membranes is expressed using mean field approach as

$$-\frac{G}{kT} = -\ln\frac{n!}{n_T!} + \ln\frac{\left(n-n_T^C\right)!}{\left(n_T-n_T^C\right)!} + \alpha n_T^C, \qquad (2\text{-}9)$$

where αkT is the difference in the pair-interaction energy between the two distribution states per Toc molecule. The most important factor which control this value is the miscibility between two molecules. The first two terms of right side represent the contribution of the ideal mixing entropy. It should be noted here that the translational entropy of liposomes and emulsions themselves can be ignored due to their large sizes. By minimizing this equation, we obtain

$$n_T^C = \frac{n - n_T\exp(-\alpha)}{1-\exp(-\alpha)}. \qquad (2\text{-}10)$$

The distribution coefficient of Toc can be approximately calculated from ${n^C}_T / {n^S}_T$ and the result is shown in Figure 2-10 ($\alpha = -1$), which shows very good agreement with the experimental results in the liposome/emulsion transition region. Therefore, we can conclude that such a simple calculation based on mean field approximation enables us to predict the proportion of emulsions and liposomes.

Transition Mechanism. Here let us summarize the physical role of Toc in lipid membranes and discuss the transition mechanism from liposomes to multiple emulsions. Figure 2-14 visualizes the proposed location of Toc molecules in lipid membranes. From the observation using pyrene, the incorporation of Toc of less than 3 mol% (R_1) into HSL membranes proved to have no significant influence on the macroscopic membrane property. When the proportion of Toc in HSL bilayer membranes exceeds R_1, there is greater reduction of the polarity inside the membrane

with an increase of the incorporated Toc. This was most likely to result from the condensation and ordering effect of Toc.[12,18] If Toc/HSL > 0.6 (R_2), the excess Toc is repelled from the membranes to produce the hydrophobic Toc core. The repelled Toc molecules seem to be located in the hydrophobic space between the outer and inner leaflets of the bilayers, by which we can explain why multiple emulsions are formed as described below.

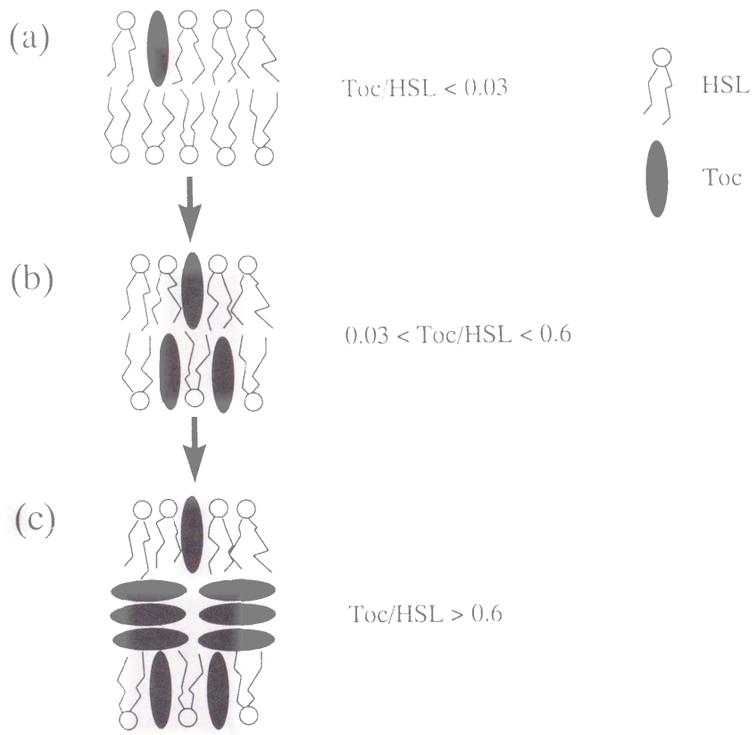

Figure 2-14. Proposed model of the effect of Toc in HSL membranes. (a) When Toc/HSL < 0.03, no significant influence on the macroscopic membrane property is exerted. (b) When 0.03 < Toc/HSL < 0.6, polarity in the membrane decreases due to the condensation effect of Toc. (c) When Toc/HSL > 0.6, Toc molecules are repelled into the hydrophobic space between inner and outer leaflets. There is coexistence of the membrane of Toc/HSL = 0.6.

Figure 2-15 shows the proposed formation process of multiple emulsions. If excess Toc molecules are repelled into the hydrophobic space as shown in Figure 2-14(c), the swollen bilayer membranes become much thicker than the usual membranes. Their thickness can be roughly expressed as $(2 + r_e)d_B$, where r_e and d_B are the Toc/HSL ratio in the emulsion phase and single bilayer thickness, respectively. In the hydration process, the swollen membranes are enclosed to prevent the hydrophobic regions from contacting the aqueous phase. However, the inner leaflet of the resulting vesicle is condensed due to the thickness of the swollen bilayer and the prevention of flip-flop by the Toc phase between the leaflets as shown as Figure 2-15(b). If we assume the radius of a droplet as r, the inner leaflets should be $r^2/\{r - (2 + r_e)d_B\}^2$ times condensed. This causes unfavorable entropic restriction of hydrophobic chains of phospholipids. To expand the interfacial area of the inner leaflet, the entrapped aqueous phase should be divided into sections which satisfy the following equations as presented as Figure 2-15(c).

$$\frac{4}{3}\pi r^3 = \sum_i \left(\frac{4}{3}\pi r_i^3\right) \tag{2-11}$$

$$\frac{r^2}{\{r - (2 + r_e)d_B\}^2}\left(4\pi r^2\right) = \sum_i \left(4\pi r_i^2\right) \tag{2-12}$$

Here r_i is the radius of the divided aqueous phases. Of course, some of the aqueous phases may be accidentally released into the outer continuum aqueous phase in the preparation process. Since NMR measurements showed that the proportion of phospholipids belonging to the most outer layer was higher for emulsions, and the entrapped volume was significantly higher for liposomes, this was likely to occur. The formed multiple emulsions are in a dynamic quasi-equilibrium state with liposomes of Toc/HSL $\fallingdotseq$ R_2.

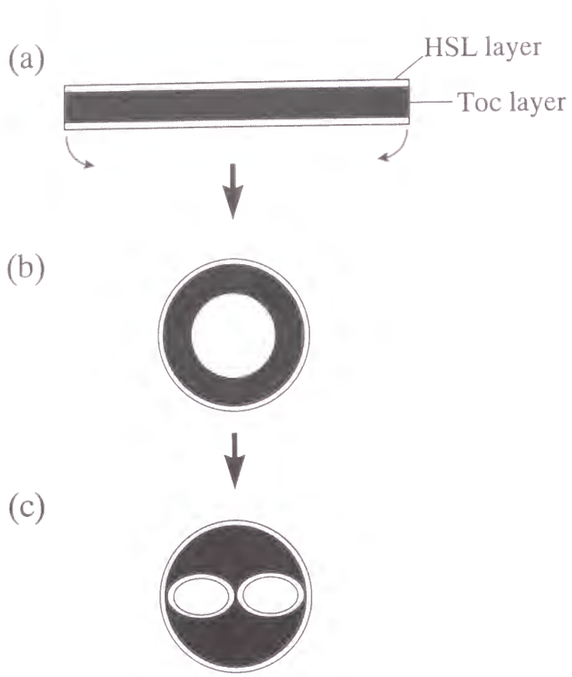

Figure 2-15. Proposed model of the formation of multiple emulsion. (a) The "excess" Toc molecules are incorporated into the hydrophobic space as described in Figure 10(c). This leads to swelling of the bilayer. (b) The swollen bilayer is enclosed in the hydration process. The inner leaflet is condensed. (c) The entrapped aqueous phase is divided into small sections to increase the interfacial area of the inner leaflet.

Comparison with Cholesterol. Capacity of cholesterol, which is also known as a membrane stabilizer, in phosphatidylcholine membrane was reported to be 66 % and not to depend on the chain length of phospholipids.[39] This is nearly as twice larger value as the case of Toc. According to our model calculation presented in Figure 2-10, α value must be larger than –0.5 in the case of cholesterol, suggesting that the pair-interaction energy between cholesterol and phospholipids is very low. This can

explain why Toc exert its physical effect on lipid membranes with much smaller amount than cholesterol.

Summary

The destruction of liposomes and their transition into multiple emulsions induced by the addition of Toc were discussed. With the increase of incorporated Toc in HSL liposomes, the polarity in the hydrophobic region of the bilayers decreased, which seemed to be due to the condensation effect of Toc. When the added Toc exceeded its capacity to be incorporated, the excess formed multiple emulsions. There were two characteristic Toc/HSL molar ratios defined as R_1 and R_2. R_1 is the molar ratio at which the alteration in the physical properties of membranes becomes significant, and R_2 is that at which emulsions begin to be formed. The proportion of the emulsions could be successively predicted by the mean field approach. The formation of multiple emulsion was explained by the repellent of excess Toc into the hydrophobic space of membranes and the following condensation of inner phospholipid leaflets during the preparation process.

References

(1) Lichtenberg, D.; Barenholz, Y. *Methods Biochem. Anal.* **1988**, *33*, 337.

(2) Szoka, F. C.; Papahadjopoulos, D. *Proc. Natl. Acad. Sci. U.S.A.* **1978**, *75*, 4194.

(3) Ralston, E.; Hjelmeland, L. M.; Klausner, R. D.; Weinstein, J. N.; Blumenthal, R. *Biochim. Biophys. Acta* **1981**, *649*, 133.

(4) Vistnes, A. I.; Puskin, J. S. *Biochim. Biophys. Acta* **1981**, *644*, 244.

(5) Oku, N.; Kendall, D. A.; MacDonald, R. C. *Biochim. Biophys. Acta* **1982**, *691*, 332.

(6) Amselem, S.; Loyter, A.; Lichtenberg, D.; Barenholz, Y. *Biochim. Biophys. Acta* **1985**, *820*, 1.

(7) Hurst, W. J.; Martin Jr., R. A. *J. Am. Oil Chem. Soc.* **1980**, *57*, 307.

(8) Ruiz, J.; Goñi, F. M.; Alonso, A. *Biochim. Biophys. Acta* **1988**, *937*, 127.

(9) McMurchie, E. J.; McIntosh, G. H. *J. Nutr. Sci. Vitaminol.* **1986**, *32*, 551.

(10) Gramms, G. W.; Eakins, K. *Biochemistry* **1972**, *11*, 606.

(11) Burton, G. W.; Ingold, K. H. *Ann. N.Y. Acad. Sci.* **1989**, *570*, 7.

(12) Stillwell, W.; Dallman, T.; Dumaual, A. C.; Crump, F. T.; Jenski, L. J. *Biochemistry* **1996**, *35*, 13353.

(13) Wassall, S. R.; Thewalt, J. L.; Wong, L.; Gorrisen, H.; Cushley, R. J. *Biochemistry* **1986**, *25*, 319.

(14) Micol, V.; Aranda, F. J.; Villalaín, J.; Gómez-Fernández, J. C. *Biochim. Biophys. Acta* **1990**, *1022*, 194.

(15) Sanchez-Migallon, M. P.; Aranda, F. J.; Gómez-Fernández, J. C. *Biochim. Biophys. Acta* **1996**, *1279*, 251.

(16) Ekiel, I. H.; Hughes, L.; Burton, G. W.; Jovall, P. A.; Ingold, K. H.; Smith, I. C. P. *Biochemistry* **1988**, *27*, 1432.

(17) Severcan, F.; Cannistraro, S. *Chem. Phys. Lipids* **1988**, *47*, 129.

(18) Wassall, S. R.; Wang, L.; Yang McCabe, R. C.; Ehringer, W. D.; Stillwell, W. *Chem. Phys. Lipids* **1991**, *60*, 29.

(19) Bisby, R. H.; Birch, D. J. S. *Biochem. Biophys. Res. Commun.* **1989**, *158*, 386.

(20) Stillwell, W.; Ehringer, W.; Wassall, S. R. *Biochim. Biophys. Acta* **1992**, *1105*, 237.

(21) Kawakami, K.; Nishihara, Y.; Hirano, K. *J. Colloid Interface Sci.* **1998**, *206*, 177.

(22) Lasic, D. D.; Papahadjopoulos, D. *Science* **1995**, *267*, 1275.

(23) Ceh, B.; Winterhalter, M.; Frederik, P. M.; Vallner, J. J.; Lasic, D. D. *Adv. Drug Delivery Rev.* **1997**, *24*, 165.

(24) Sharma, A.; Sharma, U. S. *Int. J. Pharm.* **1997**, *154*, 123.

(25) Silvander, M.; Karlsson, G.; Edwards, K. *J. Colloid Interface Sci.* **1996**, *179*, 104.

(26) Csúcs, G.; Ramsden, J. J. *Biochim. Biophys. Acta* **1998**, *1369*, 304.

(27) Miller, K. W.; Small, D. M. *Biochemistry* **1983**, *22*, 443.

(28) Rotenberg, M.; Rubin, M.; Bor, A.; Meyuhas, D.; Talmon, Y.; Lichtenberg, D. *Biochim. Biophys. Acta* **1991**, *1086*, 265.

(29) Férézou, J.; Lai, N. T.; Leray, C.; Hajri, T.; Frey, A.; Cabaret, Y.; Courtieu, J.; Lutton, C.; Bach, A. C. *Biochim. Biophys. Acta* **1994**, *1213*, 149.

(30) Saito, H.; Nishiwaki, K.; Handa, T.; Ito, S.; Miyajima, K. *Langmuir* **1995**, *11*, 3742.

(31) Kawakami, K.; Nishihara, Y.; Hirano, K. *Anal. Biochem.* **1999**, *269*, 139.

(32) Galla, H. J.; Sackmann, E. *Biochim. Biophys. Acta* **1974**, *339*, 103.

(33) Kalyanasundaram, K.; Thomas, J. K. *J. Am. Chem. Soc.* **1977**, *99*, 2039.

(34) Morris, D. A. N.; Thomas, J. K. in *Micellization, Solubilization, Microemulsions* (Proc. Int. Symp.) **1977**, *2*, 913.

(35) Ishinomori, T.; Ogino, K.; Sakai, H.; Funada T.; Masuzawa, M.; Abe, M. *Yukagaku* **1995**, *44*, 985 (in Japanese).

(36) Gruber, H. J.; Schindler, H. *Biochim. Biophys. Acta* **1994**, *1189*, 212.

(37) Hope, M. J.; Bally, M. B.; Webb, G.; Cullis, P. R. *Biochim. Biophys. Acta* **1985**, *812*, 55.

(38) Gordeliy, V. I.; Cherezov, V. G.; Teixeira, J. *J. Mol. Struct.* **1996**, *383*, 117.

(39) Huang, J.; Buboltz, J. T.; Feigenson, G. W. *Biochim. Biophys. Acta* **1999**, *1417*, 89.

Chapter 3

Effect of Hydrophilic Polymers on Physical Stability of Liposome Dispersions

Introduction

It is widely known that the stability of colloidal dispersion can be modified by adding polymers. The polymers are, in many cases, adsorbed onto the particles. When the polymer concentration is very low, it is often the case that the polymers bridge the particles and the dispersion is destabilized. However, the dispersion can be stabilized by increasing the polymer concentration to the order of 1%. This is because most of the surfaces of particles are covered by the adsorbed polymers. The entropic repulsion by the polymer tails prevent the particles from aggregating each other. The effect of the adsorbing polymers on the dispersity of the colloidal dispersion is illustrated in Figure 3-1 (a) and (b).

On the other hand, the effect of nonadsorbing polymers on the dispersity has also attracted much attention. In general, colloidal particles become aggregated due to an imbalance of osmotic pressure between the bulk and gaps caught by colloidal particles. Such attractive interaction between colloidal particles is termed the depletion force.[1-17] It is also known that the attractive force cannot work well at the very high polymer concentration. These phenomena are presented in Figure 3-1 (c) and (d). Because all the employed polymers in this chapter are highly hydrophilic, they are hardly expected to be adsorbed onto particles, that is, all of them are supposed to be nonadsorbing polymers. Liposomes are used as the hydrophilic colloidal particles. As can be imagined easily, the stability of the liposomes was found to depend strongly on the type of the polymers.

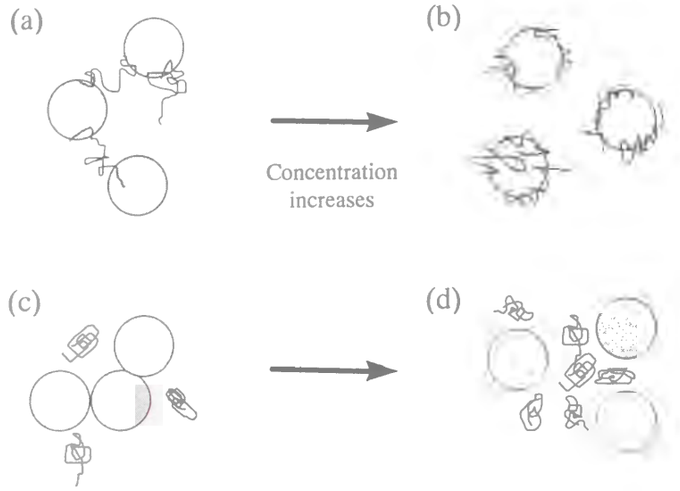

Figure 3-1. The stabilization and destabilization of the colloidal dispersion by the addition of polymers. The adsorbing polymer destabilize the dispersion by bridging the particles at lower polymer concentration (a), but stabilize them by covering the particle surfaces at higher concentration (b). The nonadsorbing polymer destabilize the particles by the depletion force at lower polymer concentration (c), but restabilize them at higher concentration (d).

Asakura and Oosawa were the first to claim that there can be attractive forces between particles suspended in a nonadsorbing polymer solution, which would be strong enough to flocculate particles.[1,2] The mechanism of the depletion-induced aggregation is shown in Figure 3-2. More than 20 years later, Vincent et al.[3] and Feigin et al.[4] showed that the depletion force could stabilize particles from flocculation at higher concentrations due to unfavorable overlap of polymer coils between colloidal particles. A theoretically acceptable explanation for such depletion stabilization was derived by Fleer et al.[5] by showing that the polymer-depleted layer around the particles was thinner at higher polymer concentrations. The change in the

depletion layer thickness is schemed in Figure 3-3. The thinning of the layer thickness could reduce the depletion energy and restabilize the particles, because the flocculation entropy loss was greater in that concentration range. In the 1990's, on the other hand, Walz et al.[10] showed the existence of repulsive barriers at larger separations by calculating in a virial expansion to the second order of particle volume fraction. Mao et al.[11] extended the calculation to the third order and found a secondary minimum in the interaction potential between particles. Recent theory proposed by Walz and Sharma[10,14-16] and their experiments have shown that the depletion energy could be enhanced by charges on the particles.

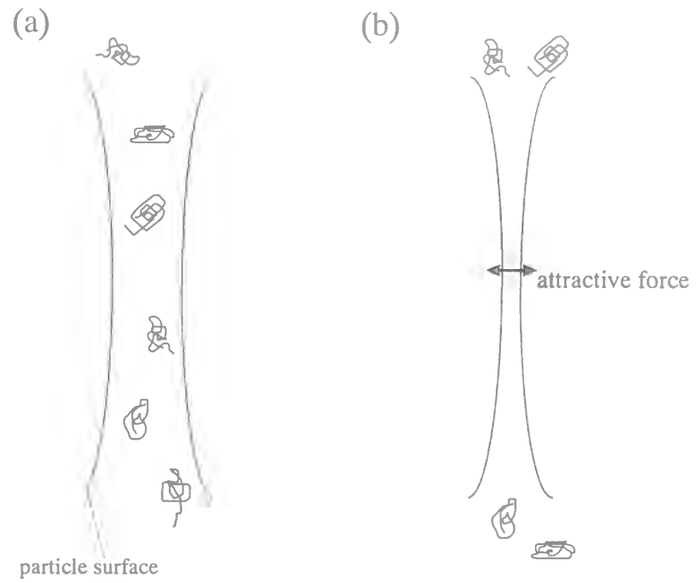

Figure 3-2. The mechanism of the depletion-induced aggregation. (a) When the distance between the particles is large enough, polymer molecules can penetrate into the gap between the particles. No interaction forces between the particles are induced. (b) When the distance between the particles are shorter than the diameter of the polymer molecules, they are excluded from the gap. The imbalance of osmotic pressure between the gap and the bulk induce the attractive force between the particles.

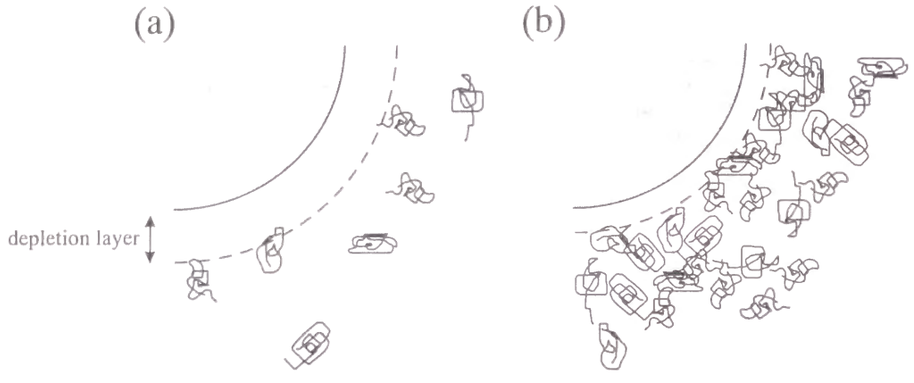

Figure 3-3. The reduction of the depletion layer thickness with polymer concentration. (a) Below the overlap concentration of polymers, the depletion layer thickness is equivalent to the polymer diameter. (b) Above the overlap concentration, the depletion layer thickness is compressed.

Direct experimental observation of the depletion force remains a difficult issue. To our knowledge, the most elegant method for the purpose has been to use the optical technique of total internal reflection microscopy,[14-16] although the application is limited to the wall-particle interaction. Surface force apparatus can also be a very powerful tool for investigating the force-distance relationship,[12] however, some parameters such as the concentration of the larger particles cannot be altered. Further development of theory and experimental technique is still required.

The interaction between cells (or liposomes) and polymers, notably polyethylene glycol (PEG) has been an attractive issue also in the field of biochemistry. This is because PEG has been frequently utilized as cell fusogen,[18-22] although its mechanism has not been clarified yet. Biologists have explained this phenomena by supposing that the hydration state of lipid membranes was altered due to the strong binding affinity between PEG and water.[18-20] Their interpretation may be partially true, but

additional experiments in the diluted system are needed to prove the nature of the interaction. A few tens of percent of PEG is usually present in experiments on cell fusion. It seems to be very meaningful to clarify the mechanism of the interaction between PEG and lipid membranes from the viewpoint of colloidal chemistry.

Liposomes have been, needless to say, hopefully regarded for nearly 30 years as possible new carriers of active agents in pharmaceutical and cosmetic fields.[23-28] Some skincare products[23,24] and injectable formulations[25-27] have already been launched and others are under development. Various other applications have also been suggested in literature, such as their use for transdermal drug delivery,[28,29] ocular delivery,[30,31] inhalation,[32,33] oral delivery,[34,35] and nonvirus vector for gene therapy.[36,37] When liposomes are utilized as drug carriers, the formulation often contains polymers for two purposes: to modify the surface characteristics,[25-27,38,39] and to increase the formulation viscosity. In the former case, lipid-conjugated polyethylene glycol is the material used most frequently and the stabilized liposomes are called stealth liposomes.[39] The polymers employed for this purpose contain hydrophobic parts, because they must bind strongly enough to liposome surfaces. The effect of the decoration by such amphiphilic polymers has been frequently studied and found to avoid the serum protein binding to liposome surfaces, which results in long circulation time after injection. On the other hand, highly hydrophilic polymers are used in the latter case,[40-42] but the studies on this topic are very few. However, recent progress in the study of the depletion force clearly indicate the importance of such work. This chapter discusses the effect of hydrophilic polymers on the liposome dispersity.

Experimental Section

Materials. Hydrogenated soybean lecithin (HSL) was purchased from Nippon Oil & Fats (Tokyo, Japan). HSL consisted of ca. 87% of distearoyl- and ca. 13% of

dipalmitoyl-phosphatidylcholine. PEG 20000 and dextran were obtained from Nacalai Tesque (Kyoto, Japan). PEG 600, sodium alginate, and methylcellulose were supplied by Wako Pure Chemicals (Osaka, Japan), Kanto Chemical (Tokyo, Japan), and Shin-Etsu Chemical (Niigata, Japan), respectively. All polymers were used as supplied but stored in a desiccator before use. Table 3-1 summarizes the polymers used in this study.

Preparation of Liposome Dispersions. Liposome dispersions were prepared by the freeze-dry method,[44,45] which was proved to yield homogeneous lipid membranes by the capillary electrophoresis analysis.[44] Briefly, weighed lipid powder was dissolved in tert-butyl alcohol at ca. 65 °C, which is above the phase transition temperature of HSL, and then the alcohol solution was freeze-dried. The powder obtained was dispersed in distilled water also above that temperature with vigorous vortexing. As described in Chapter 2,[45] the diameter of the liposomes was ca. 2 μm, and there were two lamellar layers on the average. Polymer-containing dispersions were prepared by diluting liposome dispersions with polymer solutions of given concentrations.

Table 3-1. Molecular Weight and Radius of Polymers

Polymer	Abbreviation	Molecular Weight	Radius of Gyration (nm)
PEG20000	PEG20000	20,000	5.5[a]
PEG600	PEG600	600	1.0[a]
Dextran	DEX	60,000	6.8[b]
Methylcellulose	MC	65,000	7.0[b,c]
Sodium Alginate	Alg-Na	90,000	8.1[b,c]

[a]ref. 3; [b]calculated according to ref. 43; [c]calculated by the same equation for dextran.

Preparation of Polymer Solutions. The well-dehydrated polymers were weighed and dissolved in distilled water and the solution was degassed under vacuum. These solutions were hydrated at least for 5 days at room temperature.

Turbidity Measurements. To evaluate the stability of liposome dispersions, the turbidity of dispersions was measured at 600 nm after mild centrifugation (1,500 rpm × 10 min., 25 ºC), which precipitated most of the liposomes. The size distribution of the supernatant was the same as that of the whole dispersion, suggesting that only the weakly flocculated liposome particles were precipitated by the centrifugation. Therefore, the increase in the turbidity could be attributed to the stabilization of dispersions and *vice versa*. When no polymers were contained in the samples, the observed turbidity value was ca. 0.8 for both 1 mg/ml and 2 mg/ml (HSL concentration) dispersions. The data which shown below was corrected to present the values per 1 mg/ml HSL. All measurements were done 24 hours after mixing of liposomes and polymers.

Fourier Transform Infrared Spectroscopy. The physical effect of polymers on lipid membranes was evaluated by Fourier transform infrared spectroscopy (FT-IR). ATR spectra were acquired using a Magna-IR 560 Spectrometer (Nicolet, WI, USA), by coaddition of 128 interferograms collected at 1 cm^{-1} resolution. To exclude the effect of the osmotic pressure due to the polymers outside on the FT-IR spectra, liposome dispersions for this experiment were prepared using polymer solutions. In other words, polymers were located both inside and outside the liposomes. HSL concentration was 50 mg/ml and the measurement was done at room temperature.

Surface Tension Measurements. Surface tension measurements were performed by the Wilhelmy plate method using Kyowa CBVP Surface Tensiometer A3 (Kyowa Kagaku, Tokyo, Japan). The sample room was maintained at 25 ± 0.2 ºC by circulating temperature-controlled water, and the polymer solutions were immersed in a thermobath controlled at 25 ± 0.2 ºC before use. Before every measurement, the platinum plate was heated with a burner, followed by rinsing with distilled water and acetone. All the data were read at 3 minutes after the creation of new surfaces, that is,

after pouring the sample solution into the petri dish. The measurement accuracy was ca. ± 0.1 mN/m, except for the case in which the time dependence was very strong.

Bulk Viscosity Measurements. The viscosity of polymer solutions was obtained using a Cannon-Fenske type viscometer immersed in a thermobath controlled at 25 ± 0.2 ºC. Measurements were done at least twice and experimental errors were confirmed to be within 1%. The values obtained were adopted as the bulk viscosity of polymer-liposome mixtures.

Microviscosity Measurements. Microviscosity, which can be defined as the viscosity near the liposome surfaces, was evaluated from He-Ne laser light scattering measurements on Coulter N4 Plus (Coulter, FL, USA). The scattering angle was 90 ° and the obtained data was analyzed by the cumulant method. Each measurement was repeated 3 times and the averaged self-diffusion coefficients were converted to viscosity values via the Einstein-Stokes relationship. If polymers are adsorbed onto liposome surfaces, the polymer fraction around liposomes is enriched in comparison to that of the bulk. It leads to the increase in the local viscosity, which should depress the Brownian motion of liposome particles. On the other hand, if polymers are depleted from the surfaces, the local viscosity decreases and the Brownian motion is enhanced. Therefore, the self-diffusion coefficients can provide the information on the adsorption of polymers onto liposome surfaces. The apparent change in the diameter of liposome particles due to the polymer adsorption was negligible, since liposomes were much larger than polymers. The osmotic shrinkage was also ignored, since the polymer concentration for this experiment was very low except for the case of PEG600. For example, the experiment on Alg-Na was performed under 3 mg/ml as shown later.

Results

Surface-Active Properties of Polymers. Although all the employed polymers were highly hydrophilic, they had different surface active properties depending on whether or not their hydrophobic parts could be separated from the hydrophilic parts at the water/air interfaces.[46] Figure 3-6 shows the surface tension of the polymers at 3 minutes after the creation of new surfaces. As can be seen, MC and PEG 20000 were relatively surface active, while the other polymers hardly reduced surface tension even at very high concentrations. The order of surface activity was MC > PEG 20000 >> PEG 600 > Alg-Na > DEX. Three minutes was apparently too short for the attainment of the equilibrium state, since more than several hours are required for most hydrophilic polymers.[46-48] However, the order of the polymers mentioned above was most likely to be unchanged even when a longer time had elapsed. If the hydrophobic interaction plays a dominant role in the polymer-liposome attractive interaction, the degree of the interaction should obey this order.

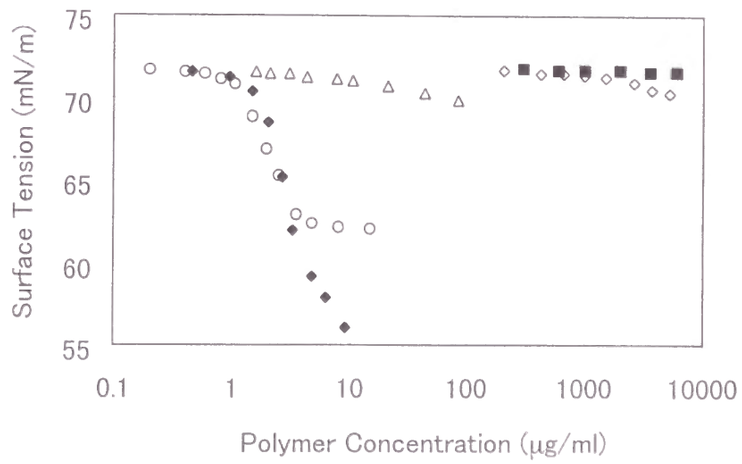

Figure 3-4. Surface tension of polymers. Polymer type: MC (◆), PEG20000 (○), PEG600 (△), Alg-Na (◇), and DEX (■).

FT-IR Measurements. Fourier-transform infrared spectroscopy (FT-IR) has been widely used to evaluate the conformational disorder of the lipid molecules.[49-51] Therefore, if polymers strongly interact with lipid membranes, the IR spectra should be affected. Figure 3-5 shows the FT-IR spectra in the presence and absence of polymers. The strongest bands from the symmetric and antisymmetric CH_2 stretching vibrations were found around 2900 cm^{-1} as reported in literature. The conformational disorder of acyl chains is usually evaluated by the shifting of these bands to higher frequencies. In the same manner, the interfacial region can be investigated from the band at ca. 1700 cm^{-1}, which reflects the C=O stretching vibrations. Information on the hydrophilic region can be obtained from the band at ca. 1250 cm^{-1}, which arises due to PO_2^- asymmetric stretching vibrations. As can be seen, the addition of DEX or PEG hardly affected the membrane structure, suggesting that the interaction between the lipid membrane and polymer was very weak. On the other hand, the addition of MC significantly affected the membrane structure. Since the influence was observed for all the regions, that is, hydrophilic, interfacial, and hydrophobic regions, MC molecules were likely to be inserted into lipid membranes. Alg-Na was also observed to affect the IR spectra, suggesting that a strong interaction also exists between the Alg-Na and lipid membrane. However, the lower concentration was found to be more effective than the higher concentration. This may be due to a change in the adsorption manner, that is, the conversion from train-type adsorption to tail-type adsorption accompanied by the increase of the Alg-Na concentration.

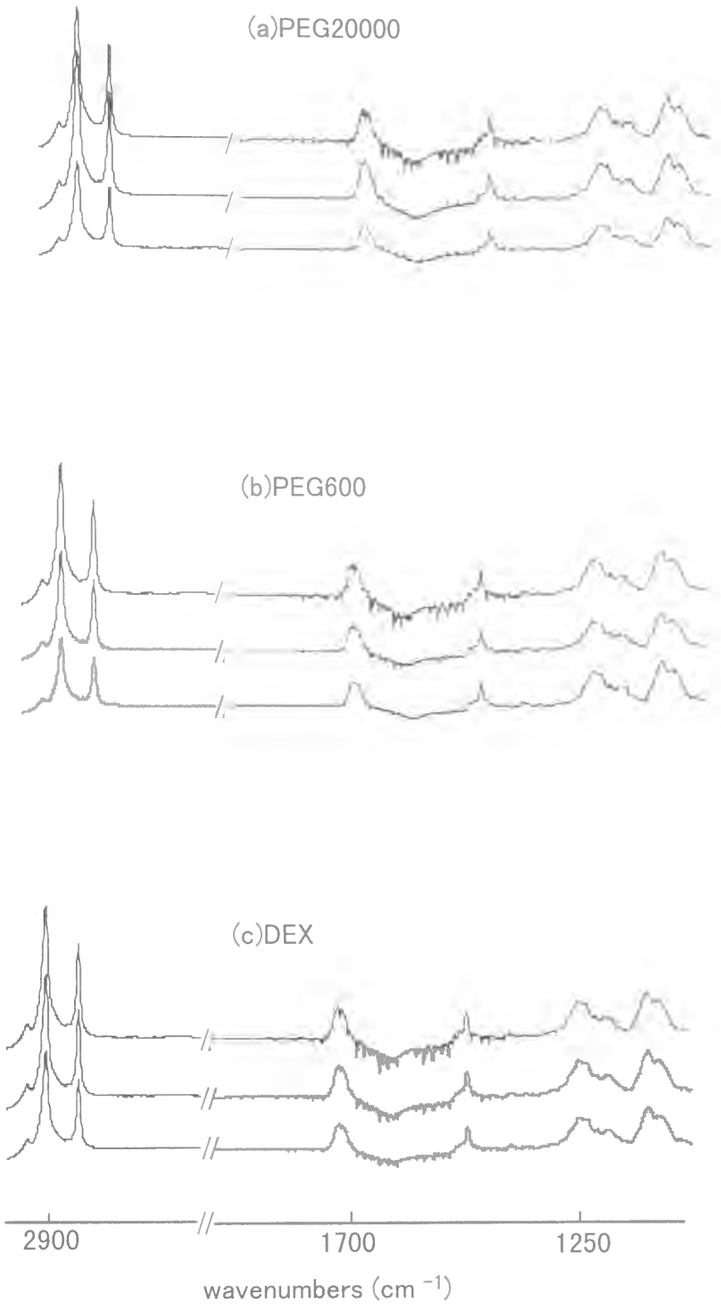

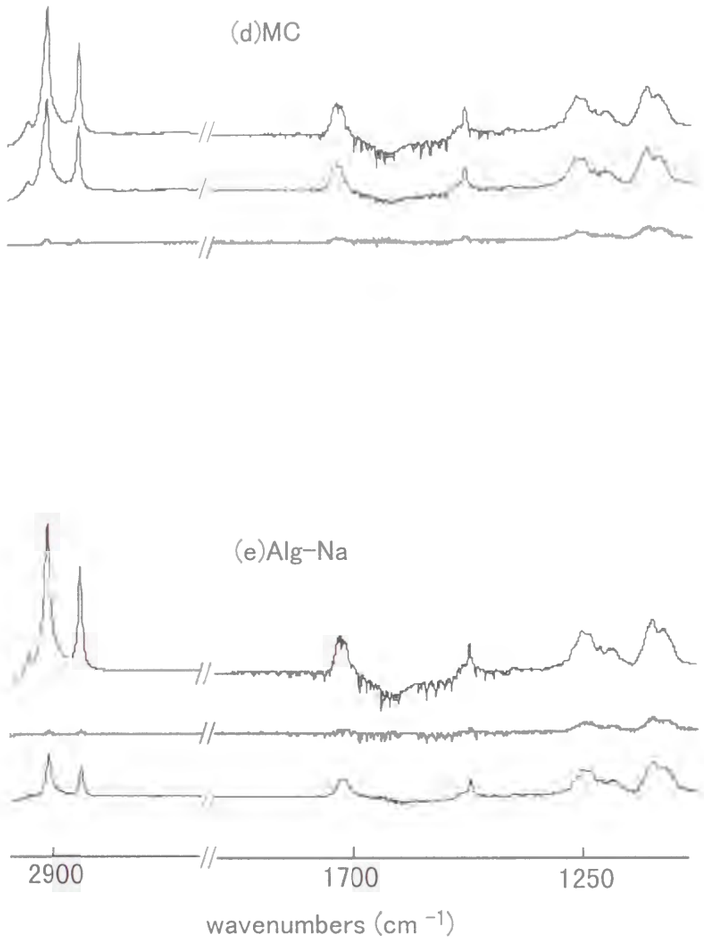

Figure 3-5. FT-IR spectra of HSL in the absence and the presence of polymers. Polymer concentration was 0 mg/ml, 0.05 mg/ml, and 5 mg/ml (top to bottom). The lipid concentration was 50 mg/ml.

Viscosity Measurements. If adsorption layers or depletion layers are formed around liposome particles, the bulk viscosity and the microviscosity should not coincide.[9,13,52] In the case of the formation of adsorption layers, the microviscosity should be higher than the bulk viscosity, and *vise versa* for the formation of depletion layers. Figure 3-6 shows the relationship between the bulk viscosity and the microviscosity for all polymers. Clearly, the polymers can be separated into two groups. The microviscosity of PEG20000, MC, and Alg-Na showed higher values than the bulk in the low polymer concentration region, whereas at higher polymer concentrations, the bulk viscosity became higher. On the other hand, the microviscosity of PEG600 and DEX always showed lower values than those of the bulk. Therefore, polymers of the former group seemed to adsorb onto liposome surfaces, however, the amount was not very large. This is schematically explained in Figure 3-7. At the low polymer concentration, the microviscosity becomes higher than the bulk if there are adsorbed polymers on the liposome surfaces regardless of the amount. However, at the high polymer concentration, the microviscosity becomes lower if the adsorbed molecules are so small that the contribution of the depletion layers are more significant. Polymers of the latter groups are most likely to be depleted from liposome surfaces without significant adsorption.

As mentioned in the Experimental Section, the change in the liposome size due to osmotic shrinkage should affect the diffusion coefficient and reduce the calculated value of microviscosity to a certain degree. However, the change in the diffusion coefficient was too large, as it reached 5 times larger values than the case when no polymer was added. Therefore, it seemed to have a minor effect on this experiment.

Evaluation of the Interaction from Surface Tension Measurements. We have found some cases in which the interaction between liposomes and polymers could be evaluated by surface tension measurements. In the case that liposomes do not have surface activities, the principle is as follows. If polymers are adsorbed onto liposome surfaces, the surface activity of the polymer decreases by mixing with liposomes. If there is no attractive interaction between polymer and liposome, the surface activity

increases slightly due to the exclusion volume of liposome. From such measurements, both types of interaction that is, attractive and repulsive interaction, between polymer and liposome can be observed. Figure 3-8 shows an example obtained for PEG20000. As can be seen, a significant decrease in the surface tension was observed at 3 minutes after mixing compared to the liposome-free solution. This decrease must be attributed to the apparent increase of PEG concentration in the bulk phase and the air/water interface due to the exclusion volume of liposomes, that is, there was no significant adsorption of PEG onto liposome surfaces. However, the surface tension measured at 1 day after the mixing showed nearly identical values to those of liposome-free solutions. Since the values were almost the same after 1 week, the quasi-equilibrium state seemed to have been attained at 2 days after the mixing. This must indicates a slow adsorption of PEG to the liposome surfaces.

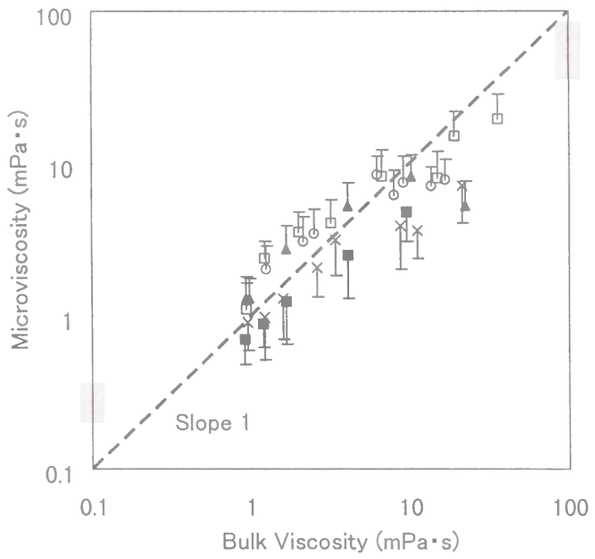

Figure 3-6. Microviscosity around liposome surfaces as a function of bulk viscosity. If symbols are located above the break line, the polymer concentration around the liposome particles is higher than the bulk concentration and *vice versa*. Polymer type: MC (▲), PEG20000 (□), PEG600 (■), Alg-Na (○), and DEX (×). The lipid concentration was 0.4 mg/ml.

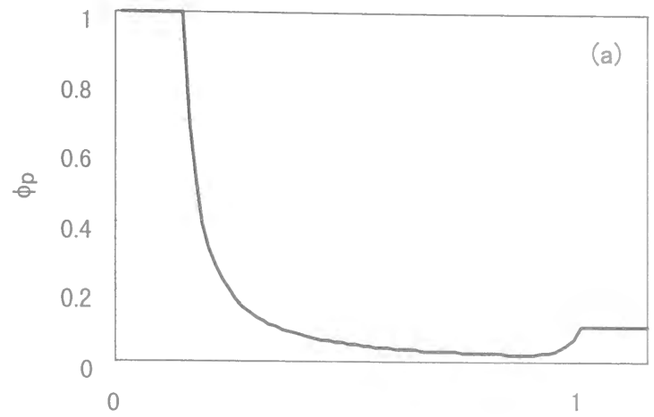

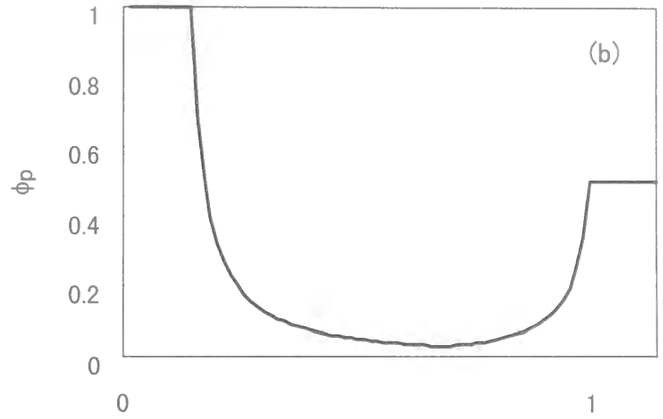

Figure 3-7. Polymer concentration profile near liposome surfaces in the presence of the polymer adsorption layer. (a) Low bulk concentration. (b) High bulk concentration.

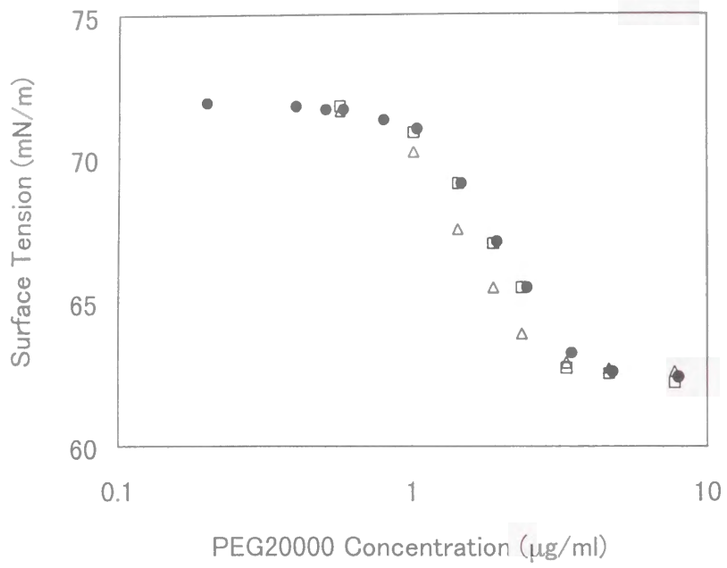

Figure 3-8. Surface tension of PEG20000/HSL liposome mixture. The data are shown as a function of the PEG concentration and the elapsed time from the mixing of the PEG solution and liposome dispersion. The elapsed time was 3 minutes (△) and 1 days (□). The surface tension of PEG20000 solution without liposome is also shown for comparison (●). The lipid concentration was 1 mg/ml.

However, it should be noted about other possibilities for the origins of the decrease in the surface tension. First, the question arises of whether phospholipids were pulled out from the liposome particles since free phospholipids may act as surface-active agents. Another possibility was the formation of PEG-lipid complex since it may have different surface-active properties compared to PEG. To exclude this possibility, the concentration of free phospholipids was measured after ultracentrifugation of the dispersions and no increase was found in the concentration of free phospholipids on addition of PEG. Therefore, the PEG/liposome interaction could be successfully evaluated by this technique.

Such evaluation was not possible for MC. When liposome was added to the MC

solution, a decrease in the surface tension was observed and it remained after 1 week incubation. However, there was also an increase in the bulk phospholipid concentration. Therefore, the decrease in the surface tension was likely to be due to the polymer-lipid complex. In the cases of DEX and PEG600, the evaluation was also difficult due to the low surface activity of these polymers. The change in the surface tension of Alg-Na by the addition of liposome was investigated in spite of its low surface activity. However, the interpretation of the results was difficult, because the increase in the bulk lipid concentration was also observed. These investigations suggested that the required property of employed polymers for this technique was surface activity but it should not affect the liposome structure. Despite a strict limitation of the systems to which it is applicable, a great advantage of this technique is that it allows the estimation of the interaction without exerting any external force on the dispersions, by which the weak interaction between liposome and highly hydrophilic polymer may be affected, as well as the high sensitivity.

Turbidity Measurements. From the various observations mentioned above, each polymer was found to interact with lipid membranes in different manners, although all the polymers employed are well-known as highly hydrophilic polymers. We next investigated the effect of the dissolved polymers on the physical stability of liposome dispersions by turbidity measurements. Figure 3-9 shows the turbidity in the presence of polymers. The stabilization of dispersions resulted in an increase in turbidity of the supernatant, since the aggregated liposome particles should precipitate. As can be clearly seen, Alg-Na was the most effective polymer to stabilize the dispersion, since the increase in the turbidity was observed over the entire concentration range. Although PEG600 was also effective over the wide concentration range, it was less effective in the middle region. DEX showed a similar tendency. However, the effect in the middle concentration region was negative rather than merely being less effective. PEG20000 destabilized the dispersity significantly. We observed two destabilization regions just above and below the overlap concentration of PEG. MC showed a similar tendency, although the clarity was reduced.

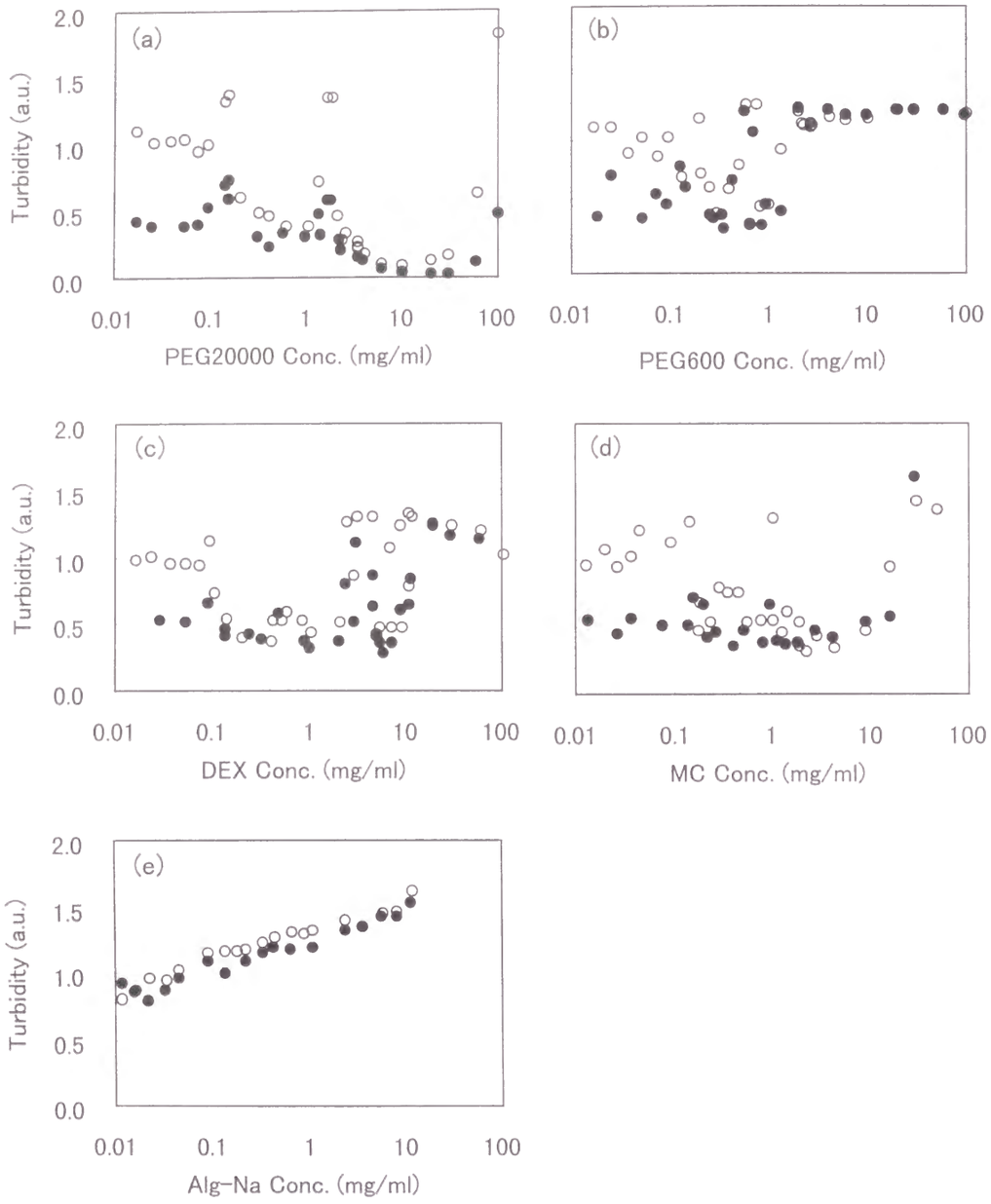

Figure 3-9. Turbidity of liposome dispersions per 1 mg/ml HSL after centrifugation in the presence of polymers. The initial (before centrifugation) lipid concentration was 1 mg/ml (○) or 2 mg/ml (●). In the absence of polymers, the turbidity was ca. 0.8 for 1 mg/ml HSL and ca. 0.4 for 2 mg/ml HSL. If the observed turbidity is higher than these values, it means that the dispersity is stabilized by the addition and polymers and *vice versa*.

Discussion

Origin of Interactions between Liposomes and Polymers. As mentioned in Results, each polymer was found to interact with lipid membranes in a different manner. Below we discuss the origin of the interactions for each polymer investigated.

Alg-Na has very low surface activity and carries negative charges. As indicated in earlier literature,[40,41] it seemed to have very strong interactions with lipid membranes, since 0.05 mg/ml was enough to change the FT-IR spectra. Microviscosity measurement also showed the presence of adsorbed layers around the liposome particles, although depletion layers also seemed to exist. The contribution to the stability of the dispersion was likely to result from the relatively strong interaction as discussed later. It is most likely to be explainable in terms of the electrostatic interaction between negative charges of Alg-Na and the local positive charges of phospholipids, since the hydrophobic interaction cannot be expected from its chemical structure and the surface tension measurement.

MC was also found to interact with liposomes strongly according to both FT-IR and microviscosity measurements. Since MC carries hydrophobic chains, hydrophobic interaction seems to be the origin of the interaction with lipid membranes.

PEG20000 was also observed to be adsorbed onto membranes from microviscosity measurements, although FT-IR measurement revealed that it did not disturb the membrane structure, which was consistent with the earlier observation made by Ariga et al.[53] They employed lipid Langmuir-Blodgett film and found that PEG20000 could not adsorb onto the air/water interface when the surface pressure was high enough. In addition to this, some NMR experiments have proven the adsorption of PEG20000 onto lipid bilayers. For example, Kuhl et al.[12] employed ^{31}P-NMR to investigate the microviscosity around liposome surfaces and concluded that PEG20000 became adsorbed onto lipid bilayers. Ohno et al.[54] also investigated that the motion of the

choline methyl group was suppressed by addition of PEG (molecular weight: 7500) by using ^{1}H-NMR, although the possibility of change in the osmotic pressure was not discussed. Therefore, it is very likely that PEG20000 can become adsorbed onto lipid bilayers. The origin of the interaction seems not to be hydrophobic interaction but surface adsorption.

PEG600 was observed to have a slightly different character from PEG20000, because the microviscosity was lower than the bulk viscosity over the entire concentration range. This trend is consistent with the well-known fact that a decrease in the chain length leads to a decrease in the adsorbed fraction.[55] However, Kuhl et al.[12] reported that PEG600 also had the ability to adsorb onto liposome surfaces from the NMR measurements mentioned above. Although the reason for this contradiction is not clear, one possible explanation is that their observation was done only in the range of 1.0 – 1.5 mPa·s. In this region, our results suggested that the difference between the microviscosity and bulk viscosity was not very large. Therefore, the contradiction may be due to the experimental error.

DEX was observed to have almost no direct interaction with lipid bilayers from both FT-IR and microviscosity measurements. In early literature, DEX was believed to interact directly with lipid bilayers, since it enhanced the aggregation.[56,57] It was also reported that the osmotic shrinkage of liposomes was not significant in the presence of DEX rather than PEG.[58,59] This was explained by supposing a direct interaction between DEX and the headgroups of lipids. These assumptions are certainly possible but each of them was based on indirect observation. Below we try to explain the experimental results by model calculations.

Polymer Concentration Profile at Liposome Surface. We concluded that Alg-Na, MC, and PEG20000 directly interacted with lipid membranes, but not DEX and PEG600. In the case that the polymer adsorbs onto lipid membranes, the self-similar grid model[60] is useful for expressing the decay profile of the polymer fraction ϕ_p, that is,

$$\phi_p(r) = \left(\frac{m}{r}\right)^{\frac{4}{3}}, \tag{3-1}$$

where m is the monomer size and r is the distance from the liposome surface. This equation means that the local mesh size is equal to the distance from the surface. If we suppose the existence of an adsorption layer of thickness a, the polymer fraction profile can be divided into four regions as shown in Figure 3-10. The first region is the adsorption layer, which can be written as

$$\phi_p(r) = 1 \qquad (0 < r < a). \tag{3-2}$$

The second region can be expressed by the self-similar grid model, that is,

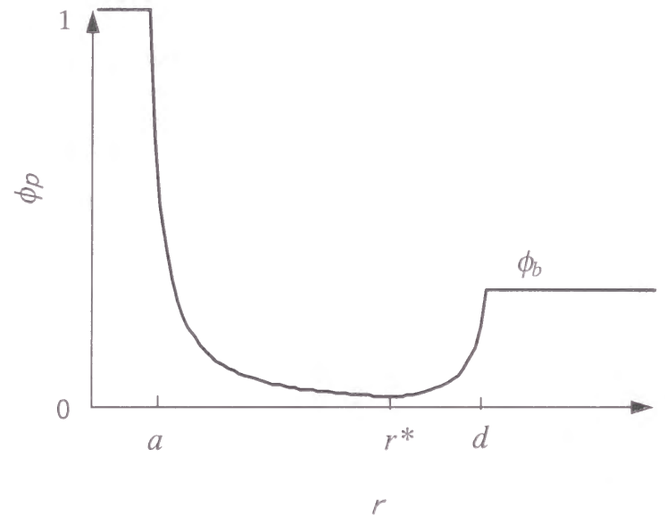

Figure 3-10. Polymer concentration profile calculated from Equations 3-2 through 3-5. This profile can be divided into four regions as described in the text.

$$\phi_p(r) = \left(\frac{m}{r - a + m}\right)^{\frac{4}{3}} \qquad (a < r < r^*), \tag{3-3}$$

where r^* is the distance at which the polymer fraction shows the minimum value. The equation for the third region can be given in a similar manner:

$$\phi_p(r) = \phi_b\left(\frac{m}{d - r + m}\right)^{\frac{4}{3}} \qquad (r^* < r < d), \tag{3-4}$$

where ϕ_b is the polymer fraction in bulk and d is the depletion layer thickness, which is equal to the polymer size when the polymer concentration is low enough. At a long distance from the liposome surface, we obtain

$$\phi_p(r) = \phi_b \qquad (r > d). \tag{3-5}$$

If no adsorption of polymers onto liposome surfaces occurs, the concentration profile is expressed by Equations 3-4 and 3-5. From these equations, we can calculate the polymer "micro-concentration" around liposome particles. To explain the difference in the bulk concentration and the micro-concentration which was obtained from the light scattering experiments, we must know the distance range which influences the Brownian motion of particles. Defining the distance range as L, we obtain the ratio of the micro-concentration and the bulk concentration R_c from the following equation.

$$R_c = \frac{\overline{\phi_p}}{\phi_b} = \frac{\int_0^L \phi_p(r)dr}{L\phi_b} \tag{3-6}$$

Here $\overline{\phi_p}$ is the averaged polymer fraction near the liposome surface. If no adsorption occurs, R_c becomes constant according to this model. Figure 3-11 shows the R_c values of all the polymers as a function of ϕ_b. As can be seen, the results investigated for

PEG600 and DEX display an apparently different trend from those of the other three polymers, with R_c being a decreasing function of ϕ_b. It seems that the R_c values of PEG600 and DEX do not depend on ϕ_b at all and can be regarded as constant within experimental error. From the plot of DEX, we can estimate L as 30 nm, because it is the only fitting parameter. However, the plot of PEG600 cannot be well explained by our model. This is most likely that PEG600 molecules are too small to discuss in the same manner.

The other three polymers seem to form an adsorption layer on liposome surfaces. The same figure also shows the profiles calculated with Equation 3-6. As can be seen, the experimental plot and the calculated line showed very good agreement. The model calculation enabled us to estimate the adsorption layer thickness a as 1.8 nm for PEG20000, 2.2 nm for MC, and 4.0 nm for Alg-Na, respectively. The employed parameters are summarized as Table 3-2.

Table 3-2. Parameters for Model Calculation of R_c

Polymer	a (nm)	m (nm)	d (nm)	L (nm)
PEG20000	1.8	0.3	11.0	30.0
PEG600	0	0.3	2.0	30.0
DEX	0	0.3	13.6	30.0
MC	2.2	0.3	13.9	30.0
Alg-Na	4.0	0.3	16.2	30.0

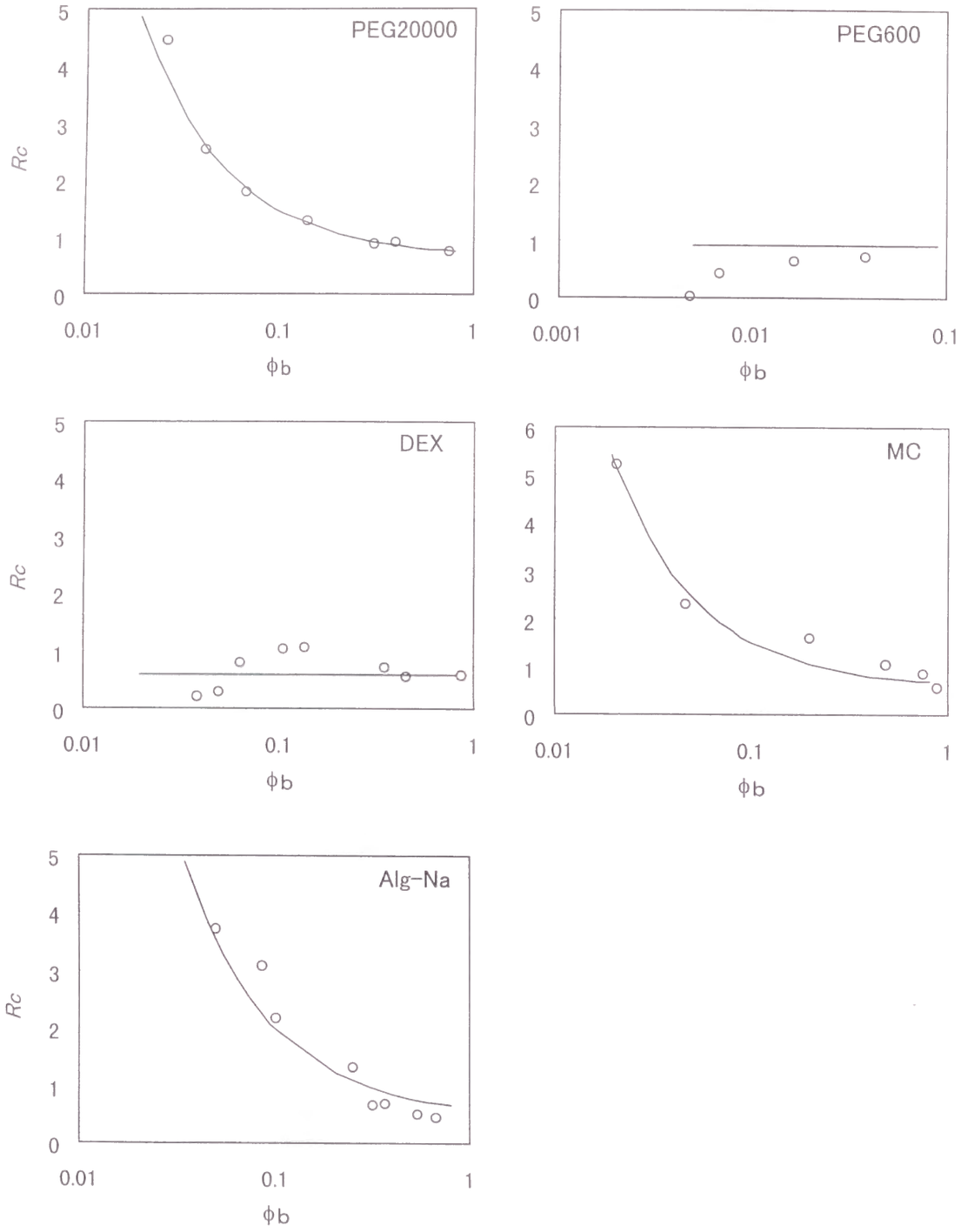

Figure 3-11. Ratio of the microconcentration and the bulk concentration as a function of polymer fraction. Symbols represent the experimental data of the light scattering and the solid lines were obtained using Equation 3-6.

Calculation of the Depletion Energy. Next, let us consider how the physical stability of liposome dispersions is affected by the presence of polymer. If polymers do not adsorb on the liposome surfaces at all, the depletion force can be an important factor which affects the dispersity. On the other hand, the adsorption of polymers often sterically stabilizes the dispersion, although the depletion interaction also exists. Below we try to calculate the depletion energy F_{dep}.

(1) Case of Reversible Adsorption. F_{dep} is given by using the Derjaguin approximation,[61] that is,

$$F_{dep} = -\pi r_L \int_0^d \Delta\Pi dh \,, \tag{3-7}$$

where r_L is the radius of liposomes and h is the shortest distance between the two liposome surfaces. $\Delta\Pi$ is the difference in the osmotic pressure between the bulk and the gap of liposome particles, which can be calculated from[62]

$$\frac{\Delta\Pi}{kT} = \frac{1}{2}\left(1-2\chi_{pw}\right)\left(\phi_b^2 - \langle\phi_p\rangle^2\right), \tag{3-8}$$

where χ_{pw} is the χ parameter between polymer and water. k and T have their usual meanings. The averaged polymer fraction between the gap, $\langle\phi_p\rangle$, can be regarded as zero if polymers between the gap can freely diffuse to the bulk in the case that liposome particles come close. However, when the bulk polymer concentration exceeds its overlap concentration ϕ_p*, the diffusion becomes restricted and the polymers between the gap become condensed during the approach of two liposome particles. The degree of the condensation seems to be difficult to estimate, since it depends on the velocity and angle of two approaching particles. Assuming that the difference in the osmotic pressure is unchanged during the approach, Equation 3-8 can be rewritten using C as a constant.

$$\frac{\Delta\Pi}{kT} = \frac{C\phi_b^2}{2}\left(1 - 2\chi_{pw}\right) \tag{3-9}$$

The depletion thickness d is also a function of ϕ_b above ϕ_p*.[5,6,9] It is calculated according to a simple geometric consideration. Assuming that the depletion thickness above ϕ_p* is equal to the size of the occupied volume per polymer molecules, we obtain

$$d = 2r_p\left\{1 - \left(\frac{\phi_w^*\phi_p - \phi_p^*\phi_w}{\phi_w^*\phi_p}\right)^{\frac{1}{2}}\right\}, \tag{3-10}$$

where

$$\phi_w^* = 1 - \phi_L - \phi_p^*. \tag{3-11}$$

r_p and ϕ_L stands for the radius of a polymer molecule and the fraction of liposome, respectively. The calculated depletion thickness is shown in Figure 3-12, which is similar to the results of earlier literature.[5]

Figure 3-13 shows the calculated depletion energy. It can be observed that significant destabilization of the dispersion occurs below ϕ_p*, whereas the restabilization is estimated above ϕ_p*.

(2) Case of Irreversible Adsorption. If polymer molecules are tightly bound to the liposome surfaces, the adsorbed layer can be regarded as the part of the liposome particles. Therefore, F_{dep} is expressed by

$$F_{dep} = -\pi r_L\int_{r^+}^{d+2a}\Delta\Pi dh\,. \tag{3-12}$$

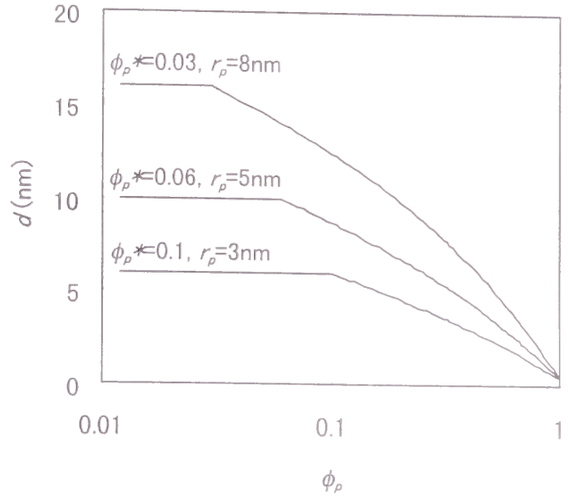

Figure 3-12. Depletion thickness calculated from Equation 3-10.

Here r^+ is the shortest distance between liposome surfaces to which they can approach each other. $\Delta\Pi$ can be calculated from Equation 3-8 and $\langle\phi_p\rangle$ from the following equation.

$$\langle\phi_p\rangle = \frac{2\int_{\frac{r^+}{2}}^{\frac{d+2a}{2}}\left(\frac{m}{r-a+m}\right)^{\frac{4}{3}}dr}{h-2a} \tag{3-13}$$

r^+ satisfies the next equation.

$$\frac{r^+}{2} - a = \int_a^{\infty}\left(\frac{m}{r+m-a}\right)^{\frac{4}{3}}dr \tag{3-14}$$

The calculated result from Equation 3-12 is also shown in Figure 3-13. This clearly indicates that the stability of the dispersity can be significantly improved by supposing the irreversible adsorption of polymer molecules. However, it should be noted that we do not assume the bridging of two surfaces by polymer molecules here.

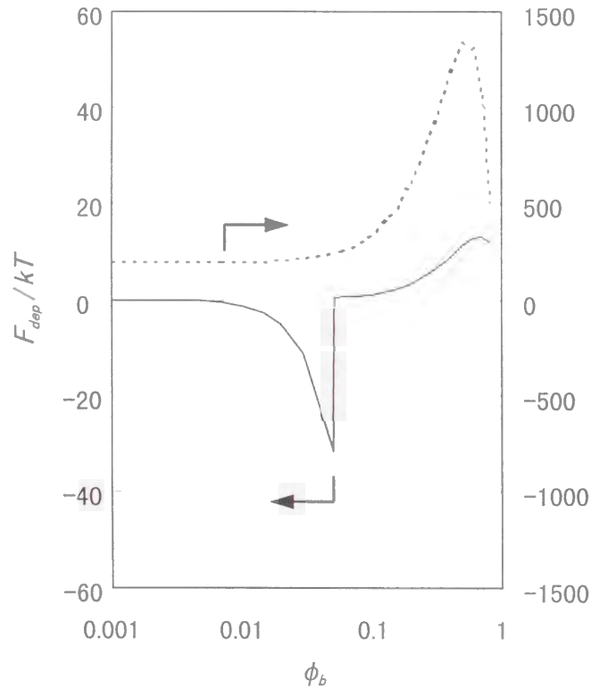

Figure 3-13. Calculated depletion energy per unit liposome surfaces by supposing the reversible adsorption of polymers (solid line, from Equation 3-7) and the irreversible adsorption (dotted line, from Equation 3-12). Parameters employed: χ_{pw} = 0.1, ϕ_p* = 0.05, ϕ_L = 0.02, d = 10 nm, r_L = 1000 nm, C = -0.01, m = 0.3 nm, a = 4 nm.

Thermodynamic Interpretation on Liposome Dispersity. The turbidity measurements revealed that there were three types of stability behavior. PEG20000 and MC destabilized dispersity over a wide concentration range and the unstabilization range seemed to be divided into two regions. DEX destabilized the dispersity at the intermediate concentration range. Alg-Na stabilized over the entire concentration range investigated. PEG600 showed the similar trend to Alg-Na except the existence of the less effective region. Below we try to explain these behaviors from the viewpoint of thermodynamics.

The difference in the free energy before and after the aggregation of particles, F, can be separated into three terms:

$$F = F_{mix} + F_{pair} + F_{dep}, \tag{3-15}$$

where F_{mix}, and F_{pair}, are the free energy change due to the mixing entropy and the pair-interaction energy, respectively. According to the Flory-Huggins mean-field theory, by defining the volume and the fraction of component i as n_i and ϕ_i, the change in the mixing entropy and the pair-interaction energy is expressed as

$$\frac{1}{kT}\left(F_{mix} + F_{pair}\right) = -\sum_i \frac{\phi_i \ln \phi_i}{n_i} + \frac{1}{2}\sum_i \sum_j \chi_{ij}\phi_i\phi_j, \tag{3-16}$$

where χ_{ij} is a χ parameter between components i and j. The first mixing entropy term can be approximated as a constant, because we do not take into account the entropy change due to the demixing of both water and polymer molecules but that which originats from the aggregation of liposome particles only, which occupy only a small fraction.

Here let us try to explain the dispersity data presented in Figure 3-9 from the thermodynamic viewpoint, although a quantitative interpretation remains forthcoming. According to the observation of light scattering, we could separate the

five polymers into two groups. DEX and PEG600 seemed to have no direct interaction with the liposome surfaces, whereas the other polymers were likely to form the adsorption layer. From the FT-IR measurements and the calculation of the adsorption layer thickness, the strength of the interaction could be ordered as PEG600, DEX < PEG20000 < MC < Alg-Na. This order agrees with that of the surface activity except Alg-Na, the interaction of which is most likely to be governed by electrostatic interaction.

According to the dispersity data, the simplest result was obtained when Alg-Na was added to the dispersion. In this case, the dispersity was improved over the entire concentration range of Alg-Na, which can be successfully elucidated by assuming that Alg-Na adsorbed onto liposome surfaces irreversibly. In other words, steric repulsion between the adsorbed Alg-Na chains played a significant role on the dispersity and the term of F_{dep} is dominant in Equation 3-15. Because a strong interaction between lipid membranes and Alg-Na has often been suggested in early literature,[40,41] this is the most likely explanation. However, from another point of view, it may lead to the destruction of lipid bilayers.

On the other hand, the effect of adding MC and PEG20000 can be interpreted by supposing reversible adsorption onto the surfaces. These two polymers affected the dispersity in a similar manner but PEG20000, which has two striking unstable concentration regions, showed a clearer trend. The overlap volume fraction of PEG20000 was derived from the model calculation as ca. 0.03.[3] Assuming the radius of PEG20000 molecules as 5.5 nm, it can be converted to ca. 1.5 mg/ml. Therefore, one unstable region was located at just below the overlap concentration and the other above that. The former region was likely to have originated due to depletion interaction, because it corresponds well to the calculated unstable region in Figure 3-13. The latter region seemed to appear due to unfavorable pair-interaction energy, that is, the direct contact between liposome surfaces and polymer molecules seemed to be thermodynamically unfavorable. In other words, the term of F_{pair} is dominant in Equation 3-15. Since polymer chains cannot escape from liposome surfaces above the

overlap concentration, it is natural to assume that the pair-interaction energy plays an important role at such a high concentration range.

The effect of adding DEX can be interpreted in a similar fashion. The only unstable region below the overlap concentration must be due to the depletion interaction. However, above that concentration, a poorly reproducible region was observed instead of the unstable region. This may be elucidated in terms of a better miscibility between DEX and liposome surfaces compared to PEG20000 and MC, and the total free energy difference in that region may be near zero. One may ask why DEX is more miscible with liposome surfaces than PEG20000 or MC despite its not adsorbing onto surfaces. The ability of the adsorption depends on whether or not there are attractive parts to surfaces in the polymer structure, that is, the total structure has a lesser effect. However, the pair-interaction energy is governed by the total structure.

PEG600 has so small a gyration radius that the effect of the depletion force is weak. This can be elucidated in terms of its size being smaller than the Flory radius,[12] and it is likely to be the reason that an unstable region was hardly observed when it was added to the dispersion.

Practical Application. Since all of the observed polymers are well-known as highly hydrophilic polymers, their interaction with lipid membranes has been frequently ignored. However, we have shown that a slight difference in the strength of the interaction can lead to significant differences in the stabilization of liposome dispersions.

Alg-Na, which carries negative charges and therefore interacts with membranes strongly, was proved to stabilize the dispersity significantly. This could be explained by the irreversible adsorption onto liposome surfaces. Therefore we conclude that Alg-Na is a very useful polymer for stabilizing liposome dispersions, and it may also be the case for other hydrophilic charged polymers such as the salt of hyaluronic acid, chondoroitin sulfate, carboxymethyl cellulose, and poly(acrylic acid). However, we must also keep in mind that these polymers can destroy the lipid membranes as

mentioned earlier.

Other hydrophilic polymers, which interact with membranes very weakly or do not interact at all, can destabilize dispersions. In other words, to add highly hydrophilic polymers to stabilize liposome dispersions is not an a good choice from the viewpoint of thermodynamics, especially below the overlap concentration. These findings provide the important information for controlling the stability of liposome dispersions by adding hydrophilic polymers.

Summary

Interactions between various hydrophilic polymers and liposomes were investigated. To stabilize liposome dispersions, some extent of the interaction between polymers and liposome membranes is needed, because lack of such interaction can lead to depletion destabilization of liposome dispersity. Alg-Na was proved to have such ability due to its charged moieties, which interact with membranes electrostatically. In the case of there being no interactions between polymers and membranes, greater amount than the overlap concentration was needed to stabilize the dispersity, whereas an intermediate strength of the interaction led to the destabilization even in a high concentration range. These observations suggest how to select polymers to stabilize or destabilize liposome dispersions.

References

(1) Oosawa, F.; Asakura, S. *J. Chem. Phys.* **1954**, *22*, 1255.

(2) Asakura, S.; Oosawa, F. *J. Polym. Sci.* **1958**, *33*, 183.

(3) Vincent, B.; Luckham, P. F.; Waite, F. A. *J. Colloid Interface Sci.* **1980**, *73*, 508.

(4) Feigin, R. I.; Napper, D. H. *J. Colloid Interface Sci*. **1980**, *75*, 525.

(5) Fleer, G. J.; Scheutjens, J. M. H. M. *Croati. Chem. Acta* **1987**, *60*, 477.

(6) Vincent, B.; Edwards, J.; Emmett, S.; Croot, R. *Colloids Surf.* **1988**, *31*, 267.

(7) Lekkerkerker, H. N. W. *Colloids Surf.* **1990**, *51*, 419.

(8) Calderon, F. L.; Bibette, J.; Biais, J. *Europhys. Lett.* **1993**, *23*, 653.

(9) Krabi, A.; Donath, E. *Colloids Surf. A* **1994**, *92*, 175.

(10) Walz, J. Y.; Sharma, A. *J. Colloid Interface Sci.* **1994**, *168*, 485.

(11) Mao, Y.; Cates, M. E.; Lekkerkerker, H. N. W. *Physica A* **1995**, *222*, 10.

(12) Kuhl, T.; Guo, Y.; Alderfer, J. L.; Berman, A. D.; Leckband, D.; Israelachvili, J.; Hui, S. W. *Langmuir* **1996**, *12*, 3003.

(13) Donath, E.; Krabi, A.; Allan, G.; Vincent, B. *Langmuir* **1996**, *12*, 3425.

(14) Sharma, A.; Walz, J. Y. *J. Chem. Soc., Faraday Trans.* **1996**, *92*, 4997.

(15) Sharma, A.; Tan, S. N.; Walz, J. Y. *J. Colloid Interface Sci.* **1997**, *190*, 392.

(16) Sharma, A.; Tan, S. N.; Walz, J. Y. *J. Colloid Interface Sci.* **1997**, *191*, 236.

(17) Ye, X.; Tong, P.; Fetters, L. J. *Macromolecules* **1997**, *30*, 4103.

(18) Maggio, B.; Lucy, J. A. *FEBS Lett.* **1978**, *94*, 301.

(19) Blow, A. M. J.; Bothan, G. M.; Fisher, D.; Goodall, A. H.; Tilcock, C. P. S.; Lucy, J. A. *FEBS Lett.* **1978**, *94*, 305.

(20) Sáez, R.; Alonso, A.; Villena, A.; Goñi, F. M.; *FEBS Lett.* **1982**, *137*, 323.

(21) Roots, D.S.; Davidson, R.L.; Choppin, P.W. *Cell Fusion*; Plenum Press, 1987.

(22) Lentz, B. R. *Chem. Phys. Lipids* **1994,** *73*, 91.

(23) Perrier, P.; Redziniak, G. *Skincare* **1989**, *Feb*, 29.

(24) Gregoriadis, G. *Biochemist* **1994**, *Feb/Mar*, 8.

(25) Lasic, D. D.; Papahadjopoulos, D. *Science* **1995**, *267*, 1275.

(26) Sharma, A.; Sharma, U. S. *Int. J. Pharm.* **1997**, *154*, 123.

(27) Storm, G.; Crommelin, D. J. A. *Pharm. Sci. Tech. Today* **1998**, *1*, 19.

(28) Mezei, M.; Gulasekharam, V. *Life Sci.* **1980**, *26*, 1473.

(29) Cevc, G.; Blume, G.; Schätzlein, A.; Gebauer, D.; Paul, A. *Adv. Drug Delivery Rev.* **1996**, *18*, 349.

(30) Pleyer, U.; Lutz, S.; Jusko, W. J.; Nguyen, K.; Narawane, M.; Rückert, D.; Mondino, B. J.; Lee, V. H. L. *Invest. Ophthalmol. Vis. Sci.* **1993**, *34*, 2737.

(31) Bochot, A.; Fattal, E.; Gulik, A.; Couarraze, G.; Coureur, P. *Pharm. Res.* **1998**, *15*, 1364.

(32) Schreier, H.; Gonzalez-Rothi, R. J.; Stecenko, A. A. *J. Control. Release* **1993**, *24*, 209.

(33) Bridges, P. A.; Taylor, K. M. G. *Int. J. Pharm.* **1998**, *173*, 117.

(34) Humberstone, A. J.; Charman, W. N. *Adv. Drug. Delivery Rev.* **1997**, *25*, 103.

(35) Rogers, J. A.; Anderson, K. E. *Crit. Rev. Ther. Drug Carrier Syst.* **1998**, *15*, 421.

(36) Chonn, A.; Cullis, P. R. *Adv. Drug Delivery Rev.* **1998**, *30*, 73.

(37) Pouton, C. W.; Seymour, L. W. *Adv. Drug Delivery Rev.* **1998**, *34*, 3.

(38) Jones, M. N. *Adv. Colloid Interface Sci.* **1995**, *54*, 93.

(39) Ceh, B.; Winterhalter, M.; Frederik, P. M.; Vallner, J. J.; Lasic, D. D. *Adv. Drug Delivery Rev.* **1997**, *24*, 165.

(40) Igari, Y.; Kibat, P. G.; Langer, R. *J. Control. Release* **1990**, *14*, 263

(41) Cohen, S.; Bañó, M. C.; Chow, M.; Langer, R. *Biochim. Biophys. Acta* **1991**, *1063*, 95.

(42) Machluf, M.; Regev, O.; Peled, Y.; Kost, J.; Cohen, S. *J. Control. Release* **1996**, *43*, 35.

(43) Snabre, P.; Mills, P. *Colloid. Polym, Sci.* **1985**, *263*, 494.

(44) Kawakami, K.; Nishihara, Y.; Hirano, K. *J. Colloid Interface Sci.* **1998**, *206*, 177.

(45) Kawakami, K.; Nishihara, Y.; Hirano, K. *Langmuir*, in press.

(46) Okubo, T.; Kobayashi, K. *J. Colloid Interface Sci.* **1998**, *205*, 433.

(47) Bailey, F. E.; Koleske, J. V. *Poly(ethylene oxide)*; Academic Press, 1976.

(48) Lu, J. R.; Su, T. J.; Thomas, R. K.; Penfold, J.; Richards, R. W. *Polymer* **1996**, *37*, 109.

(49) Mendelsohn, R.; Snyder, R. G. *Biological Membranes* (Eds. Merz Jr., K. and Roux, B.); Birkhäuser, 1996.

(50) Arrondo, J. L. R.; Goñi, F. M. *Chem. Phys. Lipids* **1998**, *96*, 53.

(51) Mendelsohn, R.; Moore, D. J. *Chem. Phys. Lipids* **1998**, *96*, 141.

(52) Hoogendam, C. W.; Peters, J. C. W.; Tuinier, R.; de Keizer, A.; Cohen Stuart, M. A.; Bijsterbosch, B. H. J. *Colloid Interface Sci.* **1998**, *207*, 309.

(53) Ariga, K.; Shin, J. S.; Kunitake, T. *J. Colloid Interface Sci.* **1995**, *170*, 440.

(54) Ohno, H.; Maeda, Y.; Tsuchida, E. *Biochim. Biophys. Acta* **1981**, *642*, 27.

(55) Scheutjens, J. M. H. M.; Fleer, G. J. *J. Phys. Chem.* **1979**, *83*, 1619.

(56) Sunamoto, J.; Iwamoto, K.; Kondo, H.; Shinkai, S. *J. Biochem.* **1980**, *88*, 1219.

(57) Evans, E.; Metcalfe, M. *Biophys. J.* **1984**, *45*, 715.

(58) Lehtonen, J. Y. A.; Kinnunen, P. K. J. *Biophys. J.* **1994**, *66*, 1981.

(59) Lehtonen, J. Y. A.; Kinnunen, P. K. J. *Biophys. J.* **1995**, *68*, 525.

(60) de Gennes, P. G. *Adv. Colloid Interface Sci.* **1987**, *27*, 189.

(61) Israelachvili, J. N. *Intermolecular and Surface Forces* ; Academic Press, 1991.

(62) de Gennes, P. G. *Scaling Concepts in Polymer Physics*; Cornell University Press, 1979.

Chapter 4

Mechanism of Protein Solubilization in Microemulsion

Introduction

A microemulsion (ME)[1-3] is a thermodynamically stable isotropic solution, which consists of at least three components: water, oil, and surfactant. The fourth component often added is a cosurfactant. The most frequently studied ME is of W/O (water-in-oil) type, in which aqueous droplets surrounded by a surfactant shell are suspended in apolar organic solvents as a continuum medium. Some applications of ME have been developed for use as drug carriers.[4-6]

W/O ME can incorporate various types of drugs in the same manner as liposome dispersions. To derive the advantageous characteristics of ME at most, drugs should be incorporated in the water pool of ME droplets. In other words, highly hydrophilic drugs are the most applicable for W/O ME. However, needless to say, when guest molecules are incorporated into ME droplets, structural change or deformation of the droplets may occur. This problem cannot be overcome by preparation methods, because ME is in an equilibrium state.

This chapter discusses the solubilization mechanism of water-soluble protein in W/O microemulsion droplets. The mechanism is not well understood although much work has been performed.[7-13] What needs to be answered are questions such as: what is the driving force of the solubilization, where are the incorporated proteins located, do the incorporated proteins allow the native structure to be retained, and what factors to determine the incorporation rate.

Some intuitive images for the localization of proteins in ME droplets, as illustrated in Figure 4-1, have been proposed.[14-17] The most typical is the water-shell model,[14] which assumes that proteins are located in the central part of the ME water pool without adsorbing surfactant molecules on their surfaces. However, this

approximation seems to be too simple, because the significance of the electrostatic interaction between charged head groups of surfactants and charged residues of proteins, by which electrostatic adsorption is most likely to occur, have been pointed out by thermodynamic calculations.[18-21] Therefore, the protein molecules may be adsorbed on the inner wall of ME droplets as shown in Figure 4-1 (b). If the protein molecules are surface-active, they may locate on the water-oil interface as presented in Figure 4-1 (c).

In this work, sodium bis(2-ethylhexyl) sulfosuccinate (AOT), which is well known to form ME droplets without the aid of cosurfactant, was employed as a surfactant to prepare ME solutions. The model protein selected was α-chymotrypsinogen A (CTN), which is a precursor of chymotrypsin. This selection was based on the fact that chymotrypsin had been regarded as the most typical protein in early studies[22-27] since it seems to be solubilized in the water pool of ME droplets without undergoing significant denaturation. A precursor was chosen to avoid autolysis. The differences of these proteins, such as molecular weight, conformation, and pI value, are not significant.

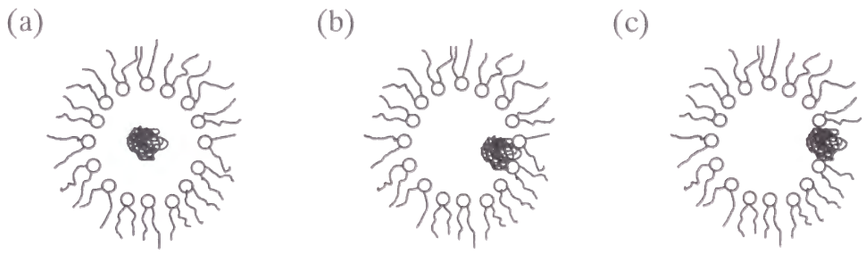

Figure 4-1. The possible location of protein molecules in W/O ME droplets. (a) Protein molecules are located in the central part of water pool. (b) Protein molecules are adsorbed on the inner wall of the droplets. (c) Protein molecules are on the water-oil interfaces.

The time-dependent behavior of the incorporation process and the analysis of the conformational state of CTN after the incorporation are discussed first. As the next step, several factors which control the incorporation behavior, such as CTN/AOT ratio, species of organic solvents, and salinity conditions, are changed to further elucidate the solubilization mechanism. From these observations, the protein incorporation model into ME droplets is proposed, and it was confirmed by the new methodologies which utilize the chromatography technique. Our conclusion is that the direct interaction, that is, the electrostatic and hydrophobic interactions between surfactant and protein molecules and the curvature effect of ME droplets were identified as playing key roles in the incorporation behavior.

Experimental Section

Materials. CTN from bovine pancreas type Ⅱ, AOT and ATR (sodium ditridecanoyl sulfosuccinate) were obtained from Sigma, Tokyo Kasei, and Cyanamid, respectively. BCA protein assay reagent was supplied from Pierce. Bis[2-[(5-chloro-2-pyridyl)oxo]-5-(diethylamino)-phenolato]cobalt (Ⅲ) chloride (Co-PADAP) was purchased from Dojin Kagaku. All chemicals were at least of reagent grade and used as supplied.

Phase-Transfer Method. Several experimental methods have been performed to investigate the incorporation behavior of proteins into ME droplets.[13] One of the simplest is the "phase-transfer method." Equivalent volumes of organic solvents containing AOT and CTN buffer solution were mixed in test tubes with vigorous shaking, and centrifugation (2,000 rpm × 10 min.) was done to separate the two phases. Immediately after this separation process, each phase was subjected to various measurements. Figure 4-2 shows the image of the resultant ME solution. In the experiment on the time-dependence, each tube was incubated in a thermobath at 25 ℃. Phosphate-buffered saline of pH 7.5 was used as the aqueous phase unless

otherwise mentioned. Total Na^+ concentration of the buffer was usually 0.2 M.

Continuous Measurement of the Time-Dependence of CTN Distribution between Aqueous and Organic Phases. The incorporation behavior of CTN into ME droplets strongly depends on the elapsed time. To investigate this time-dependent behavior continuously, we constructed the experimental set-up shown in Figure 4-3. After careful pouring of the two phases, the aqueous phase was circulated using a peristaltic pump. The circulated stream was fed back through the ME phase in the form of water droplets. The CTN concentration of the aqueous phase was followed by UV absorption at 282 nm by an on-line UV spectrometer.

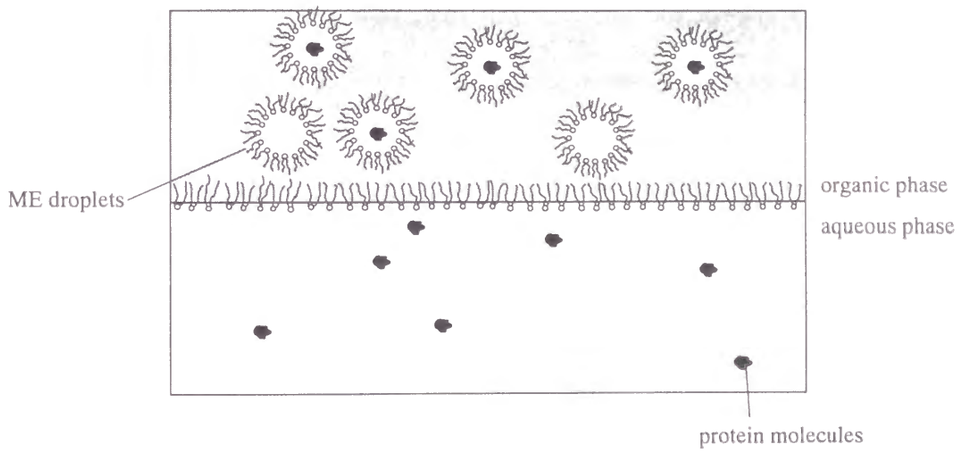

Figure 4-2. The resultant ME solution obtained by the phase-transfer method.

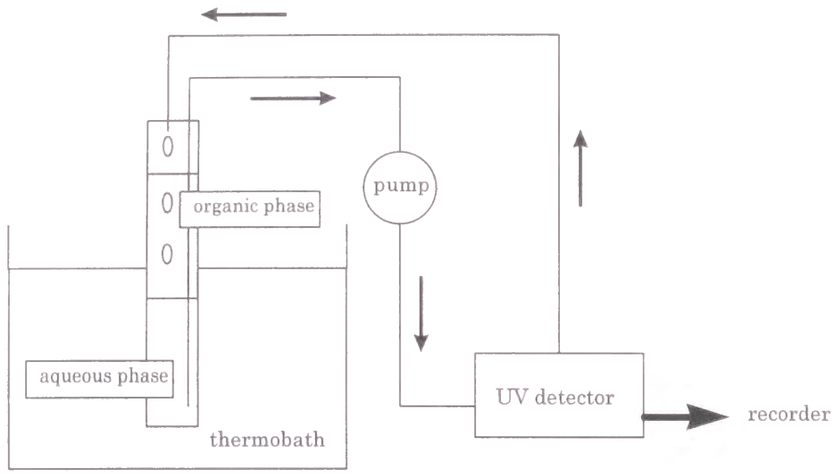

Figure 4-3. Experimental set-up for the measurement of time-dependent CTN incorporation behavior into ME.

Determination of CTN Concentration. The CTN concentration in the ME phase was analyzed by UV absorption at 282 nm, except when toluene, cyclohexane, or n-dodecane was used as the organic solvent. These exceptions are because that these solvents have UV absorbance. In these cases and when the incorporation rate was very high, the CTN concentration in the aqueous phase was measured by the BCA method,[28] which could avoid the effect of denaturation of CTN.

Determination of AOT and ATR Concentration. The AOT concentration in both phases was determined by using Co-PADAP,[29,30] which has been frequently used to quantify the concentration of anionic surfactants. 0.5 ml of 0.04 wt% Co-PADAP aqueous solution, 1 ml of 2 M HCl, 5 ml of distilled water, and 5 ml of benzene were mixed in test tubes. After the addition of an appropriate amount of samples and subsequent vigorous hand shaking, each solution was incubated at room temperature for 1 day. The obtained organic phases were subjected to UV measurement at 560 nm,

and the AOT concentration was determined from a standard curve.

Hydrophobic Interaction Chromatography. Hydrophobic interaction chromatography was employed to investigate the adsorption states of AOT molecules onto CTN surfaces. The used column was Econopack HIC cartridge (Biorad). First, the column was equilibrated using distilled water, and then a small amount of aqueous sample in contact with the ME phase was loaded at the entrance of the column. The unbound CTN was detected by a UV detector at 282 nm. Phosphate-buffered saline containing 0.2 M Na^+ was introduced as an eluent after that, and the eluted CTN was detected as the bound CTN.

Cation Exchange Chromatography. Cation exchange chromatography was also employed to investigate the adsorption states of AOT molecules onto CTN surfaces. The column was Econopack CM cartridge (Biorad). The experimental procedures were the same as for the hydrophobic interaction chromatography, except that the eluent contained 1 M Na^+.

Other Analysis. The amount of water in organic phases was measured by Karl-Fisher method (Hiranuma AQ-6). The size and shape of microemulsion droplets in both the presence and absence of CTN was determined by a small-angle X-ray scattering method (Rigaku Goniometer E7). The conformational state of CTN in both aqueous and organic phases was analysed by circular dichroism spectra (Jasco J-720).

Results and Discussions

Time Dependent Behavior of CTN Incorporation into ME Droplets. The extraction of CTN from the aqueous buffer phase to the organic ME phase was investigated using the apparatus shown in Figure 4-3, and the typical results are shown in Figure 4-4. The ordinate represents the fraction of unextracted CTN, (1-E), where E represents the extracted fraction of CTN. As can be seen, a rapid increase of E was observed immediately after the contact of two phases, and the maximum

extraction was attained after a few hours. Thereafter, a subsequent slow back-extraction process was observed. This time dependent behavior is similar to the study reported before using cytochrome C as the guest protein.[31]

Figure 4-5 presents the effect of the AOT concentration on the extraction behavior. As can be seen, the higher the AOT concentration was, the faster was the extraction. However, too high a concentration was observed not to work well. For example, when AOT concentration was 1 M, almost no extraction proceeded. This can be elucidated in terms of the increase in the viscosity of the organic phase. The figure also shows an increase in the maximum extraction rate with an increase of the AOT concentration. This is most likely to have originated from the enhancement of the back-extraction process, since a much higher extraction rate could be obtained by more vigorous mixing of the two phases even at a low AOT concentration.

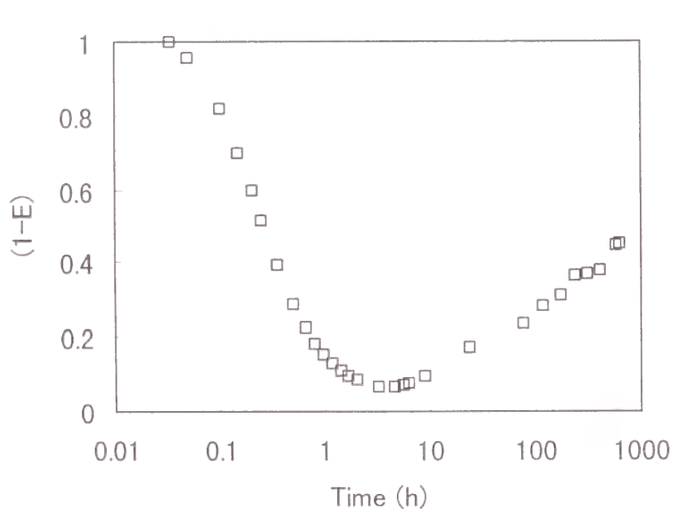

Figure 4-4. An example of the time dependent extraction behavior of CTN in AOT/n-heptane/phosphate buffer microemulsion system. The phosphate-buffered saline contains 0.2 M of NaCl and the pH was adjusted to 7.5. Initial CTN concentration in the aqueous phase and AOT concentration in the organic phase was 18 μM and 250 mM, respectively.

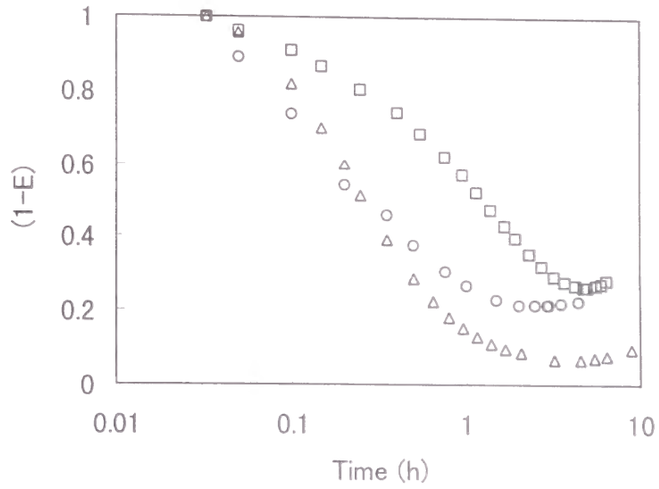

Figure 4-5. Effect of AOT concentration in the organic phase on the extraction behavior. AOT concentration was 10 mM (□), 100 mM (○), and 250 mM (△). Other conditions were the same as for Figure 4-4.

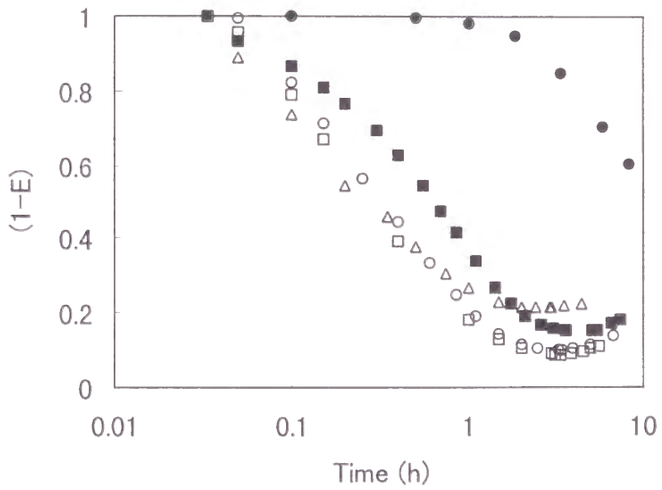

Figure 4-6. Effect of salt concentration (Na^+) in the aqueous phase on the extraction behavior. Na^+ concentration was 170 mM (□), 190 mM (○), 200 mM (△), 250 mM (■), and 400 mM (●). Other conditions were the same as for Figure 4-4, except that AOT concentration was 100 mM.

Figure 4-6 presents the effect of the salt concentration on the extraction behavior. These results can also be elucidated as the effect of the size of ME droplets, since the increase in salt concentration results in a decrease of the ME size. As can be seen, when the salt concentration was in the range between 170 and 250 mM, where the radius of the water pool was in the range between 4 and 5 nm, the extraction behavior did not have the significant difference. However, when the salt concentration increased to 400 mM, where the radius of the water pool was 3.2 nm, the extraction was strongly suppressed. Since the radius of the CTN molecule is ca. 3.5 nm[32], the radius of the water pool was smaller. Therefore, this suppressed extraction was arose due to the size-exclusion effect of the ME droplets.[33-35]

Figure 4-7 shows the effect of the pH of the aqueous phase on the extraction behavior. The pH value 9.5 was selected for comparison because it is the isoelectric point of CTN, i.e., the net charge of CTN was neutral at this pH. As can be seen, the higher pH resulted in the suppression of the maximum extraction due to significant enhancement of the back-extraction. At this pH, a small amount adsorption of AOT caused by the hydrophobic interaction makes CTN negatively charged. Since AOT is an anionic surfactant, it is natural to assume that negatively charged CTN is repelled from AOT ME very rapidly. We also tried the same experiment at pH 11, at which CTN was strongly negatively charged, but the extraction did not proceed at all due to the denaturation of CTN.

Figure 4-8 presents the time dependent distribution coefficient of CTN between the ME phase and the aqueous phase. The extraction was performed by the vigorous hand shaking, by which 10 minutes was long enough to attain the maximum extraction. The abscissa represents the AOT concentration in the organic phase, [AOT]org, which was not altered during the experiment The ordinate shows the CTN concentration ratio, D, between the organic phase and the aqueous phase. As can be seen, the results showed the same tendency as the former experiment, i.e., the extraction process consisted of a fast forward extraction and a slow back extraction.

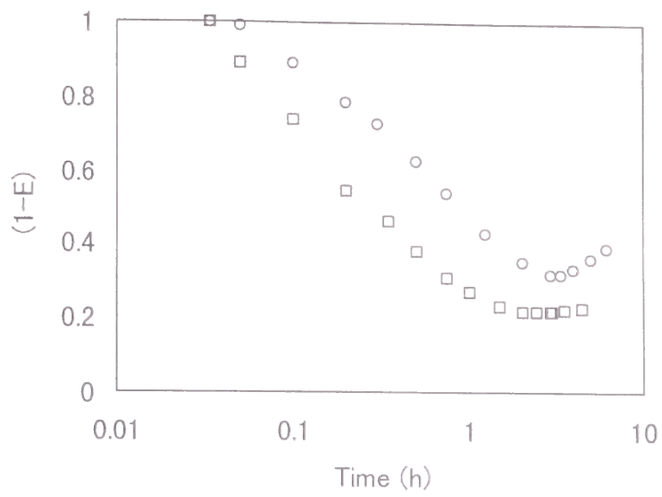

Figure 4-7. Effect of pH of the aqueous phase on the extraction behavior. The pH was adjusted to 7.5 (□) or 9.5 (○). Carbonic buffer was used to adjust the pH at 9.5. Other conditions were the same as for Figure 4-4, except that AOT concentration was 100 mM.

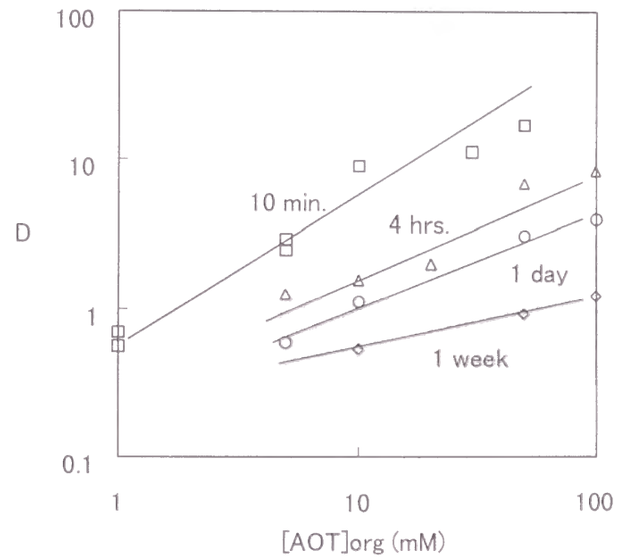

Figure 4-8. Time dependent CTN extraction behavior into the AOT/n-heptane ME phase after the vigorous hand shaking. The aqueous phase was phosphate-buffered saline at pH 7.5 containing 0.2 M Na^+ and 12 μM CTN initially. D is defined as CTNorg/CTNaq.

10 minutes after the contact of the two phases, the D value was observed to be proportional to [AOT]org in the low concentration range, and it remained the same for ca. 2 hours. This is the evidence that CTN molecules are incorporated in the water pool of ME droplets with very little or no adsorption of AOT molecules on their surfaces. However, the proportionality disappeared after a long period due to enhanced back extraction in the high AOT concentration range. This is likely to be elucidated in terms of the great adsorption of AOT molecules on CTN surfaces as in the case of cytochrome C.[31]

The time dependent extraction behavior in the protein extraction process was often ignored in early works. Although Luisi et al.[13,36] and Hatton et al.[37,38] observed such behavior, their interest was only in the required time to attain the maximum extraction. No information of the back extraction process was provided. This slow back extraction behavior may have been the reason for the inconsistent data among the different studies as suggested by Wolbert et al.[39]

Conformational States of CTN molecules in the Extraction Processes. It is very important to know whether or not protein molecules maintain their activities in ME. However, CTN has no activities because CTN is a precursor of chymotrypsin. Therefore we tried to obtain information on the conformational states of CTN molecules from spectroscopic measurements.

First, the UV adsorption spectra of CTN in the ME phase was investigated. Figure 4-9 shows the alteration of UV spectra with time. As can be seen, the spectra were observed to be blue-shifted after the slightly red shift within a few hours. The red shift might be related to the presence of negative charges of AOT molecules near CTN molecules. The subsequent blue shift may indicate a slight conformational change of CTN molecules. However, the alteration in the spectra is rather weak as in the case of α-chymotrypsin[22], when compared to the change in the visible light absorption of cytochrome C.[40]

Measurements of CD spectra can provide the information about the secondary structure of proteins. Figure 4-10 shows the CD spectra in the ME phase. As can be

seen, the ellipticity of the 230 nm band measured after 10 minutes in the ME phase was almost identical to that of the native state, whereas that after 1 week the difference became clear, suggesting an increase in the content of α-helices as in the case of α-chymotrypsin.[22] However, we concluded that the structural change of CTN due to incorporation into ME droplets is rather small, since cytochrome C showed a drastic change in the CD spectra.[40]

From these two spectroscopic measurements, CTN seems to retain the higher-order structure and macroscopic characters in the extraction processes.

Dependence of AOT/CTN Ratio on the Extraction Behavior. The extraction behavior was strongly affected by the AOT/CTN ratio. Figure 4-11 presents the extraction rate, E, as functions of total AOT/CTN ratio and AOT concentration. From this figure, it can be clearly seen that the extraction rate increases gradually when the AOT concentration is low, but a drastic increase occurs at ca. AOT/CTN = 40 when AOT concentration is high. This difference is likely to arise from the aggregation behavior of CTN molecules. In other words, when both AOT and CTN concentrations are high, CTN aggregates are easily formed by the addition of AOT, and the CTN transfer into the ME phase proceeds as aggregates. This leads to a drastic change in the extraction rate by a small addition of AOT. The change in Wo, which is defined as the number of water molecules per AOT molecule in the organic phase, is presented in Figure 4-12. Both curves show a sharp peak, which can be elucidated in terms of the change in ME shape as detected by SAXS measurements. Details of SAXS measurements will be discussed later. In this concentration range, several tens of CTN molecules were loaded per ME droplet, and this high loading may be the reason for the shape-change of ME.

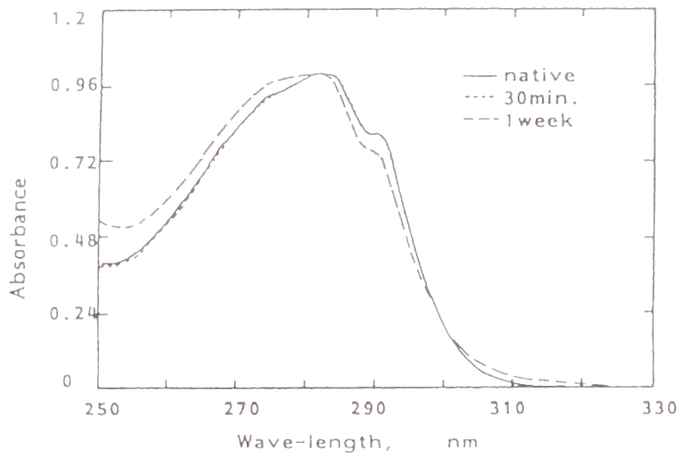

Figure 4-9. UV spectra of CTN in AOT/ n-heptane ME phase. The initial concentration of Na^+ and CTN in the aqueous-buffered phase was 200 mM and 13 μM, respectively. The initial AOT concentration in the organic phase was 50 mM. The elapsed time is shown in the figure.

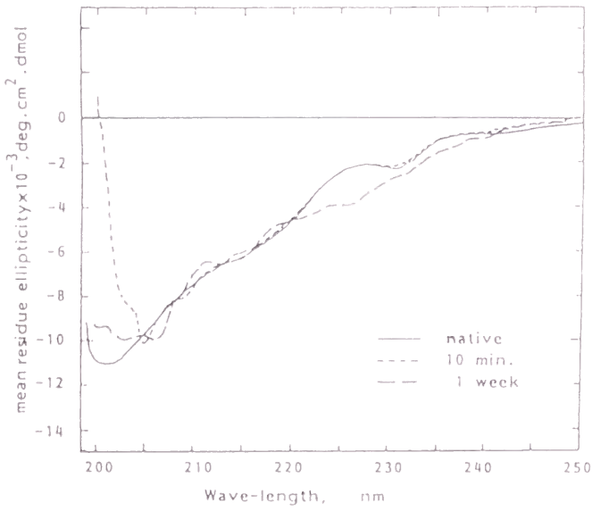

Figure 4-10. CD spectra of CTN in AOT/ n-heptane ME phase. The initial concentration of CTN in the aqueous phase was 130 μM. Other conditions were the same as for Figure 4-9.

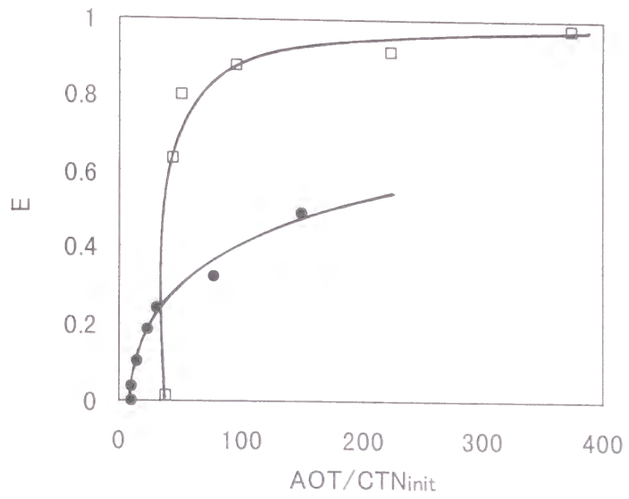

Figure 4-11. Dependence of the extraction rate of CTN into the ME phase on AOT concentration and the total AOT/CTN molar ratio. AOT concentration was 1 mM (●) and 30 mM (□).

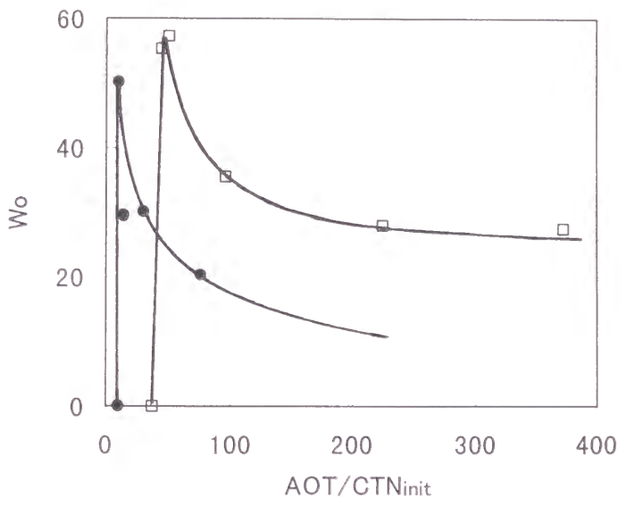

Figure 4-12. Dependence of the Wo of the ME phase on AOT concentration and the total AOT/CTN molar ratio. AOT concentration was 1 mM (●) and 30 mM (□).

Figure 4-13 presents the AOT concentration in the aqueous phase, which was corrected by subtracting the monomer concentration, as a function of the CTN concentration in the aqueous phase. The obtained AOT concentration can be regarded as the adsorbed AOT onto CTN surfaces in the aqueous phase. As can be seen, the AOT/CTN ratio showed a constant value at ca. 10 regardless of the CTN concentration and species of the organic solvent. In addition to this, both AOT and CTN concentrations in the organic phase were under the detection limit when the total AOT/CTN ratio was lower than 10 regardless of the species of the organic solvents. These results suggest that the value "10" is the number of adsorbed AOT molecules per CTN molecule, i.e., each CTN molecule seems to adsorb ca. 10 AOT molecules and the excess AOT molecules form ME droplets in the organic phase. At pH 7.5, CTN carries14 positively charged residues and 4 negatively charged residues. Thus, there is a capacity to adsorb 14 AOT molecules. However, all of the residues are not on the surface of CTN molecules, where AOT molecules can easily bind. If a negatively charged residue is close to a positively charged one, this positively charged one might not bind an AOT molecule. These considerations indicate that "10" is the ideal value of the AOT adsorption capacity per CTN molecule.

Dependence of ME Size on Salt Concentrations and Solvent Species. As described in the next section, the extraction behavior of CTN into the ME phase was observed to depend strongly on the ME size. In this section, we introduce briefly the factors which affect the ME size before proceeding further. Figure 4-14 shows the dependence of ME sizes, which was determined by the Guinier plot of the SAXS data, on salt concentrations and solvent species. As can be seen, the increase in the salt concentration or the decrease in the molecular volume of organic solvents led to a decrease in the diameter as frequently reported in previous literature.[41] This effect can be elucidated in terms of the change in the apparent shape of the AOT molecule. The increase in the salt concentration shields the electrostatic repulsion between AOT headgroups, and therefore the apparent size of the headgroups becomes small. On the other hand, the decrease in the molecular size of the organic solvents leads to their

enhanced penetration between AOT hydrophobic chains, and therefore the apparent volume occupied by the hydrophobic chains becomes large. Figure 4-14 shows this tendency very well.

A linear relationship has frequently been reported between the ME radius and Wo.[11,42-44] In our system, the relationship is expressed as

$$(radius, nm) = 0.18Wo + 1.2 \qquad (4\text{-}1)$$

as shown in Figure 4-15. This slope is slightly steeper than the reported values. It is likely that this is due to the higher salt concentration compared to the earlier experiments.

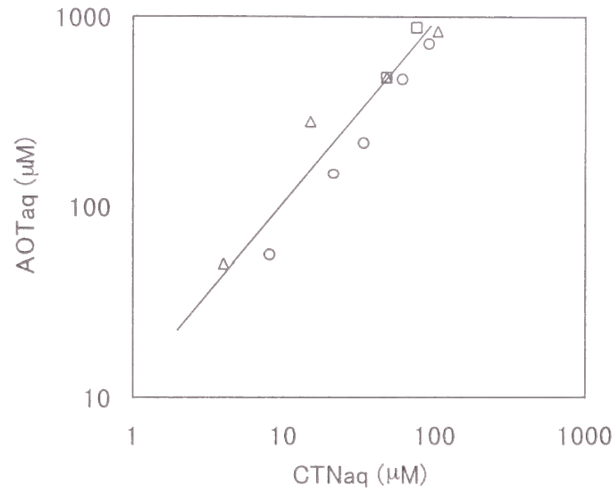

Figure 4-13. Relationship between AOT and CTN concentration in the aqueous phase. Used solvents were n-hexane (□), n-heptane (◯), and isooctane (△). The indicated line has a slope of 1.

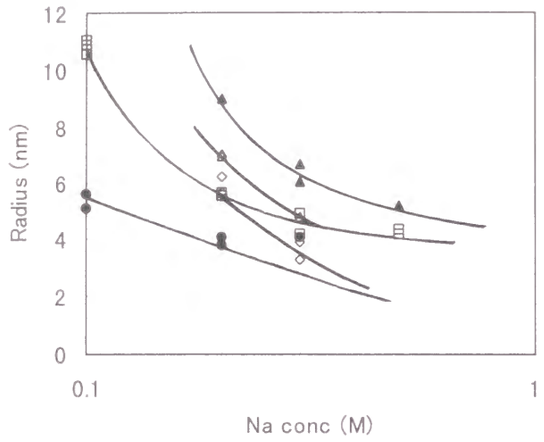

Figure 4-14. ME radius as a function of salt (Na^+) concentration and organic solvent species. Used solvents were n-decane (▲), isooctane (△), n-heptane (□), n-hexane (◇), and cyclohexane (●).

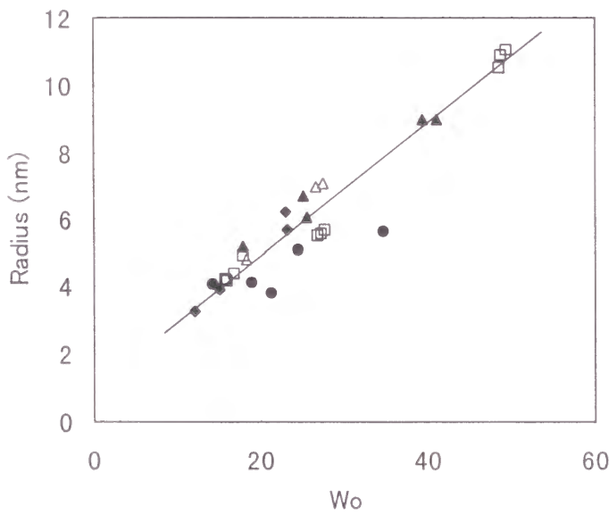

Figure 4-15. Relationship of the ME radius and Wo. Used solvents and the symbols are the same as for Figure 4-14.

Dependence of the Distribution Coefficient on Wo. Many researchers have thought that the extraction behavior is controlled by the electrostatic interaction between ME membranes and proteins.[18-21] However, a recent study using synchrotron X-ray diffraction indicates no perturbation of the geometry of ME droplets upon the incorporation of chymotrypsin,[45] suggesting that there is no direct electrostatic interaction between incorporated proteins and charged ME walls. Figure 4-16 shows the dependence of D, which is defined as CTNorg/CTNaq, on the salt concentration and the solvent species. As can be seen, the distribution coefficient is strongly affected by the salt concentration. Since the increase in the salt concentration leads to the enhanced shielding of the electrostatic interaction, this result seems to indicate that the electrostatic interaction is the controlling factor of the extraction behavior. However, we must keep in mind that the increase in the salt concentration also leads to the decrease in the ME size as described in the previous section. From Figure 4-16, it can also be proved that the decrease in the molecular size of the organic solvents leads to the decrease in the distribution coefficient. These results show that the conditions for the decreased distribution coefficient are consistent with those for the decreased size of ME droplets. Therefore, we plotted these distribution coefficients as a function of Wo, in Figure 4-17. This figure clearly indicates that the obtained distribution coefficient values fall on a single curve when Wo is used as a variable, suggesting that the bending energy[46-49] of AOT membranes is the controlling factor for the extraction process. The figure also presents the data in which KCl was used as the salt in place of NaCl, and ATR, which has the same headgroup as AOT but has longer chains, was used as the surfactant in place of AOT. These employment was due to the difficulty of reducing the ME size. As can be seen, the importance of Wo was proved in spite of the difference in the experimental conditions. In other words, ME size was found to play a dominant role in the extraction behavior, because it was proportional to Wo.

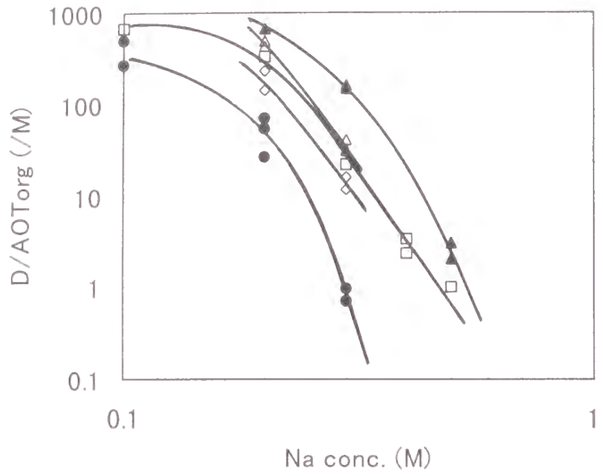

Figure 4-16. Dependence of D on the salt concentration and the solvent species. Used solvents and the symbols are the same as for Figure 4-14.

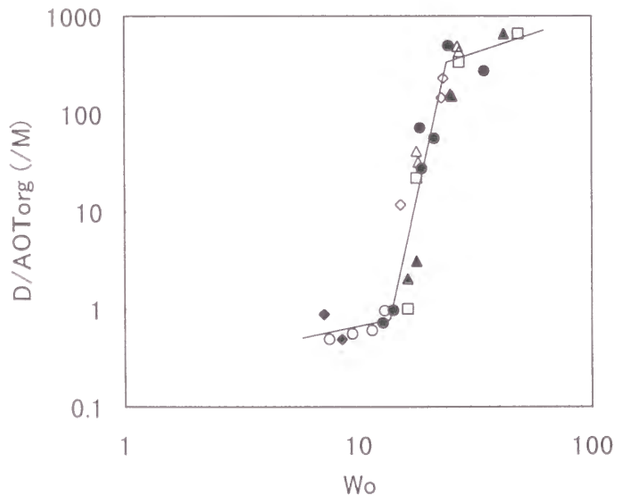

Figure 4-17. Plot of D values as a function of Wo. Used solvents and the symbols are the same as for Figure 4-14, except ○ (KCl was used as the salt; the organic solvent was n-heptane) and ◆ (ATR was used as the surfactant; the organic solvent was n-heptane).

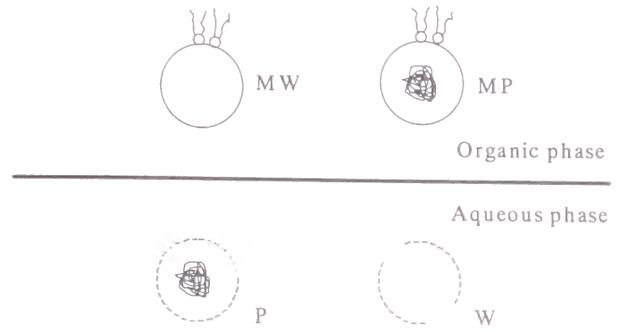

Figure 4-18. Scheme of the model of protein incorporation into ME droplets.

A phenomenological model for CTN incorporation in ME droplets is illustrated in Figure 4-18. The water pool of a ME droplet, which is free from proteins, is defined as MW, and that containing proteins is defined as MP, having volumes of v_{MW} and v_{MP}, respectively. The aqueous phase is divided into the element, which have the same volume, v_{WP}. The empty elements are designated as *W*, and the elements containing CTN molecules as *P*. The CTN incorporation process is described as,

$$P + MW \leftrightarrow MP + P\,. \tag{4-2}$$

In other words, we assumed that there are no size changes of ME droplets during the incorporation. The equilibrium relationship for Equation 4-2 is expressed as

$$K\phi_P\phi_{MW} = \phi_{MP}\phi_W\,. \tag{4-3}$$

Here, K is the equilibrium constant and ϕ_i the volume fraction of i. If we suppose the total volume fraction of water pools to be ϕ_M, it can be expressed as

$$\phi_M = \phi_{MW} + \phi_{MP} = v_{ME}[ME]\,, \tag{4-4}$$

where v_{ME} and *[ME]* are the volume of water per mole of the droplets and the concentration of ME droplets in the organic phase, respectively. Therefore, we can obtain the following equations for each volume fraction.

$$\phi_P = v_{ME}\frac{[CTN]}{n} \tag{4-5}$$

$$\phi_W = 1 - v_{ME}\frac{[CTN]}{n} \tag{4-6}$$

$$\phi_{MP} = \frac{K\phi_M\phi_P}{\phi_W + K\phi_P} \tag{4-7}$$

Here *[CTN]* and n are the CTN concentration in the aqueous phase and the number of CTN molecules per CTN cluster. If CTN molecules are dissolved individually, n = 1. We can obtain an expression for the distribution coefficient D from these equations as

$$D = \frac{\phi_{MP}}{\phi_P} = \frac{[ME]}{\dfrac{[CTN]}{n} + \dfrac{\dfrac{1}{v_{ME}} - \dfrac{[CTN]}{n}}{K}}. \tag{4-8}$$

The radius of water pools r can be related to Wo by

$$r = \frac{3v_W Wo}{\Sigma_S}, \tag{4-9}$$

where v_W and Σ_S are the molecular and ME surface area occupied by an AOT molecule. This equation enables us to obtain the expressions for v_{ME} as

$$v_{ME} = \frac{4\pi}{3}\left(\frac{3v_W}{\Sigma_S}\right)^3 Wo^3 N_A\ , \tag{4-10}$$

where N_A is the Avogadro's number. In our system, ($3v_W/\Sigma s$) was 0.18 nm as shown in Equation 4-1, and Σs can be calculated as 0.50 nm^2 geometrically. *[ME]* is expressed as

$$[ME] = \frac{\Sigma_S[AOT]}{4\pi\left(\dfrac{3v_W}{\Sigma_S}\right)^2 Wo^2}, \tag{4-11}$$

where *[AOT]* is the AOT concentration in the organic phase. Therefore, Equation 4-8 can be simplified as

$$D = \phi_M \qquad \text{for } K = 1, \tag{4-12}$$

$$D = Kv_{ME}[ME] \qquad \text{for } \frac{v_{ME}[CTN]}{n} << \frac{1}{K-1}, \tag{4-13}$$

$$\frac{[CTN]}{n} = [ME] \qquad \text{for } \frac{v_{ME}[CTN]}{n} >> \frac{1}{K},\ K >> 1. \tag{4-14}$$

Figure 4-19 is the plot of *D/[ME]* against Wo, which can be divided into three regions as in Figure 4-17.

In the first region, which is observed in the range of Wo > 25, *D/[ME]* is proportional to Wo^3. This can be elucidated in terms of Equation 4-13, and the K value is evaluated as 680. Therefore the free energy change upon the incorporation of CTN into ME droplets can be calculated as –RTlnK = -16 kJ/mol. Since the dissolution energy of C_6H_{14} into water can be estimated as 32 kJ,[50] the hydrophobic tails of adsorbed AOT molecules on CTN surfaces are likely to interact weakly with the surfactant membranes of droplets. In this region, CTN molecules are likely to be incorporated into ME droplets as aggregates as observed by Matzke et al. using chymotrypsin,[51] since the water pools are much larger than the CTN size.

In the second region, which is seen in the range of 14 < Wo < 25, *D/[ME]* steeply

decreases with a decrease in Wo. Wo = 14 corresponds to r = 3.7 nm. Since this value is nearly consistent with the radius of CTN[32] as mentioned earlier, this shows that the incorporation mechanism differs when the ME radius is smaller than the CTN radius. The strong dependence of the distribution coefficient on Wo is most likely to be controlled by the bending energy of the ME droplets.

In the third region, which is found in the range of Wo < 14, the apparent distribution coefficient seems too large if we support the importance of the bending energy of ME droplets. It seems that another extraction process is dominant in this case, i.e., the adsorption of AOT molecules onto the CTN surface may cause the transfer of CTN from the aqueous phase into the organic phase. This assumption is supported by the earlier observation, i.e., the required time to attain the maximum extraction rate was very long and the back extraction did not proceed at all when the ME size was small. Of course, this extraction mechanism should exist in other two regions, although the effect is negligible due to the low amount of extraction by this mechanism. Figure 4-20 summarizes the illustrations of the supposed states of CTN molecules in the organic phase for three ranges of Wo.

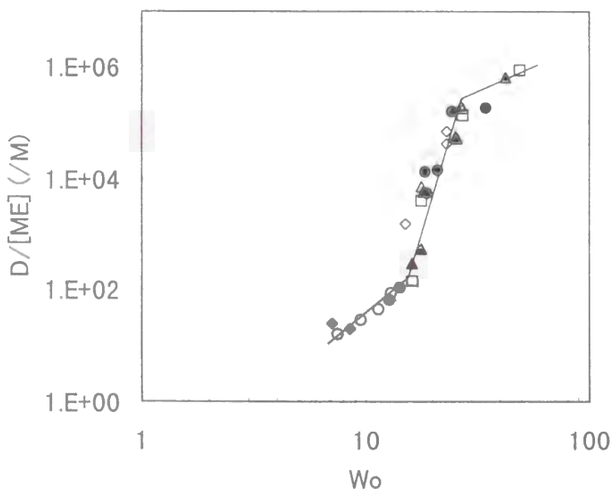

Figure 4-19. Dependence of D/[ME] on Wo. Symbols are the same as for Figure 4-15.

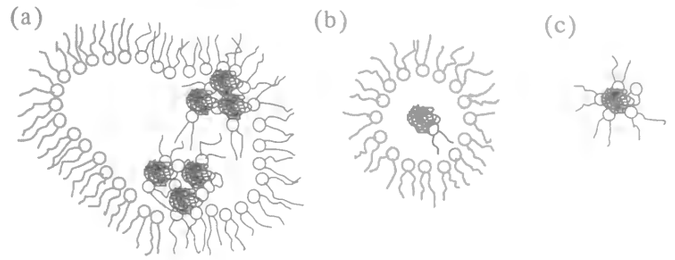

Figure 4-20. Illustrations of the state of CTN molecules in the organic phase. (a) Wo >25. CTN molecules are incorporated into ME droplets as clusters via AOT molecules. (b) 14 < Wo < 25. CTN molecules are incorporated as a single molecule with adsorption of a small amount of CTN. (c) Wo < 14. CTN molecules are extracted into the organic phase with adsorption of AOT molecules, and are not incorporated into ME droplets.

Solubilization Model. From these observations, the CTN solubilization model into the organic ME phase is proposed as illustrated in Figure 4-21. This model requires an adequate ME size to incorporate CTN molecules (14 < Wo < 25). If the ME size is too large, CTN molecules are incorporated as clusters as shown in Figure 4-20 (a). After that, the CTN/AOT complexes may be divided into small aggregates in the organic phase.

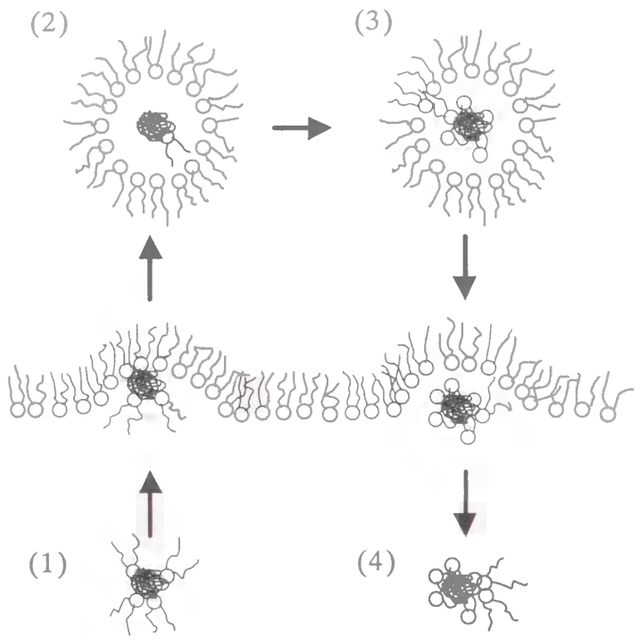

Figure 4-21. Proposed model of the CTN incorporation process into ME droplets. (1) Immediately after contact of the organic phase containing AOT and the aqueous CTN solution, fast adsorption of AOT molecules onto CTN surfaces proceeds via electrostatic interaction. This makes CTN molecules hydrophobic. (2) The "hydrophobic" CTN molecules are extracted into the organic phase with accompanying water molecules to form ME droplets. In this stage, CTN molecules are nearly in the native state. (3) With a long lapse of time in the organic phase, CTN molecules adsorb AOT molecules via hydrophobic interaction. This may be due to perturbation of the CTN structure by electrostatic interaction. This gradually changes the conformational state of the CTN molecules but not to a significant degree, and makes them hydrophilic. (4) The "hydrophilic" CTN molecules are back-extracted to the aqueous phase. Since the driving force of the back-extraction is the collision of droplets to the macroscopic oil/water interface, this proceeds very slowly, except when the net charge becomes negative due to much adsorption of AOT molecules. In the case of pH 7.5, more than 5 molecules must be adsorbed by the hydrophobic interaction.

Cation Exchange Chromatography. Chromatographic experiments were performed to confirm our proposed model by investigating the surface state, that is, hydrophilicity and charges, of CTN molecules. The time-dependent chromatograms obtained by cation exchange chromatography are presented in Figure 4-22. The samples loaded were aqueous solutions of CTN in contact with the ME phase or the AOT-free aqueous CTN solutions. The first peak corresponds to the CTN which passed through the column without interactions, and the height of the peak is denoted as p_1. The eluent was subsequently introduced and the obtained peak could be related to CTN which was adsorbed onto the column, and its peak height is denoted as p_2. These peak heights were proportional to the total amount of CTN fed to the column. Since the native CTN is positively charged, it should be adsorbed onto the chromatographic column, that is, the first peak should not be observed. As can be seen, the native CTN molecules are completely adsorbed as expected, whereas this is not the case for all the CTN molecules in the two-phase systems, suggesting that a certain degree of the interaction between CTN and AOT molecules always exists. With the lapse of time, p_1 was observed to increase, while p_2 was found to decrease. In addition to this, the second peak split into two peaks after a long time had elapsed. One of the peaks was at the same elution time as the second peak, but the other peak shifted to a longer elution time, suggesting that the apparent amount of positive charge increased more than that of the native CTN. However, this cannot be explained by the AOT adsorption. It is most likely that the positive charge of CTN buried inside in the native state appears at the surfaces due to the structural change. The height of the new third peak is denoted as p_3.

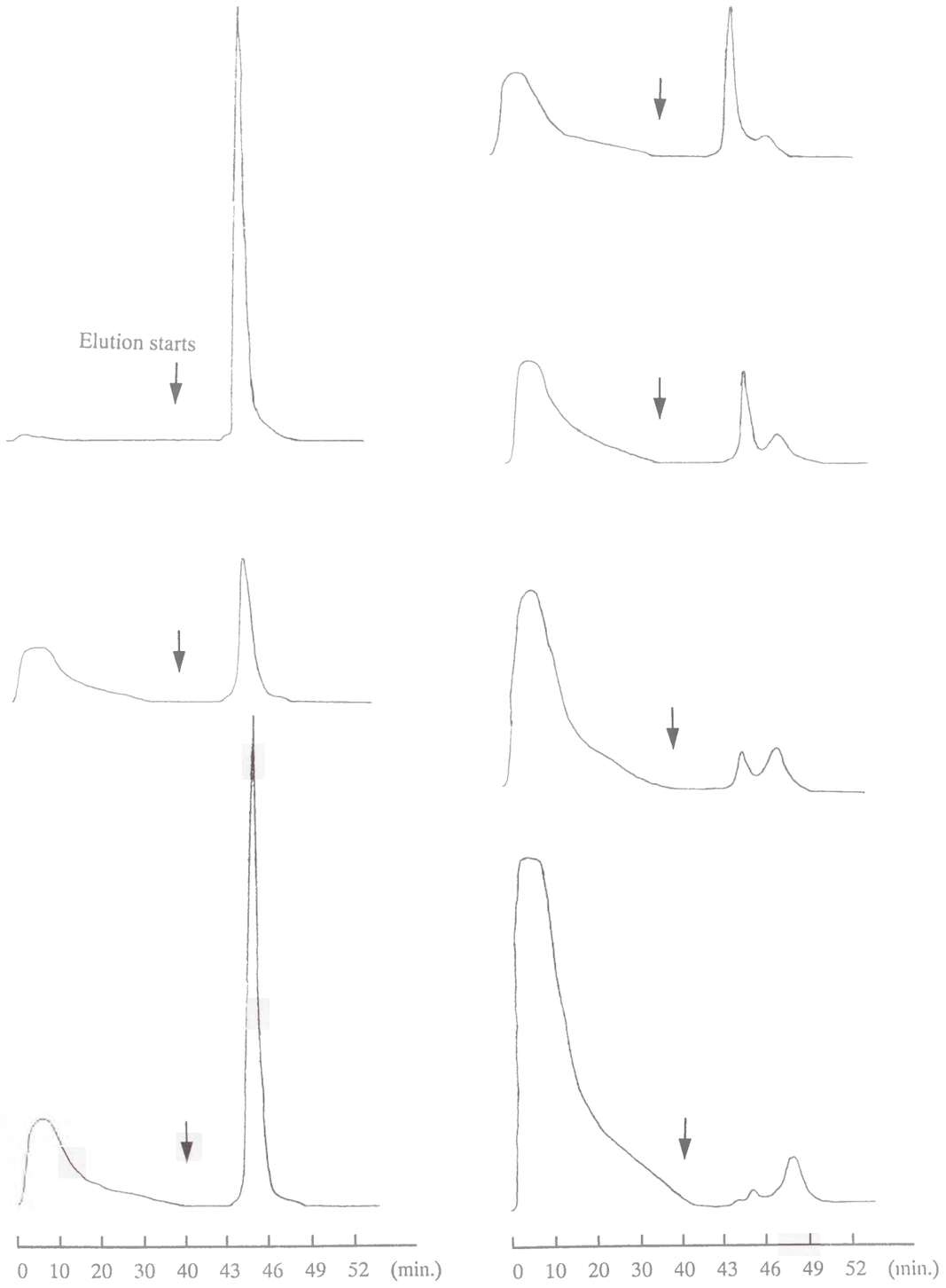

Figure 4-22. Time-dependent chromatograms obtained by cation exchange chromatography. Left side (top to bottom): native state, 3.3 μM; 10 minutes from contact, 3.8 μM; 30 min., 7.5 μM. Right side: 60 min., 6.4 μM, 2 hours, 9.0 μM; 8 hrs., 19 μM; 24 hrs., 29 μM. Eluent was introduced at the indicated point.

Here we take the ratio of p_1 to p_2 or the sum of p_2 and p_3 as the parameter to evaluate quantitatively the degree of AOT adsorption. The ratio is defined as *Rc* and its dependence on the contact time is shown in Figure 4-23. As can be seen, this ratio greatly increased with time except the ratio at 30 minutes. This result indicates the occurrence of time-dependent AOT adsorption onto CTN surfaces. The decrease in the AOT adsorption at 30 minutes can be elucidated as the conversion period from the electrostatic adsorption to the hydrophobic adsorption. Therefore, these results serve as an evidence for the incorporation model described in Figure 4-21.

When a very high salt concentration was employed, say Na = 0.4 M, we observed a slow increase in *Rc*. This can be elucidated in terms of a slow adsorption of AOT onto CTN surfaces due to the shielding effect of salt. The conversion period mentioned above was observed to be 24 hours after the contact. This suggests that the denaturation due to electrostatic adsorption of surfactants can be prevented by increasing the salt concentration.

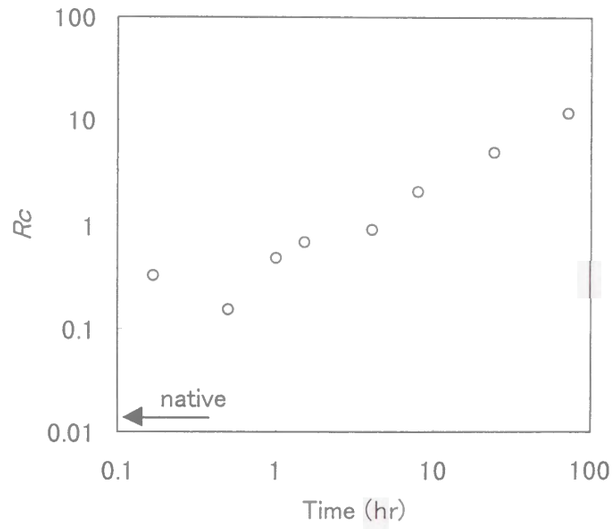

Figure 4-23. Dependence of the parameter of AOT adsorption *Rc* on the contact time. Native CTN yields *Rc* = 0.015 (indicated in the figure), regardless of the CTN concentration.

Hydrophobic Interaction Chromatography. Figure 4-24 presents the time-dependent chromatograms obtained by the hydrophobic interaction chromatography. The samples loaded were the aqueous CTN solutions as in the experiments of cation exchange chromatography, and each peak height obtained is also defined as p_1 and p_2. From this figure, it is apparent that p_2 diminished gradually with time, suggesting that the CTN molecules became more hydrophilic. Figure 4-25 shows R_H, which is defined by p_1/p_2, as a function of time. This figure quantitatively shows the increase of CTN hydrophilicity with time. However, if our model is correct, the hydrophilicity should be smaller than that of the native state during the electrostatic interaction period, that is, within a few tens of minutes from contact. This can be elucidated in terms of the hydrophobic interaction between AOT molecules and the column. In other words, since the column and AOT molecules can interact hydrophobically, it can be supposed that the AOT molecules, which are adsorbed onto CTN surfaces via electrostatic interaction, were removed during the chromatographic experiment. Therefore, these results also serve as the evidence for the incorporation model presented in Figure 4-21.

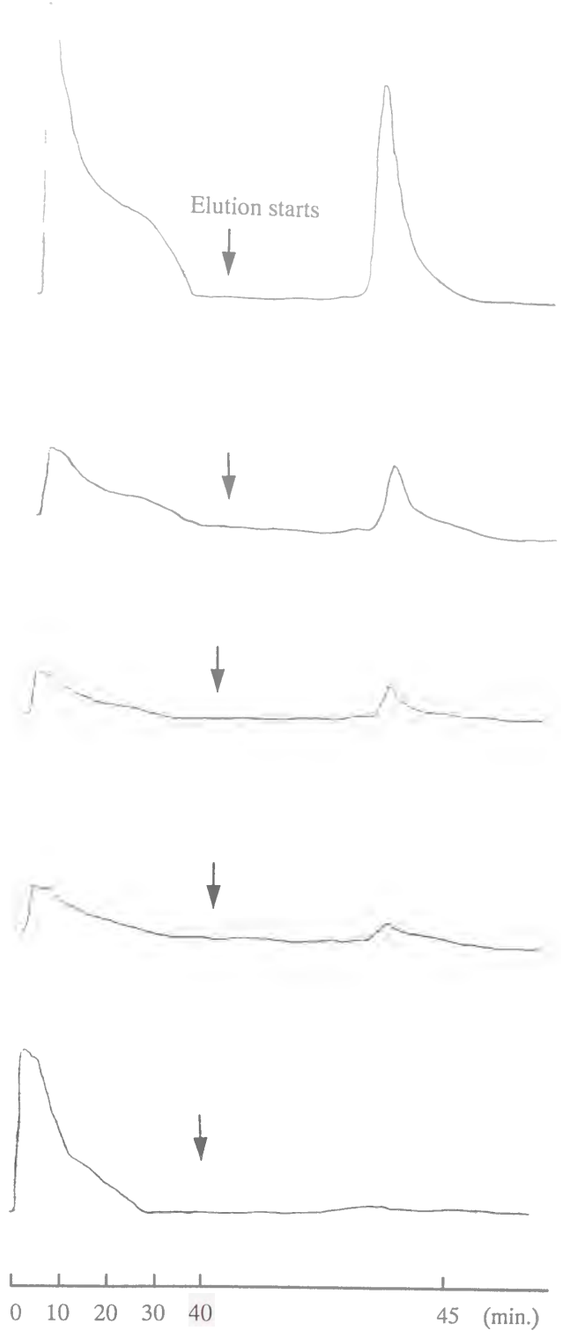

Figure 4-24. Time-dependent chromatograms obtained by hydrophobic interaction chromatography. Top to bottom: native state, 26 μM; 10 minutes from contact, 6.5 μM; 30 min., 4.3 μM; 60 min., 5.8 μM, 24 hrs., 24 μM. Eluent was introduced at the indicated point.

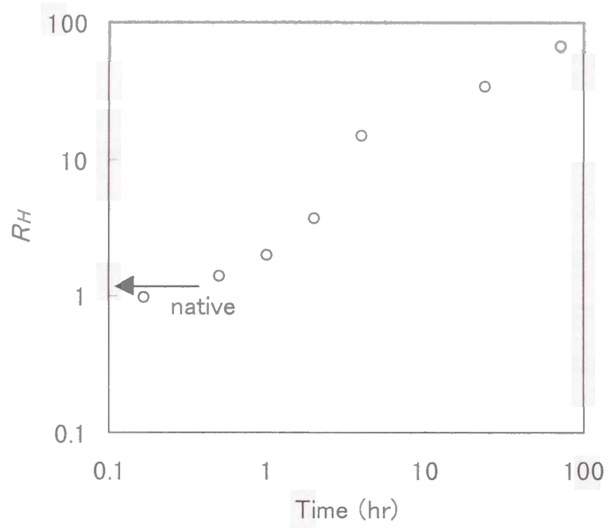

Figure 4-25. Dependence of the parameter of AOT adsorption R_H on the contact time. Native CTN yields R_H = 1.2 (indicated in the figure), regardless of the CTN concentration.

Summary

We presented here the importance of the adsorption of surfactants onto protein surfaces, in the solubilization process into ME droplets, even for the highly hydrophilic proteins. The solubilization process consists of two stages, a fast forward extraction and slow backward extraction, due to the two types of interactions between surfactants and proteins. This process is summarized in Figure 4-21.

The importance of ME size for the incorporation behavior was also investigated. If the ME droplets are large enough, protein molecules are incorporated as clusters. In the case of the ME size comparable to protein molecules, the size is a controlling factor of the incorporation rate. Small ME droplets cannot incorporate larger proteins, but the adsorption of surfactants onto protein surfaces enables a small amount of protein to extract into the organic phase. These findings are illustrated in Figure 4-20.

Our proposed model seems to be valid for all surfactants and proteins, if we take into account the stiffness of the protein structure, the charge of proteins and surfactants, etc. The model can provide an important information for the tailoring of ME formulation.

References

(1) Hoar, T. P.; Schulman, J. H. *Nature*, **1943**, *152*, 102.

(2) de Gennes, P. G.; Taupin, C. *J. Phys. Chem.* **1982**, *86*, 2294.

(3) Leung, R.; Shah, D. O. *J. Colloid Interface Sci.* **1987**, *120*, 320.

(4) Bhargava, H. N.; Narurkar, A.; Lieb, L. M. *Pharm. Tech.* **1987**, *March*, 46.

(5) Schwuger, M. J.; Stickdorn, K.; Schomäcker *Chem. Rev.* **1995**, *95*, 849.

(6) Schmalfuß, U.; Neubert, R.; Wohlrab, W. *J. Control. Release* **1997**, *46*, 279.

(7) Luisi, P. L.; Henninger, F.; Joppich, M. *Biochim. Biophys. Res. Commun.* **1977**, *74*, 1384.

(8) Luisi, P. L. *Angew. Chem. Int. Ed. Engl.* **1985**, *24*, 439.

(9) Martinek, K.; Levashov, A. V.; Klyachko, N.; Khmelnitski, Y. L.; Berezin, I. V. *Eur. J. Biochem.* **1986**, *155*, 453.

(10) Luisi, P. L.; Steinmann-Hofmann, B. *Methods Enzymol.* **1987**, *136*, 188.

(11) Luisi, P. L.; Giomini, M.; Pileni, M. P.; Robinson, B. H. *Biochim. Biophys. Acta* **1988**, *947*, 209.

(12) Pileni, M. P. "Structure and Reactivity in Reverse Micelles." Elsevier, Amsterdam, **1989**.

(13) Leser, M. E.; Luisi, P. L. *Chimia* **1990**, *44*, 270.

(14) Ramakrishnan, V. R.; Darszon, A., Montal, M. *J. Biol. Chem.* **1983**, *258*, 4857.

(15) Pileni, M. P.; Zemb, Th.; Petit, C. *Chem. Phys. Lett.* **1985**, *118*, 414.

(16) Luisi, P. L.; Magid, L. *Crit. Rev. Biochem.* **1986**, *20*, 409.

(17) Petit, C.; Brochette, P.; Pileni, M. P. *J. Phys. Chem.* **1986**, *90*, 6517.

(18) Caseli, M.; Luisi, P. L.; Maestro, M.; Roselli, R. *J. Phys. Chem.* **1988**, *92*, 3899.

(19) Bratko, D.; Luzar, A.; Chen, S. H. *J. Chem. Phys.* **1988**, *89*, 545.

(20) Bruno, P.; Casselli, M.; Luisi, P. L.; Maestro, M.; Traini, A. *J. Phys. Chem.* **1990**, *94*, 5908.

(21) Rahaman, R. S.; Hatton, T. A.; *J. Phys. Chem.* **1991**, *95*, 1799.

(22) Barbaric, S.; Luisi, P. L. *J. Am. Chem. Soc.* **1981**, *103*, 4239.

(23) Fletcher, P. D. I.; Rees, G. D.; Robinson, B. H.; Freedman, R. B. *Biochim. Biophys. Acta* **1985**, *832*, 204.

(24) Marcozzi, G.; Correa, N.; Luisi, P. L.; Caselli, M. *Biotech. Bioeng.* **1991**, *38*, 1239.

(25) Oldfield, C.; Freedman, R. B.; Robinson, B. H. *J. Chem. Soc., Faraday Trans.* **1996**, *92*, 73.

(26) Shioi, A.; Kishimoto, T.; Adachi, M.; Harada, M. *J. Chem. Eng. Japan* **1997**, *30*, 1130.

(27) Almeida, F. C. L.; Valente, A. P.; Chaimovich, H. *Biotech. Bioeng.* **1998**, *59*, 360.

(28) Smith, P. K.; Krohn, R. I.; Hermanson, G. T.; Mallia, A. K.; Gartner, F. H.; Provenzano, M. D.; Fujimoto, E. K.; Goeke, N. M.; Olson, B. J.; Klenk, D. C. *Anal. Biochem.* **1985**, *150*, 769.

(29) Taniguchi, S.; Goto, K. *Talanta* **1980**, *27*, 289.

(30) Kobayashi, T.; Adachi, M.; Iida, H.; Oba, K.; Oda, K.; Okumura, H.; Tsuji, K.; Numata, H.; Morimoto, Y. *Eisei Kagaku* **1986**, *32*, 391.

(31) Adachi, M.; Harada, M. *J. Colloid Interface Sci.* **1994**, *165*, 229.

(32) Boyer, P. D. "The Enzymes." Academic Press, London, **1971**.

(33) Hatton, T. A. "Surfactant-Based Separation Process." (Ed. Hinze, W. L. and Armstrong, D. W.), ACS Symp. Ser. Vol. 342, **1987**.

(34) Laane, C.; Dekker, M. "Surfactants in Solution. Vol. 9" (Ed. Mittal, K. L.) Plenum Press, NY, **1989**.

(35) Leser, M. E.; Luisi, P. L.; Palmieri, S. *Biotech. Bioeng.* **1989**, *34*, 1140.

(36) Luisi. P. L.; Bonner, F. J.; Pellegrini, A.; Wiget, P.; Wolf, R.; *Helv. Chim. Acta* **1979**, *62*, 740.

(37) Goklen, K. E.; Hatton, T. A. *Biotechnol. Prog.* **1985**, *1*, 69.

(38) Goklen, K. E.; Hatton, T. A. *Sep. Sci. Technol.* **1987**, *22*, 831.

(39) Wolbert, R. B. G.; Hilhorst, R.; Voskuilen, G.; Nachtegaal, H.; Dekker, M.; van't Riet, K.; Bijsterbosch, B. H. *Eur. J. Biochem.* **1989**, *184*, 627.

(40) Adachi, M.; Harada, M. *J. Phys. Chem.* **1993**, *97*, 3631.

(41) Mat, H. B.; Stuckey, D. C. "Solvent Extraction in the Process Industries, Vol. 2." Elsevier Applied Science, London **1993**.

(42) Fletcher, P. D. I.; Parrot, D.; *J. Chem. Soc., Faraday Trans.* 1 **1988**, *84*, 1131.

(43) Brochett, P.; Petit, C.; Pileni, M. P. *J. Phys. Chem.* **1988**, *92*, 3505.

(44) Adachi, M.; Harada, M.; Shioi, A.; Sato, Y. *J. Phys. Chem.* **1991**, *95*, 7925.

(45) Hirai, M.; Takizawa, T.; Yabuki, S.; Kawai-Hirai, R.; Oya, M.; Nakamura, K.; Kobashi, K.; Amemiya, Y. *J. Chem. Soc., Faraday Trans.* **1995**, *91*, 1081.

(46) Helfrich, W. *Z. Naturforsch.* **1973**, *28c*, 693.

(47) Winterhalter, M.; Helfrich, W. *J. Phys. Chem.* **1988**, *92*, 6865.

(48) Mitchell, D. J.; Ninham, B. W. *Langmuir* **1989**, *5*, 1121.

(49) Szleifer, I.; Kramer, D.; Ben-Shaul, A.; Gelbart, W. M.; Safran, S. A. *J. Chem. Phys.* **1990**, *92*, 6800.

(50) Tanford, C. *J. Phys. Chem.* **1972**, *76*, 3020.

(51) Matzke, S. F.; Creagh, A. L.; Haynes, C. A.; Prausinitz, J. M.; Blanch, H. W. *Biotech. Bioeng.* **1992**, *40*, 91.

Concluding Remarks

Two types of molecular assemblies, liposomes and microemulsions, were investigated from the viewpoint of drug carriers for topical applications. These two aggregates have opposite characters; the former is not in the equilibrium state while the latter is thermodynamically stable.

Thermodynamically unstable structures such as liposomes are significantly affected by their preparation process. This is one of the reasons why relatively only a few liposomal products are on the market. We demonstrated in Chapter 1 that the capillary electrophoresis can be a powerful tool for investigating compositional homogeneity of liposomes. Our observation showed the importance of organic solvents in the preparation process, although the utilization of such harmful solvents is not favored. In addition to this, we presented that the capillary electrophoresis could be used for investigating other various characteristics of liposomes.

Topical formulations contain a large amount of drugs and have high viscosity in most cases. These issues were discussed in Chapters 2 and 3. In Chapter 2, we showed that α-tocopheryl acetate significantly affected the membrane structure and could induce the formation of multiple emulsions. To add polymers to solutions is the normal strategy to gain viscosity, and this is also the case for liposomal dispersions. However, the interactions between polymers and liposomes may affect the physical stability of liposomes due to the depletion force, the perturbation of membranes, etc., although the interactions are normally weak. In Chapter 3, we demonstrated that FT-IR, dynamic light scattering, and surface tension measurements could be convenient tools for investigating such weak interactions, and found that the type of interaction strongly depends on the polymer species. These observations provided an important information for designing liposomal formulations for topical uses.

Microemulsion formulations are not affected by their preparation process. However, much detailed observation of the incorporation process of drugs is needed, since it is

not possible to solubilize drugs by mechanical forces. The incorporation process of proteins into microemulsion droplets was investigated in detail in Chapter 4, with the importance of surfactant-protein interactions and the size of the droplets being shown. This result offers a useful information for the design of microemulsion formulations.

The observations discussed here offer an important information and useful methodologies for designing topical formulations, which contain molecular assemblies as drug carriers. Since the efficaciousness of molecular assemblies has been frequently reported, we hope that the information we have presented can promote the development of such useful formulations.

List of Publications

Chapter 1

(1) "Compositional Homogeneity of Liposomal Membranes Investigated by Capillary Electrophoresis."

Kawakami, K.; Nishihara, Y.; Hirano, K. *J. Colloid Interface Sci.* **1998**, *206*, 177.

(2) "Rigidity of Lipid Membranes Detected by Capillary Electrophoresis."

Kawakami, K.; Nishihara, Y.; Hirano, K. *Langmuir* **1999**, *15*, 1893.

(3)"Applications of Capillary Electrophoresis for Analysis of Liposome Dispersions."

Kawakami, K.; Nishihara, Y.; Hirano, K. *Hydrocolloids 2: Fundamentals and Applications in Food, Biology, and Medicine*; Elsevier, 2000, in press.

Chapter 2

(4) "Determination of the Entrapped Volume of Liposomes; Dilution Method."

Kawakami, K.; Nishihara, Y.; Hirano, K. *Anal. Biochem.* **1999**, *269*, 139.

(5) "Liposome/Emulsion Transition Induced by α-Tocopheryl Acetate."

Kawakami, K.; Nishihara, Y.; Hirano, K. *Langmuir*, **1999**, *15*, 7454.

Chapter 3

(6) "Effect of Hydrophilic Polymers on Physical Stability of Liposome Dispersions."

Kawakami, K.; Nishihara, Y.; Hirano, K. *J. Phys. Chem. B*, submitted.

Chapter 4

(7) "Mechanism of Protein Solubilization in Sodium Bis(2-ethylhexyl) Sulfosuccinate Water-in-Oil Microemulsion."

Kawakami, K.; Harada, M.; Adachi, M.; Shioi, A. *Colloids Surf. A* **1996**, *109*, 217.

Acknowledgment

This study was performed from 1992 to 1994 at the Department of Chemical Engineering, Graduate School of Engineering, Kyoto University, and from 1994 to 1999 at Formulation R & D Laboratories, Shionogi & Co., Ltd. The author expresses his great gratitude to Professor Ko Higashitani of Department of Chemical Engineering, Graduate School of Engineering, Kyoto University. His kind support and detailed suggestions were very helpful on the preparation of this thesis.

Sincere gratitude is due to Professor Masataka Tanigaki of Department of Chemical Engineering, Graduate School of Engineering, Kyoto University, and Associate Professor Kazunari Akiyoshi of Department of Synthetic Chemistry & Biological Chemistry, Graduate School of Engineering, Kyoto University for their useful comments on this thesis.

The author would like to express his grateful acknowledgment to Professor Makoto Harada of Institute of Advanced Energy, Kyoto University for his kind advice on the preparation of this thesis and fruitful discussion on Chapter 4. Sincere gratitude is due to Dr. Motonari Adachi of Institute of Advanced Energy, Kyoto University for his helpful and concrete suggestions on Chapter 4. Special thanks are also due to Dr. Akihisa Shioi of Institute of Advanced Energy, Kyoto University for his pertinent suggestions on Chapter 4.

The author is grateful to Dr. Koichiro Hirano, General Manager, Formulation R & D Laboratories, Shionogi & Co., Ltd. for his providing an opportunity to prepare this thesis and his kind continuous support. The author also appreciates the instructive comments on Chapters 1 through 3 provided by Mr. Yoshitaka Nishihara, Formulation R & D Laboratories, Shionogi & Co., Ltd. Experimental support on NMR measurements by Dr. Tohru Yamaguchi, Discovery Research Laboratories, Shionogi & Co., Ltd. is also deeply acknowledged.

December, 1999

Kohsaku Kawakami